DISSERTATION

submitted to

the Combined Faculties for the Natural Sciences and for Mathematics

of the Ruperto-Carola University of Heidelberg, Germany

for the degree of

Doctor of Natural Sciences

presented by

Xiaobo Fan

born in Hunan, China

Oral-examination: 2014

The antimicrobial activity and mechanism of action of recombinant Ib-AMP4, an antimicrobial peptide from *Impatiens balsamina*

Referees: Prof. Dr. Michael Wink

Prof. Dr. Jürgen Reichling

I hereby declare that I have written the submitted dissertation myself and in this process have used no other sources or materials than those expressly indicated.

I hereby declare that I have not applied to be examined at any other institution, nor have I used the dissertation in this or any other form at any other institution as an examination paper, nor submitted it to any other faculty as a dissertation.

List of publications:

Fan, X., J. Reichling, and M. Wink. 2013. Antibacterial activity of the recombinant antimicrobial peptide Ib-AMP4 from *Impatiens balsamina* and its synergy with other antimicrobial agents against drug resistant bacteria. Pharmazie **68:**628-30

Fan, X., H. Schäfer, J. Reichling, and M. Wink. 2013. Bactericidal properties of the antimicrobial peptide Ib-AMP4 from *Impatiens balsamina* produced as a recombinant fusion-protein in *Escherichia coli*. Biotechnol J **8:**1213-20.

Fan, X., H. Schäfer, J. Reichling, and M. Wink. Interaction between Ib-AMP4 with LPS and lipids (in preparation).

Fan, X., H. Schäfer, J. Reichling, and M. Wink. 2013. Antimicrobial properties of Ib-AMP4 and the inhibitory effect of calcium. (Poster submitted on the first EMBO|EMBL Symposium on New Approaches and Concepts In Microbiology, Heidelberg, 14-16 October, 2013)

Acknowledgement

I want to express my sincere appreciation to my PhD mentors Prof. Dr. Michael Wink and Prof. Dr. Jürgen Reichling for their generous support during the time of my research, their consistent interest in the progress of my work as well as valuable suggestions and discussions. Furthermore, I want to thank Prof. Dr. Michael Wink for an overall pleasant atmosphere, his accessibility anytime, and the opportunity to choose the topics and course of my research studies.

I thank Prof. Guoqiu Wu (Southeast University, China) and Prof. Tao Xi (China Pharmaceutical University, China), for collaboration and fruitful discussions on protein production.

I thank Dr. med. Stefan Zimmermann for providing access to bacteria and essential materials.

I thank Prof. Dr. Motomu Tanaka and his group, especially Dr. Ali Makky and Agatha Korytowski, for their collaboration and fruitful discussions on the physical-chemistry experiments, such as surface isotherm and QCM-D.

I thank Prof. Dr. Thomas Ruppert and Dr. Merker for measurement of mass spectra.

I thank Prof. Dr. Matthias Mayer for Circular dichroism spectra.

I also thank my colleagues, in particular Dr. Holger Schäfer, Ms Petra Fellhauer, Mr Ikhwan Resmala Sudji, Ms Hedwig Sauer-Gürth, Ms Heidi

Staudter, and Ms Astrid Bakhaus for their ideas, suggestions, discussions, and generous support.

I want to specially thank Mr Markus Braun for translation of the summary.

I want to thank China Scholarship Fund to support my PhD research and studies.

I am deeply grateful for the consistent and strong support from my beloved family, Guorong, Lin, Hui and Weiwei, for their support to my academic career.

Abbreviations

g	gram
h	hour
l	liter
m	milli
µ	micro
A	molecular area
M	molar per liter
N	newton
P	surface potential
Π	surface pressure
rEk	recombinant enterokinase
rpm	round per minute
AMP	antimicrobial peptide
APS	ammonium persulfate
BSA	bovine serum albumin
CD	circular dichroism
Da	Dalton
DLS	dynamic light scattering
DOPC	1,2-dioleoyl-*sn*-glycero-3-phosphocholine
DOPG	1,2-di-(9Z-octadecenoyl)-*sn*-glycero-3-phospho-(1'-*rac*-glycerol)
DTB	dextrose tryptone broth
EDTA	ethylenediaminetetraacetic acid
ESBL	extended spectrum β-lactamase
FICI	fractional inhibitory concentration index
GUVs	giant unilamellar vesicles
Ib-AMP4	*Impatiens balsamina* antimicrobial peptide 4
IPTG	isopropyl β-D-1-thiogalactopyranoside
ITO	indium tin oxide
LPS	lipopolysaccharide
LB	Luria–Bertani broth
MBC	minimal bactericidal concentration
MDR	multiple drug resistance
MIC	minimal inhibitory concentration
MRSA	methicillin-resistant *Staphylococcus aureus*
PS	phosphatidylserine

PG phosphatidylglycerol

QCM-D quartz crystal microbalance with dissipation

RT room temperature

SDS sodium dodecyl sulfate

SDS-PAGE sodium dodecyl sulfate–polyacrylamide gel electrophoresis

TEM transmission electron microscopy

Trx thioredoxin

WHO World Health Organization

Summary

Drug resistant microbes have become widely prevalent and are a large clinical burden. Infectious diseases have again become life threatening and affect millions of people each year because of the rapid evolution of drug resistance. Therefore, the development of antibiotics with novel antimicrobial mechanisms of action is highly prioritized. AMPs are antimicrobials with potential to fulfill this need because of their differences from traditional antibiotics.

Ib-AMP4 has been isolated from *Impatiens balsamina* and exhibits broad antimicrobial activity against plant pathogens. Large amounts of Ib-AMP4 were prepared by expressing the peptide in *Escherichia coli*. Bacteria showing resistance to current antibiotics are susceptible to AMPs. No cross-resistance was observed between present antibiotics and AMPs. Ib-AMP4 has shown promising antimicrobial effects against human pathogens, including the most prevalent MDR species of MRSA and ESBL-producing *E. coli*. When combined with other antimicrobials, Ib-AMP4 restored the susceptibility of MDR strains and greatly reduced the amount of antimicrobial agents required for efficacy. However, the antimicrobial efficiency of Ib-AMP4 was also largely affected by cations, especially divalent cations.

To determine the mechanism of action underlying the antimicrobial activity of Ib-AMP4, LPS from bacterial cell walls and lipids from biomembranes were used to construct an *in vitro* model system. We found that in the presence of Ca^{2+}, our model system of the LPS-Re monolayer absorbed Ca^{2+} and became increasingly compact. Bacterial pathogens used Ca^{2+} to repel Ib-AMP4 electrically, thereby reducing cell wall permeability to Ib-AMP4.

The cytoplasmic membrane is the primary target of Ib-AMP4's rapid bactericidal effect. Liposome leakage assays and QCM-D indicate that Ib-AMP4 may intercalate into the DOPC bilayer membrane, thereby resulting in liposomal leakiness, surface swelling, and wrinkling. The development of pores develop within the lipid bilayer is still unknown. However, pore development most likely follows the "sinking raft" model because the Ib-AMP4 structure includes a large hydrophilic headgroup coupled to a short and small hydrophobic tail. After the initial insertion of Ib-AMP4, a rapid and intensive leakage occurred for approximately 20 min. Along with this leakage, the insertion of Ib-AMP4 continued in a "self-promoting" pattern, in which the initial insertion of Ib-AMP4 induced further insertions of Ib-AMP4. Surface pressure, line tension, and curvature strain were likely involved in the formation and resealing of the pores. Studies using single DOPC and DOPC/DOPG binary monolayers in calcium-loaded and -free buffers indicated that the charge properties of the lipids and cations in the buffer affect the insertion of Ib-AMP4 regardless of surface pressure. Cholesterol may inhibit calcein leakage caused by Ib-AMP4 by changing the membrane's compressibility and curvature. Cations may also inhibit Ib-AMP4 insertion into membranes either by interrupting the conformational change of Ib-AMP4 during the insertion stage or by electrically repelling Ib-AMP4. Such inhibition is similar to that with cell wall LPS.

Zusammenfassung

Medikamtentenresistente Mikroorganismen sind heutzutage weit verbreitet und stellen ein bedeutsames klinisches Problem dar. Dabei ist es der rapiden Evolution von Resistenzen geschuldet, dass Infektionskrankheiten mittlerweile wieder lebensbedrohliche Ausmaße annehmen können. Folgerichtig kommt der Entwicklung von Antibiotika mit neuartigen Wirkmechanismen oberste Priorität zu. AMPs sind antimikrobielle Substanzen, die sich von herkömmlichen Antibiotika unterscheiden und über das Potential verfügen dieser Anforderung gerecht zu werden.
Ib-AMP4 wurde aus *Impatiens balsamina* isoliert und zeigte breite antimikrobielle Aktivität gegenüber Pflanzenpathogenen. Große Mengen von Ib-AMP4 wurden durch die Expression des Peptids in *Escherichia coli* hergestellt. Auch Bakterien, welche gegen gegenwärtige Antibiotika resistent sind, sind für Ib-AMP4 empfänglich. Es wurden keinerlei Kreuzresistenzen zwischen Ib-AMP4 und sich im Umlauf befindlichen Antibiotika festgestellt. Ib-AMP4 offenbarte vielversprechende Effekte gegen humane Krankheitserreger, wie zum Beispiel die am weitesten verbreiteten MDR-Stämme von MRSA und ESBL-produzierende *E. coli*. In Kombination mit anderen antimikrobiellen Stoffen, stellte Ib-AMP4 die Empfindlichkeit von MDR-Stämmen wiederher und reduzierte die Menge der benötigten antimikrobiellen Substanzen erheblich. Jedoch vermochten es Kationen – insbesondere divalente Kationen – die antimikrobielle Wirksamkeit zu beeinflussen.
Um den der antimikrobiellen Aktivität zu Grunde liegenden Mechanismus des Ib-AMP4 aufzuklären, wurden LPS aus bakteriellen Zellwänden und Lipide aus Biomembranen dazu benutzt, um ein *in vitro* Modell zu entwerfen. Daraus wurde ersichtlich, dass das Modellsystem aus LPS-Re in Gegenwart von Ca^{2+} selbiges absorbierte und kompakter wurde. Bakterielle Pathogene benutzten Ca^{2+}, um Ib-AMP4 elektrisch abzustoßen und somit dessen Zellwandpermeabilität herabzusetzen.
Die Zellmembran ist der Hauptangriffspunkt des bakterizid wirkenden Ib-AMP4. Die gestörte Liposomenintegrität in „Liposome leakage assays“ und QCM-D deutet darauf hin, dass Ib-AMP4 in die DOPC-Doppelschicht interkaliert und dadurch Lecks in den Liposomen, das Anschwellen der Oberfläche und Runzelbildung induziert. Die Entstehung von Poren innerhalb der Lipiddoppelschicht ist noch immer ungeklärt. Am wahrscheinlichsten ist allerdings die Bildung entsprechend dem „sinking raft“ Modell, da Ib-AMP4 eine große hydrophile Kopfgruppe besitzt, welche an einen kurzen hydrophoben Schwanz gekoppelt ist. Nach der anfänglichen Insertion des Ib-AMP4 kam es zu raschen und intensiven, ungefähr 20 Minuten andauernden Leckverlusten. Zusammen mit diesen Leckverlusten, waren weitere, sich selbst fortpflanzende Insertionen von Ib-AMP4 zu beobachten, die durch den initialen Einbau von Ib-AMP4 vermittelt wurden. Oberflächenspannung, Linienspannung und Krümmungspannung trugen wohl zur Entstehung und Versiegelung der Poren bei. Untersuchungen, die binäre DOPC und DOPC/DOPG Einzelschichten in calciumhaltigem und calciumfreiem Puffer lassen vermuten, dass die Ladung der Lipide und Kationen im Puffer die Insertion von Ib-AMP4 unabhängig von der Oberflächenspannung beeinflusst. Cholesterin könnte die Calceinfreisetzung durch Ib-AMP4 unterbinden, indem es die Membrankompressibilität und die Krümmung verändert. Kationen könnten die Insertion von Ib-AMP4 in Membranen ebenfalls inhibieren, indem sie entweder dessen Konformationsänderung während der Insertionsphase unterbrechen oder Ib-AMP4 elektrisch abstoßen. Diese Art der Inhibierung ähnelt jener durch Zellwand-LPS.

Contents

THE ANTIMICROBIAL ACTIVITY AND MECHANISM OF ACTION OF RECOMBINANT IB-AMP4, AN ANTIMICROBIAL PEPTIDE FROM *IMPATIENS BALSAMINA*

List of Figures

List of Tables

Chapter 1. General introduction

1.1 Global infectious diseases and drug resistant bacteria

A study performed in 2009 reported that more than 15% of clinical *Escherichia coli* isolates in Europe were resistant to third generation cephalosporins (WHO 2011). Furthermore, MRSA infections have been occurring in Latin America, and more than 26% of clinical isolates have been drug resistant (WHO 2007). According to a recent release from the World Health Organization (WHO), *Escherichia coli* and *Klebsiella pneumoniae* resistant to cephalosporins and *Staphylococcus aureus* resistant to methicillin have exceeded 50% of isolates found in multiple sites nationally as shown in Table1 (WHO 2014). Bacterial resistance to third generation cephalosporins means that infections with these bacteria can only be treated using carbapenems, which are generally considered a last resort when treating severe infections. Notably, in some regions, the proportion of *Klebsiella pneumoniae* resistant to carbapenems has reached over 50% of isolates (Table 1). Community acquired bacteria, such as *Streptococcus pneumoniae,* nontyphoidal *Salmonella, Shigella* species and *Neisseria gonorrhoeae,* have also displayed a rapid increase in antimicrobial resistance. Overall, resistance has increased the burden on and doubled the mortality in clinical practices (Table 2). Presently, approximately 60,000 people in Europe and the United States die each year due to serious infections

caused by antimicrobial resistant bacterial pathogens, primarily those acquired in health-care settings (WHO 2014).

Table 1 Bacteria commonly causing infections in hospitals and communities (WHO, 2014)

Name of bacterium/ resistance	Examples of typical diseases	No. of 194 states providing national data	No. of WHO regions with national reports of 50 % resistance or more	Range of reported proportion of resistance
Escherichia coli	Urinary tract infections, blood stream infections			
-vs 3rd gen. cephalosporins		84	5/6	0-82
-vs fluoroquinolones		90	5/6	3-96
Klebsiella pneumoniae	Pneumonia, blood stream infections, urinary tract infections			
-vs 3rd gen.cephalosporins		85	6/6	2-82
-vs carbapenems		69	2/6	0-68
Staphylococcus aureus	Wound infections, blood stream infections			
-vs methicillin "MRSA"		42	3/6	0-36

Table 2 Risk of death is higher in patients infected with drug resistant bacterial strains (WHO, 2014)

Name of bacterium/ resistance	Outcome (number of studies included)	Deaths (%)	
		Patients with resistant strains	Patients with non-resistant strains
Escherichia coli			
-vs 3rd gen. cephalosporins	Bacterium attributable mortality (n=4)	23.6	12.6
-vs fluoroquinolones	Bacterium attributable mortality (n=1)	0	0
Klebsiella pneumoniae			
-vs 3rd gen.cephalosporins	Bacterium attributable mortality (n=4)	10	10.1
-vs carbapenems	Bacterium attributable mortality (n=1)	27	13.6
Staphylococcus aureus			
-vs methicillin "MRSA"	Bacterium attributable mortality (n=46)	26.3	16.9

1.2 Antibiotic targets and development

All organisms share a large number of common traits, such as cellular structure and metabolism, but, due to millions of years of evolution in some cases, also differ greatly. In particular, microorganisms have evolved unique cellular structures and metabolic properties as compared to eukaryotes that have potential to serve as targets for antibiotics. Currently, antibiotic development has targeted the four major metabolism pathways of DNA synthesis, RNA synthesis, protein synthesis and cell wall synthesis (Kohanski et al. 2010; Lewis 2013). Antibiotics have been developed to target bacteria specific proteins and substrates as shown in Figure 1.

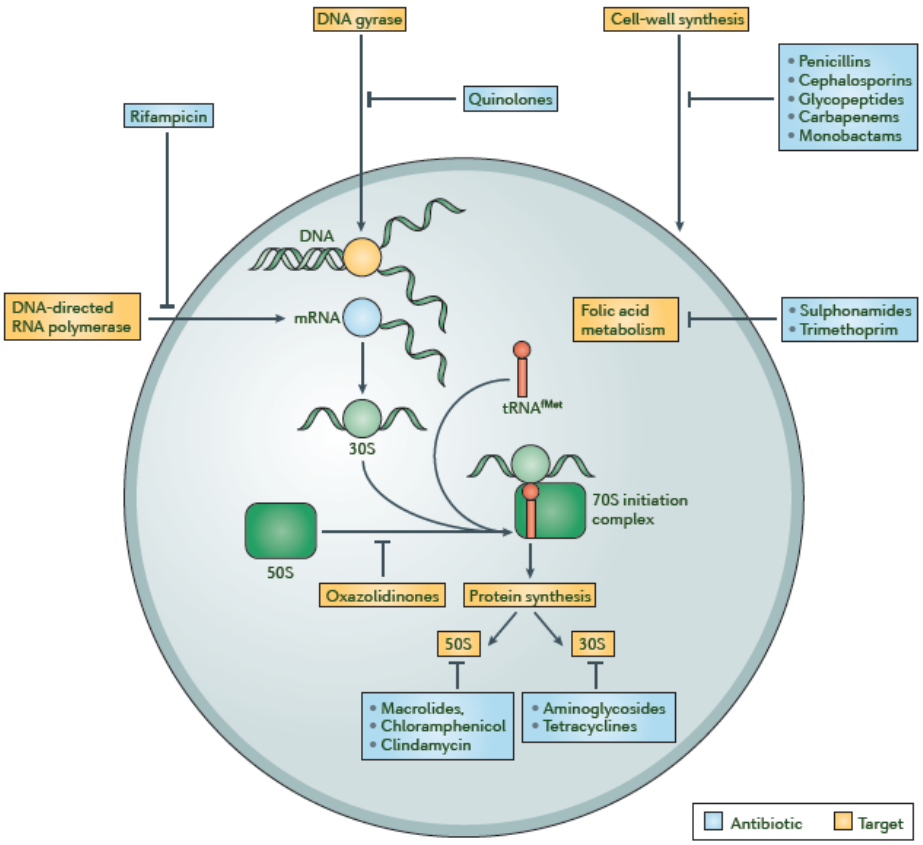

Figure 1. Antibiotics primarily target bacterial metabolism pathways (Lewis 2013).

Since the first antibiotic, penicillin, was discovered in 1929, dozens of naturally occurring antibiotics have been identified. As their underlying mechanisms of actions are deciphered, the drug–target interactions have been determined. This has led to the development of more novel artificial antibiotics via molecular modification of preexisting antibiotics. These efforts have greatly enhanced treatment in clinical practices. However, despite the increasing prevalence of drug resistance, the research and development for new antibiotics has almost halted. This is evident in the fact that there have been no major novel types of antibiotics developed in the last two decades (Figure 2). The antibiotic candidates currently in the pipeline are variations of previous antibiotics and, due to the similarity between the antibiotic structures and their targets, are likely to provoke new resistance (Carlet et al. 2012; Spellberg et al. 2004). Thus, we are heading towards a post-antibiotic era in which common infections and minor injuries will be fatal. Therefore, the discovery of new antibiotics with novel antimicrobial mechanisms of action has become a matter of great urgency.

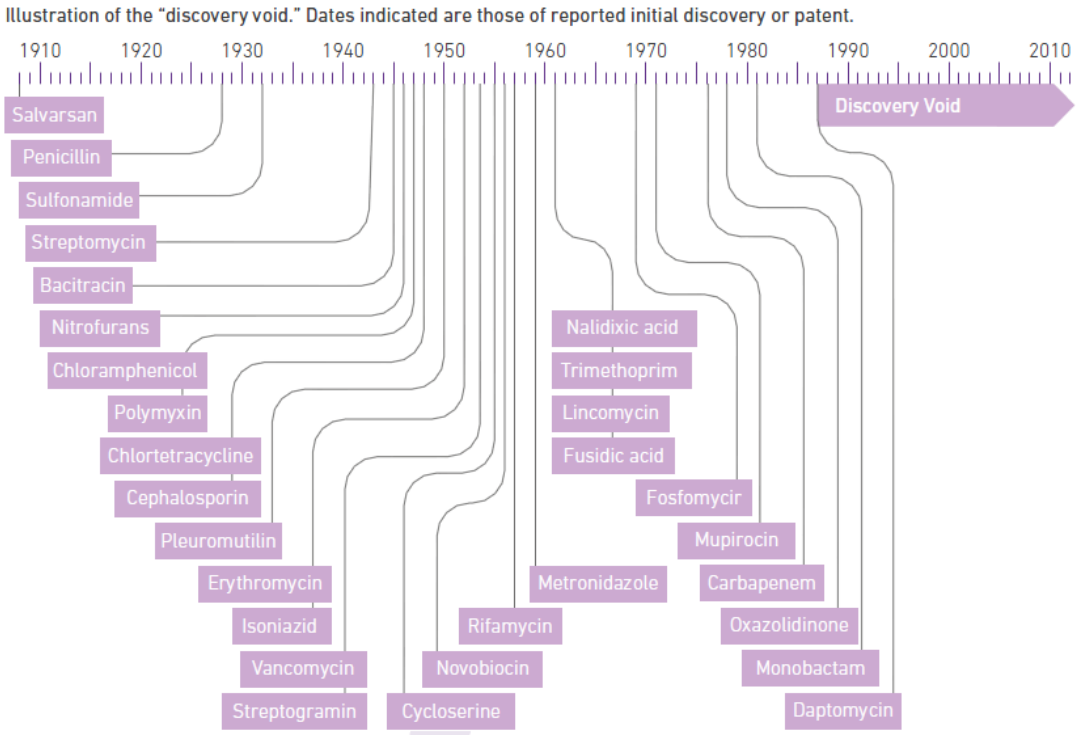

Figure 2. Timeline of discovery of distinct classes of antibacterial drugs (Higgins 2011).

1.3 Drug resistance mechanism

Evolution occurs naturally when microorganisms replicate themselves erroneously or exchange traits under selective pressure. Drug resistance has evolved in nature since ancient people started to use herb medicine well before the antibiotics era. Phylogenetic researches reveal that some classic resistant genes such as metallo-β-lactamases originated more than two billion years ago (Garau et al. 2005). Drug resistance is now widely spread all over the world because of antibiotic abuse and inadequate infection control practices.

Antibiotics inhibit or alter essential cellular functions in bacteria by selective pressure. Antibiotic abuse, especially the improper administration of antibiotics below sufficient dosage, accelerates drug resistance. The major strategies

used by bacteria against antibiotics have been reported and are well understood (Figure 3). A possible strategy is antibiotic destruction. β-lactam antibiotics, such as penicillin, can be hydrolyzed by bacteria bearing the ESBL gene coding for a β-lactamase. Bacteria also use mutations to overcome antibiotics. Streptomycin resistance requires special mutations within the bacterial 30S ribosomal protein RpsL (Alekshun and Levy 2007). Another resistance mechanism involves reducing the accumulation of antibiotics by decreasing drug permeability or active pumping out. An example is AcfAB-TolC (Alekshun and Levy 2007) that could actively pump out multiple antibiotics with targets located inside cells. Furthermore, susceptibility of bacteria to antibiotics is highly related to the bacterial stage. Non-growing cells after the log exponential phase are relatively more tolerant to antibiotic treatments. The underlying mechanism is still largely unknown, but might be caused by the absence of active targets for antibiotics in non-growth cells (Kumar et al. 2013).

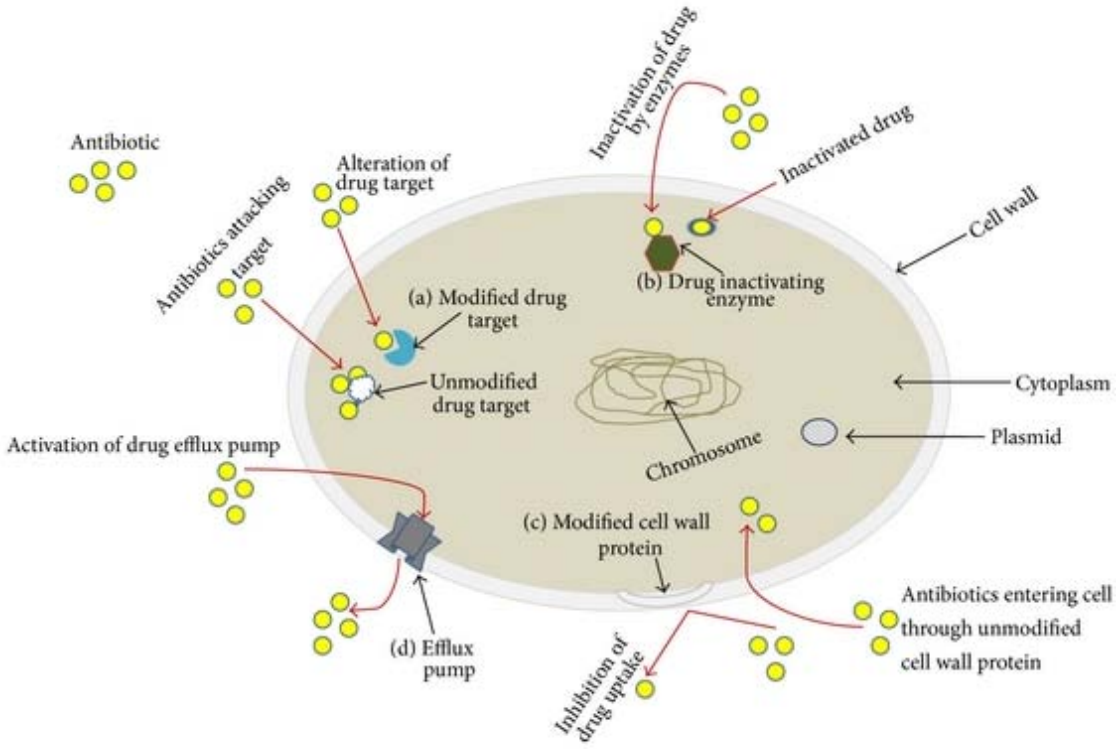

Figure 3. Bacterial cells employ multiple mechanisms to overcome antibiotics (Alekshun and Levy 2007).

1.4 Source distribution and physiological roles of antimicrobial peptides (AMPs)

AMPs have been highlighted because of their potential to solve the drug resistance problem. AMPs are part of the ancient, nonspecific innate immune system in many organisms. AMPs represent a universal feature of systematic defense for all life forms and are found in various organisms ranging from bacteria to plants and animals (Jenssen et al. 2006).

The fruit fly is a model organism for invertebrates and has been the main subject of AMP studies (Engstrom 1999). Invertebrates lack an adaptive immune system found in vertebrates. Thus, AMPs are more important in

invertebrates than in vertebrates. The innate immune system seems very effective because the fruit fly can survive in hostile environments where pathogenic microorganisms thrive. The main types of AMPs in vertebrates are defincins and cathelicidins, which are characteristic of a conserved N-terminate or a conserved disulfide bridge crosslink (Jenssen et al. 2006). Amphibian skin glands contain elevated levels of AMPs. Up to 500 AMPs have been discovered from different amphibian species (Rinaldi 2002). Besides their function against infection, AMPs in bacteria also act as competition regulators. Bacteria secrete AMPs to kill other microorganisms that compete for nutrients in the same environment (Chatterjee et al. 1992; Klaenhammer 1988).

Plant AMPs always contain multiple disulfide bonds which bring a great obstacle for their production in bacteria, yeast or other organisms (Hammami et al. 2009) and thereby little attention has been drawn to plant peptides. Plant AMPs are mainly divided into 8 classes: snakin, defensin, thionin, knottin, hevein-like, cyclotide, impatiens and lipid-transfer. These are important in defending plants against bacteria, fungi, viruses and even parasites, though the production of secondary metabolites remains the main antimicrobial defence strategy in plants in most cases (Hammami et al. 2009). Along with their antimicrobial activity, they seem have more activity on the inorganic

defense such as frost, cold and dry (Hammami et al. 2009), and more and more attention has been drawn to understand their roles during development.

1.5 Action of AMPs on bacteria

The initial interaction between AMPs with their target microbes occurs through electrostatic attraction. Negatively charged membrane lipids seem to provide for a mutual and vigorous attraction to highly charged cationic antimicrobial peptides. Numerous studies have demonstrated that the charge of AMPs is highly associated with their membrane binding activity (Bessalle et al. 1992; Lee et al. 2013; Matsuzaki et al. 1997; Sato and Feix 2006; Yeaman and Yount 2003). This view is also supported by the fact that AMPs from different species are conserved of highly positive charge (Gueguen et al. 2006; Seshadri Sundararajan et al. 2012; Wang et al. 2009). Given the facts that electrostatic forces exist in long distance range and that interactions between lysine or arginine with phosphate groups in lipid bilayers are particularly strong, electrostatic interactions likely drive the initial attraction between lipids and AMPs (Mavri and Vogel 1996).

The event that follows the initial binding is a transition stage where the peptides dramatically increase their affinity towards the membrane by altering their geometric conformation; a self-promoting association or multimerization would occur and peptides are positioned perpendicular to the membrane (Huang 2000; Prado Montes de Oca 2013; Yeaman and Yount 2003). This

phenomenon is supported by oriented circular dicroism (OCD) studies on the orientation of peptides on the membrane surface. Most of these peptides are in alpha-helix form. The alpha-helices are oriented parallel to the membrane surface initially, but are then re-oriented perpendicular to the membrane when the threshold concentration is reached. The membrane finally develops a transmembrane deficiency, which could either be a hole or a channel, after the transition stage. Different speculations have been described for this stage, namely, barrel-stave, toroid-pore, and carpet theories (Prado Montes de Oca 2013; Wimley 2010; Yeaman and Yount 2003).

The barrel-stave model suggests that the peptides binding to the membrane surface would push the local lipids aside. The peptide would then be inserted into the bilayer along with a conformational change that orients the hydrophobic residues of peptides in such a way that they face the lipids. The hydrophilic residues form a pore lining. The barrel-stave pore only consists of peptides. Thus, the peptides require a sufficient length to expand across the bilayer. Similar to the barrel-stave model, the toroid-pore model uses peptides to form the pore lining. However, the toroid-pore model is different from the barrel-stave one because in the toroid-pore model, the pore lining forms a mosaic with both headgroups from the peptide and lipid. The carpet theory is much simpler than the previous two theories because the peptide does not have to intercalate or align with the lipids. The continuous accumulation of the

peptides on the membrane surface would displace the lipids and finally disrupt the membrane. This mechanism can be observed in the segmentation and fragmentation of the lipid membrane by most surfactants.

Aside from the three classic models mentioned above, many experiments suggest that an external electric field can open the membrane transiently (Teixeira et al. 2012). A comprehensive practice in previous studies is to introduce DNA molecules into bacterial cells using electroporation. A minimal voltage of ~1 V is required to form pores on the cell membrane when a short pulse is applied. However, this threshold would be significantly decreased to ~0.2 V when the electric field is constant or lasting. Thus, the electroporation theory is an alternative to the stable channel/pore complex formation suggested by carpet barrel or toroid theory. Electroporation theory suggests that a transient pore is formed because of an external electric field, which is generated from peptide binding. A highly positively charged peptide binds to the outer membrane, thereby creating an electric field that points toward the inner plasma. The membrane breaks and forms a transient channel when it reaches a threshold that allows the translocation of the peptide-anchored lipid-raft into the inner lipid leaflet. The leakage of inner molecules, such as ions and proteins, occurs along with the translocation of the peptide–lipid raft. The external potential falls below the threshold again, which results in the closure of the transient channel. Slightly different from electroporation theory,

sinking-raft theory suggests that the transient pore formation was due to mass imbalance caused by peptide preferential binding by self-association or self-assembly (Teixeira et al. 2012).

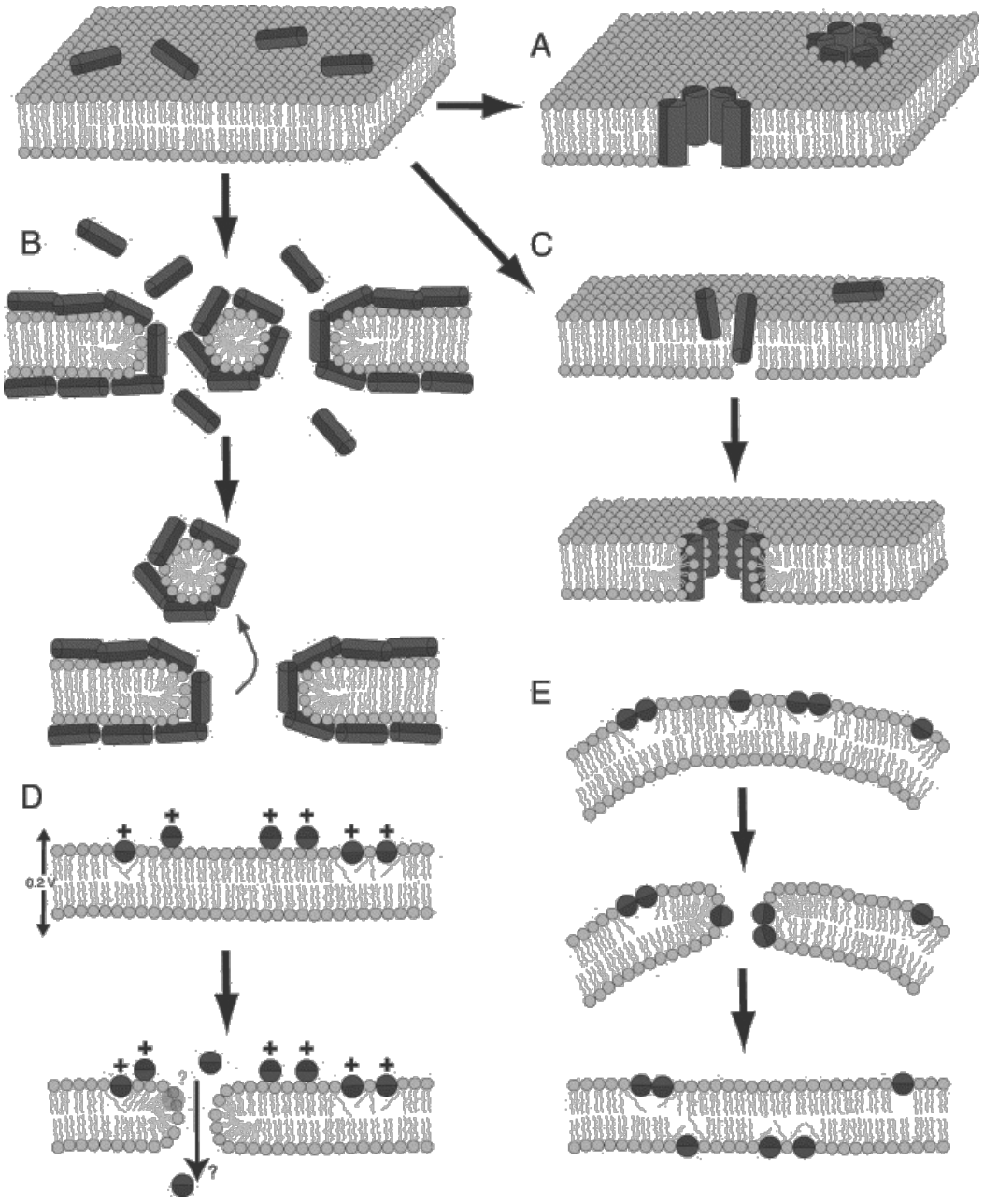

Figure 4. AMP mechanisms in the formation of transmembrane pores (Teixeira et al. 2012). A) barrel-stave model; B) carpet model; C) toroid-pore model; D) electroporation model; E) sinking-raft model.

1.6 Bacterial cell wall and membrane offer selective targeting for AMPs

All biomembranes are composed of a fluid mosaic of amphiphilic substances, such as lipids and protein. However, biomembranes significantly differ in terms of the presence of lipid species and their composition in different organisms to which AMPs exert different binding affinities. A possible source for AMP selectivity is the charge difference created by the lipid composition and architecture within the membrane (Epand et al. 2007; Nizet 2006; Spector and Yorek 1985). Biomembranes contain phosphatidylcholine (PC), phosphatidylethanolamine, and sphingomyelin, which are general zwitterionic lipids without any net charge. The incorporation of ionic lipids, including PS, PG, and cardiolipin, can create a negative charge on the membrane surface, which in turn attracts AMPs. Enriched membranes in acidic lipids are commonly found in bacteria. The proportion of PG and cardiolipin exceeds 50% of the total membrane lipids for some species, such as *Escherichia coli* (Epand et al. 2007). By contrast, ionic lipids are typically present at extremely low levels (generally less than 5%) in mammalian cells. Mammalian membranes are also structured asymmetrically with most of their acidic lipids aligned at the inner leaflet facing the cytoplasm. Thus, the charged moiety is no longer exposed to the external environment.

Outside of the plasma membrane, bacteria use a particular envelope known as a cell wall to wrap their fragile plasma membrane. Such a structure improves bacterial compatibility to environments with extreme levels of salt, pH, and organic solvent (Yeaman and Yount 2003). Based on Gram-staining method, bacteria are generally divided into two classes—the Gram-positive and -negative bacteria. Except the peptidoglycan murein which is a basic element for all bacterial cell walls, Gram-negative and -positive bacteria differ greatly from each other.

In Gram-positve bacteria, the cell wall composition is much simpler and mainly consists of multiple layers of peptidoglycan interspersed with teichoic acids. The teichoic acids run perpendicular towards the peptidoglycan sheets and are unique to Gram-positive cell walls (Figure 5A).

Different from Gram-positive bacteria, the cell wall of Gram-negative bacteria is much complicated. Outside of the peptidoglycan layer, there is an extra layer of lipid membrane termed “outer membrane” for Gram-negative bacteria. This outer membrane is linked to the inner peptidoglycan by lipoproteins and is anchored with lipopolysaccharide (LPS) at the outer leaflet (Figure 5B).

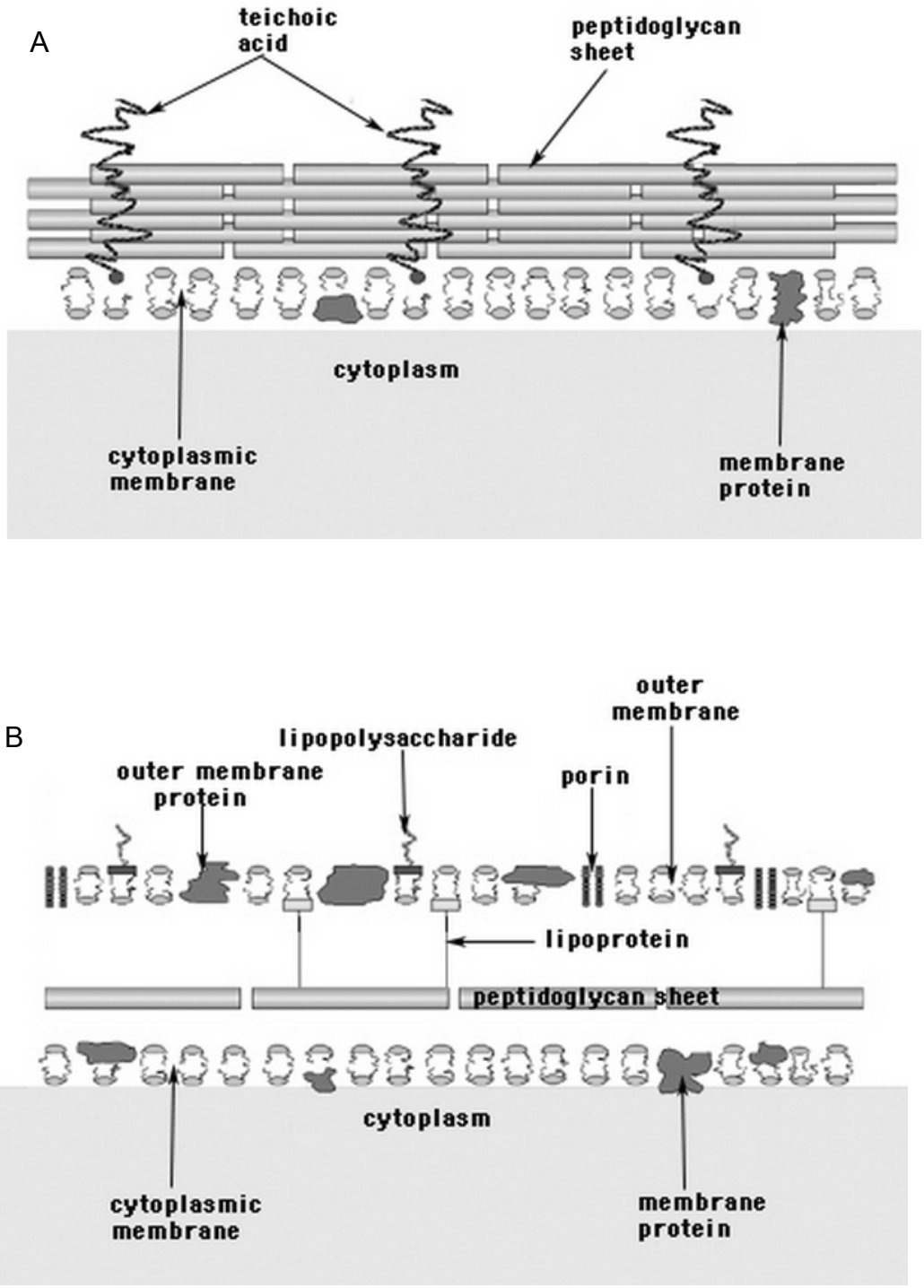

Figure 5. Structures of Gram-positive and –negative bacterial cell envelopes (mol-biol4masters.masters.grkraj.org, by Dr. Kenneth Todar**).** A) Structure of Gram-positive bacteria cell wall. The wall is relative thick and consists of multiple layers of peptidoglycan with teichoic acids running perpendicular to the peptidoglycan sheets. B) Structure of Gram-negative bacteria cell wall. The wall is relative thin and contains an extra layer of outer membrane with LPS anchored at the outer leaflet.

This unique envelope is also negatively charged either by teichoic acid or LPS for Gram-positive and Gram-negative bacteria. These components can attract highly positively charged AMPs. These AMPs aggregate on the cell surface before inserting into the membrane. Several findings suggest that LPS induces AMP targeting.

The above mentioned perspectives show that bacteria are considered electrostatically more attractive for positively charged AMPs. Besides, the thermomechanical lipid bilayer properties, which significantly affect membrane stability, are regulated by the presence or absence of lipid species and their lipid composition. The most comprehensive example is cholesterol, which comprises up to 50% of the lipids in the mammalian cell membrane, but is rarely present in bacterial membrane. The cell membrane becomes packed, but still exhibits good fluidity in the presence of cholesterol (Yeagle 1985), thereby preventing insertion or breakage.

Table 3. Representative membrane lipid composition of Gram-negative and Gram-positive bacteria, fungi and mammalian erythrocytes (Fischer 1994; Morein et al. 1996; Ratledge and Wilkinson 1988; Teixeira et al. 2012).

Lipid (%)	Microorganism						
	Escherichia coli (Gram-negative bacteria)			*Staphylococcus aureus* (Gram-positive bacteria)	*Saccharomyces cerevisiae* (Fungi)	Erythrocyte	
	OM	CM	Total lipid			Outer leaflet	Inner leaflet
Cardiolipin (CL) *a.k.a.* diphosphatidylglycerol (DPG)	6	12	3	5*		–	–
Phosphatidylglycerol (PG)	3	6	19	57		–	–
Lysylphosphatidylglycerol (LPG)	–	–	–	38		✓	✓
Phosphatidylethanolamine (PE)	90	82	74	–	**	20	40
Phosphatidylcholine (PC)	–	–	–	–	**	40	20
Sphingomyelin (SM)	–	–	–	–		40	10
Phosphatidylserine (PS)	–	–	–	–	✓	–	30
Phosphatidic acid (PA)	–	–	<1	–		–	–
Phosphatidylinositol (PI)	–	–	–	–		✓	✓
Sterol	–	–	–	–	Ergosterol	Cholesterol	

✓ Present in trace or undetermined amounts. * Lipids composition in exponential growth phase. ** Inconsistent data

1.7 Structure vs. efficacy

The disulfide bridges, generally present in the AMP sequence, are closely related to the AMP antimicrobial activities. Spatial restraint by disulfide bonds provides the prerequisite for AMPs to fold into the correct conformation (Fan et al. 2013; Jenssen et al. 2006). AMPs exert membrane activity by conformation transition.

AMPs represent a unique and diverse group of proteins with a length of 12 to 50 amino acids. These AMPs are divided into subgroups based on their residue composition and structure. AMPs contain two or more basic amino acids. Their secondary structures follow four patterns, namely, α-helix, β-sheet, loop/coil, and extended (Jenssen et al. 2006). Most AMPs dissolve in aquatic buffer with a random structure, but adopt a special 3D structure upon partitioning into biological membranes. Within this special structure, hydrophobic residues are concentrated on one side, whereas hydrophilic residues are found on the other side. This amphipathicity allows AMPs to partition into membranes.

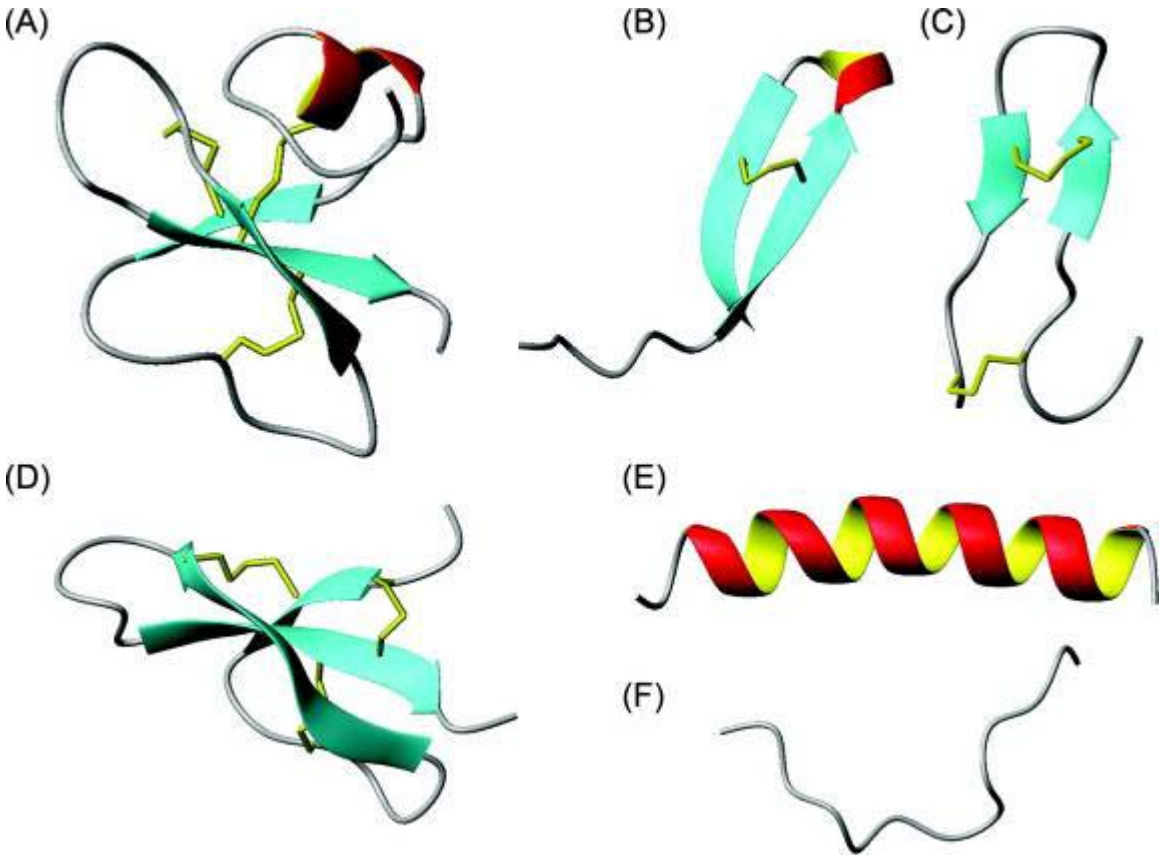

Figure 6. Structural classes of antimicrobial peptides (Jenssen et al. 2006). Examples of Different AMPs structures are given by (A) Mixed structure of human β-defensin-2 (PDB code 1FQQ) and (D) rabbit kidney defensin-1 (PDB code 1EWS); (B) looped thanatin (PDB code 8TFV); (C) β-sheeted polyphemusin (PDB code 1RKK); (E) α-helical magainin-2 (PDB code 2MAG); (F) extended indolicidin (PDB code 1G89).

1.8 Objective of this research

The antimicrobial peptide Ib-AMP4 has two disulfide bonds. Ib-AMP4 has been isolated from *Impatiens balsamina* and exhibits broad antimicrobial activity against plant pathogens. In this study, we aimed to do the following: 1) to produce recombinant Ib-AMP4 in large amounts by *Escherichia coli* expression and purification; 2) to estimate Ib-AMP4‘s potential as a clinical treatment and its combination potential with traditional antimicrobial agents; 3) to determine the target of Ib-AMP4 and the underlying mechanism for Ib-AMP4

to exert a rapid bactericidal effect; 4) to investigate the role of the cell wall and membrane during Ib-AMP4 targeting; and 5) to show the effect of cations, particularly divalent Ca^{2+}, during the antimicrobial process of Ib-AMP4.

Chapter 2. Materials and methods

2.1 Reagents and Chemicals

Restriction enzymes *Hin*dIII, *Kpn*I, ligase, and recombinant enterokinase (rEk) were purchased from New England Biolabs (Beverly, MA, USA). Tryptone and yeast extract were sourced from GE Healthcare Biosciences (Pittsburgh, USA). Ampicillin and isopropyl β-D-1-thiogalactopyranoside (IPTG) were obtained from Sigma (Sigma-Aldrich Chemie GmbH, Munich, Germany).

DOPC and DOPG from Avanti (Avanti Polar Lipids, Alabaster, Alabama) were dissolved in chloroform/methanol (9:1) at 2.5 mg/ml and used as stock solutions. Calcein, cholesterol, and BSA (lyophilized powder) were purchased from Sigma (Sigma-Aldrich, Munich, Germany). Deep rough mutant LPS (LPS Re) was extracted from *Escherichia coli* strain F515, whereas LPS Ra was purified from the bacterial rough strains of *Salmonella enterica (Galanos et al. 1969).* All chemicals and organic solvents used in this study were of analytical grade or higher.

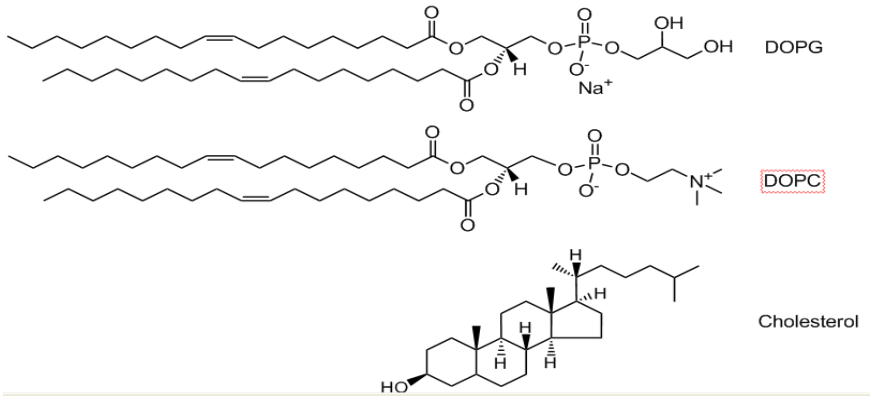

Figure 7. Structures of DOPC, DOPG and cholesterol. DOPG and DOPC share a very similar structure with only small differences existing at the headgroup, which introduced a negative charge to the DOPG. Cholesterol is a truly neutral compound.

2.2 Buffers

MilliQ water was used to prepare all aqueous solutions. The following buffers were used for Ib-AMP4 purification: lysis buffer (50 mM Tris, 200 mM NaCl, and 1 mM EDTA; pH 8.0), loading buffer (50 mM Tris and 200 mM NaCl; pH 8.0), washing buffer (50 mM Tris, 200 mM NaCl, and 5 mM imidazole; pH 8.0), and elution buffer (50 mM Tris, 200 mM NaCl, and 0.25 M imidazole; pH 8.0). Cleavage buffer (25 mM Tris, 50 mM NaCl, and 2 mM $CaCl_2$; pH 8.0) was used for rEk cleavage. The following buffers were used in the mechanism study: calcium-free buffer (10 mM HEPES, and 150 mM NaCl; pH 7.4) and calcium-loaded buffer (10 mM HEPES, 150 mM NaCl, and 50 mM $CaCl_2$; pH 7.4).

2.3 Bacteria, cells, and plasmids

Escherichia coli JM109 and BL21/DE3 were purchased from NEB (New England Biolabs, Beverly, MA, USA), and the plasmid *pET32a* bearing a lac promoter for the expression was bought from Novagen Company (Novagen, Madison, Wisconsin, USA). Adenocarcinomic human alveolar basal epithelial cell line A549 was purchased from ATCC.

The antimicrobial activity of Ib-AMP4 was evaluated by testing its MIC against 29 clinical isolates and 20 standard reference bacteria, including MRSA and ESBL-producing *E. coli*. These strains were human clinical isolates: (1) Gram-negative bacteria: *Acinetobacter calcoaceticus, Proteus vulgaris, Proteus mirabilis*, *Enterobacter cloacae, Enterobacter aerogenes*, *Escherichia coli, Serratia marcescens, Pseudomonas stutzeri, Pseudomonas aeruginosa*, *Klebsiella oxytoca*, *Klebsiella aerogenes, Citrobacter freundii*; (2) Gram-positive bacteria: *Bacillus megaterium, Bacillus subtilis, Enterococcus faecium*, *Enterococcus casseliflavus, Micrococcus luteus, Staphylococcus haemolyticus*, *Staphylococcus epidermidis*, *Staphylococcus aureus, Staphylococcus oralis, Staphylococcus saprophyticus, Streptococcus agalactiae, Streptococcus pyogenes* and *Streptococcus pneumoniae*. The clinical isolates were obtained from the Center of Medical Laboratory of Zhongda Hospital, Southeast University, China. The standard reference bacteria were purchased from ATCC.

2.4 Protein expression

2.4.1 DNA design, plasmid design

The Ib-AMP4 DNA containing an rEk cleavage site with flanking *Hin*dIII and *Kpn*I sites (ATCGGGTACC GATGACGATG ACAAACAGTG GGGTCGTCGT TGCTGCGGTT GGGGTCCGGG TCGTCGTTAT TGCCGTCGTT

GGTGCTAATA AAAGCTTATC G) was synthesised by GeneRain Company (Shanghai, China). The synthesized DNA was inserted into the plasmid *pET32a*.

2.4.2 Construction of plasmid pET32A-Trx-Ib-AMP4

Ib-AMP4 DNA and the plasmid *pET32a* were digested by *Hin*dIII and *Kpn*I separately and then ligated by DNA ligase. We followed the protocols in molecular cloning (Green and Sambrook, 3rd edition 2001) and Novagen manuals. The resulting recombinant plasmid was transferred into *Escherichia coli* JM109 for screening on plates with ampicillin. DNA was isolated from positive clones and sent for sequencing to confirm the correct sequence of the construct.

2.4.3 Preparation of Escherichia coli DH5a and BL21 competent cells and transformation

Competent cells were prepared using the classic calcium chemical method to introduce the plasmid into the *Escherichia coli* cells. This method is simple to operate, requires no special instruments, and yields good transformation efficiency. The procedure was performed as follows:

1. Frozen bacteria were activated from -80 °C by drawing the bacteria on a dish plate containing fresh solid LB medium. This set-up was incubated overnight.

2. A single colony from the LB plate was inoculated into 4 ml of fresh LB liquid medium and incubated overnight. Ampicillin was added as a negative control.

3. The overnight cell culture was inoculated into 100 ml of the fresh medium at a ratio of 1:100 and incubated for ~2 h with an OD_{600} between 0.2 and 0.3.

4. Cells were retrieved by centrifugation at 4,000 rpm and at 4 °C. Cell pellets were resuspended in 20 ml cold buffer containing 0.1 M $CaCl_2$.

5. The cells were stored in ice for 30 min.

6. The cells were retrieved by centrifugation, and the pellets were resuspended in 1 ml 0.1 M $CaCl_2$.

7. Approximately 100 µl of the cell suspension was pipetted in each micro-centrifuge tube.

8. The competent cells were ready for usage or were stored at -80 °C for one month.

The constructed plasmid was introduced into the competent cells following the standard molecular cloning manual. An aliquot of the competent cells (100 µl) was obtained from -80 °C storage and thawed on ice. After adding 0.5 µl of 200 µg/ml plasmids, the competent cells were immediately translocated into a 40 °C water bath for exactly 45 s. The cells were then maintained on ice for another 30 min and spread on a dish plate with fresh medium containing 100 µ g/ml ampicillin for screening.

2.4.4 Expression of pET32A-Trx-Ib-AMP4

Escherichia coli cells containing *pET32a-Trx-Ib-AMP4* were seeded and grown in 1 ml LB broth (10 g peptone, 5 g NaCl, and 5 g yeast extract/l LB broth) overnight. The overnight culture was trans-inoculated into flasks with 250 ml fresh LB medium with 0.01% ampicillin. Flasks were shaken at 200 rpm at 37 °C overnight. Induction with 1 mM IPTG was performed at 28 °C for 7 h.

2.5 Purification

2.5.1 Cell lysis

The cells were collected after expression induction by centrifugation at 4,000 rpm for 10 min. Cells were resuspended in a lysis buffer. The cell suspension was subjected to two cycles of thaw-freeze before ultrasonication to lyse the cells sufficiently. Ultrasonication was performed in an ice bath at 300 W for 40 min with an impulse of 5 s/5 s. The cell suspension cleared up after the cells were broken. The insoluble cellular debris was removed by centrifugation at 8,000 rpm for 25 min. The supernatant was collected for Ni-affinity chromatography.

2.5.2 Ni-Affinity chromatography

Soluble proteins were retrieved by collecting the supernatant after cell lysis, and the supernatant was applied to a nickel affinity column (Madison, Wisconsin, USA) that was pre-equilibrated with a loading buffer. Nonspecific

bound impurities were eliminated by a washing buffer. The final process involved the retrieval of the bound protein by applying an elution buffer to the column. The steps of the procedure were monitored by an ultraviolet spectrophotometer with a wavelength of 280 nm.

2.5.3 rEk cleavage

The elution from Ni-Affinity chromatography mainly contained the expressed fusion protein of Trx-Ib-AMP4, with Ib-AMP4 fused with Trx. The fusion partner of Ib-AMP4, Trx, was removed by enterokinase cleavage to obtain the pure peptide of Ib-AMP4. The elution was first dialyzed against a cleavage buffer to complete the rEk cleavage. After dialysis, the protein solution was concentrated to a concentration of 4 mg/ml by ultrafiltration (10,000 kD pore size, Millipore Corporation, Billerica, MA, USA) followed by rEk digestion. Enterokinase was added at a ratio of 5 units of rEk per 2.5 mg fusion protein. The cleavage was performed at 37 °C for 18 h. The proteins after rEk cleavage were examined by SDS–PAGE.

2.5.4 G-25 size exclusion chromatography

The proteins were filtered through a 0.5 micron membrane after rEk cleavage and subsequently applied to a G-25 molecular filter column (80 cm × 5 cm^2). Pure water was used as washing and elution buffer. The flow was maintained at a constant rate of 5 ml/min. The loading amount of digested protein was

fixed at 5 ml for each purification cycle. Fractions with OD_{280} absorption were collected and examined by SDS–PAGE, HPLC, and mass spectrometry (MALDI-MS). The fraction containing Ib-AMP4 was lyophilized and stored at -20 °C.

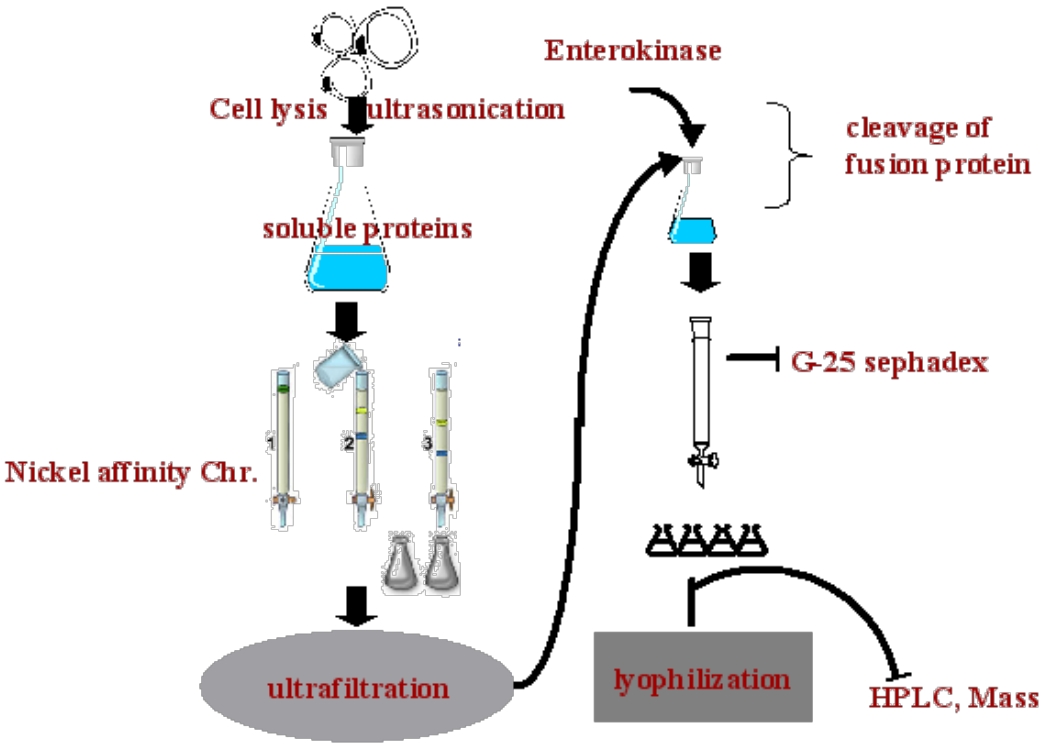

Figure 8. Scheme of Ib-AMP4 purification. The fusion protein carried 6 X His tag was mainly expressed in a soluble form. The fusion protein could be easily retrieved by nickel affinity chromatography. After rEk cleavage and G-25 sephadex chromatography, Ib-AMP4 was separated from its fusion partner of Trx.

2.6 Activity test

2.6.1 Activation and stability

The lack of post-translational modification in *Escherichia coli* cells called for an extra step to oxidize the disulfide bonds of Ib-AMP4 after purification. In order to optimize the condition for oxidation, three lyophilized samples were

processed under different temperature with or without a adding of 5 µg/ml H_2O_2. The activation of Ib-AMP4 samples was evaluated by comparing its MIC against *Staphylococcus aureus* ATCC 25923. Duplicate wells were used each time and the results were recorded after the plates were incubated at 37 °C for 24 h.

2.6.2 Minimal inhibitory concentration (MIC)

MIC tests were carried out according to the NCCLS broth microdilution method (Ferraro 2005). Briefly, bacteria were seeded in 1 ml medium and shaken overnight. A dilution was prepared with an OD600 of 0.8 from this culture, which was further diluted into a fresh medium (5 : 1000; v/v) for micro-volume plate assay on 96 well plates. The peptide was diluted across rows by two-fold serial dilutions. The results were recorded after the plates were incubated at 37 °C for 24 h. Experiments were run in duplicates and each test was repeated independently. Ampicillin and 0.001% H_2O_2 were used as positive and negative controls, respectively.

2.6.3 Time killing curve

Bactericidal kinetics were determined by counting viable bacteria after treatment with 2 X MIC of Ib-AMP4. Briefly, *Staphylococcus aureus* ATCC25923 was seeded and grown in fresh dextrose-tryptone-broth (DTB) medium overnight. The overnight culture was then transferred into fresh DTB

containing 20 μg/ml Ib-AMP4. Every 2 min after incubation 10 μl aliquots of the culture medium were diluted into 990 μl ddH_2O, and 100 μl of the dilution were immediately plated on sheep blood agar plate (37°C). The viable colonies were counted after incubation of 24 h.

2.6.4 Two-drug combination and FICI

The classic checkboard method was used in the combination tests of Ib-AMP4 with silver nitrate, thymol, oxacillin, EDTA, vancomycin, or other antimicrobial agents. A medium serial was pre-supplemented with different concentrations of an antimicrobial agent, such as EDTA or vancomycin, ranging from 0× MIC to 1× MIC to a given bacterium. The MICs of Ib-AMP4 against the corresponding bacteria were measured in the medium serials. Another method used in the combination tests was similar to the above mentioned one, except that Ib-AMP4 was pre-supplemented into the medium. Only three concentrations (i.e., 0.2x, 0.4x, and 0.6x MIC) of Ib-AMP4 were tested on corresponding bacterium via several combinations to economize on Ib-AMP4 usage .

FICI was introduced to estimate the combination effect and analyze the results of the two-drug combination. FICI is a summary of each individual's contribution to the combination and could be expressed as follows (Elion et al. 1954; Hall et al. 1983):

$$FICI = \frac{\text{MIC of substance A in combination}}{\text{MIC of substance A alone}} + \frac{\text{MIC of substance B in combination}}{\text{MIC of substance B alone}}$$

Based on FICI, the combination was subjected to three patterns: i) antagonistic effect with FIC > 2.0; ii) additive effect with 0.5 < FIC < 2.0; and iii) synergistic FIC < 0.5.

2.6.5 Cytotoxicity in cancer cells

A suspension of A549 cells (~10,000 cells/ml) was prepared in fresh DMEM medium containing 10% bovine serum then 100 µl were added to each well of a 96-well plate. The plate was incubated at 37 °C plus 5% CO_2 until the cell density reached about 30% of each well, then 100 µl fresh media containing serial dilutions of Ib-AMP4 ranging from 400 to 25 µg/ml were added. Afterwards, the plate was incubated for another 24 h before carrying out the MTT assay as described before (Plumb 2004). Three duplicates were analyzed and the test was repeated for three times.

2.6.6 Heamolysis activity

The haemolysis assay was carried out as previously described (Shimojo and Iwaoka 2000). Briefly, a volume of 1 ml heparinised sheep blood was washed 6 times with 8 X volume of saline; then the blood cells were retrieved and resuspended in 4 ml saline for use. The haemolysis assay was carried out in a 96-well plate loaded with 100 µl blood cell suspension per well. Afterwards, 100 µl Ib-AMP4 (400 µg/ml) were then added to the first well and diluted

twofold across rows. The plate was then incubated at 37 °C for 45 min followed by centrifugation. A volume of 50 µl supernatant was taken from each well and measured photometrically at 540 nm to reveal haemoglobin that had been released from erythrocytes. Haemolysis caused by 0.5 mg/ml SDS and 0.9% saline was defined as 100% and 0% activity, respectively. Three duplicates were analyzed and the test was repeated for three times.

2.6.7 Surfactant activity

Surfactant activity of Ib-AMP4 was evaluated by measuring the surface tension of pure water in the presence of different concentrations of Ib-AMP4 ranging from 5 µg/ml to 1 mg/ml. This measurement was carried out with a Langmuir film balance (Kibron, Helsinki, Finland).

2.7 Study of model of action with membrane models

2.7.1 Liposome/vesicle preparation

Calcein-encapsulated small unilammellar liposomes were prepared by the extrusion method (Balhara et al. 2013). A lipid film was dried from a chloroform/methanol solution under a stream of nitrogen followed by 3 h of vacuum drying. The dry film was subsequently rehydrated with 80 mM calcein in HEPES buffer (pH 7.4) containing 10 mM HEPES and 150 mM NaCl followed by extrusion for 21 times through a polycarbonate membrane of 200 nm pore size. The yielded homogenous liposomes were collected and

passed through a PD-10 column (GE Healthcare, Freiburg, Germany) to remove the free calcein. The elution fractions from chromatography were prepared for the calcein leakage assay.

Calcein-free unilammellar DOPC liposomes were prepared using the above mentioned method, but were rehydrated with a HEPES buffer without calcein. LPS-Re vesicles were prepared by sonicating 1 mg/ml LPS in HEPES buffer for 60 min. The vesicle size was checked by DLS.

Four different types of liposomes were prepared to estimate the effect of DOPG and cholesterol during membrane disruption. Their molar composition were as follows: DOPC (100%) as control; DOPC/cholesterol (7:3) to mimic blood cells; DOPC/DOPG (85:15) to mimic *Staphylococcus aureus*; and DOPC/DOPG (40:60) to mimic *E. coli.*

2.7.2 Liposome leakage assay

Liposomal leakage caused by Ib-AMP4 was studied by monitoring the release of calcein loaded

liposomes (Balhara et al. 2013). Calcein was self-quenched at a high concentration inside the liposome, but showed an increase in fluorescence intensity after being released from the liposome when the membrane bilayer became leaky.

Black plate (Ibidi GmbH, Martinsried, Germany) was incubated overnight before usage with HEPES buffer containing 5% BSA to block the unspecific

binding sites. A concentration serial of Ib-AMP4 in the HEPES buffer was initially prepared in wells by diluting twice and mixing with 50 µl liposome solution. After mixing, the plate was immediately analyzed using a fluorescence reader (Tecan, Mainz, Germany) with exiting and emission wavelengths of 295 and 325 nm, respectively. The fluorescence intensity was recorded over time.

2.7.3 Giant unilamellar vesicle (GUV) preparation

The GUV was prepared by electroformation with indium thin oxide (ITO) coated slides as reported previously (Bi et al. 2013; Herold et al. 2012). The ITO slides were cleaned by sonication in ethanol, isopropanol, and deionized water thrice, followed by annealing for activation. Annealing was performed by placing the slides in a heating chamber of 150 ℃ for 20 min and then cooling down to room temperature (RT) (Morales-Penningston et al. 2010). The slides were always placed with their ITO-coated sides exposed to the air to avoid contamination.

The lipid thin layer was coated onto one slide by the flat-coating method (Bi et al. 2013; Estes and Mayer 2005). Approximately 300 µl of 2.5 mg/ml DOPC in chloroform was dropped onto a slide surface. A needle was used to carefully spread the solution back and forth. Before the lipid dried, the slide was placed in the center of a horizontal centrifuge and centrifuged at 1,000 rpm for 10 min to homogenize the film. The slides were placed in a vacuum for another 2 h.

After the solvent evaporated completely, two slides were assembled in an electroformation chamber with their ITO coated sides facing each other. The chamber was then filled with 300 mM sucrose. A sinusoidal AC electric field of 10 Hz and 1.5 V was applied for 3 h to form GUVs.

2.7.4 Time elapse photography

GUV liposome solution (30 µl) mixed with 120 µl glucose (300 mM) was injected into the sample slide chamber (Ibidi GmbH, Martinsried, Germany). The mixture was incubated for 10 min to allow the precipitation of the GUVs. Ib-AMP4 (400 µg/ml) at 50 µl was gently injected from the right side. The diffusion of peptide started from the right side. A dynamic gradient of the peptide concentration was introduced onto the GUV sample. The dynamic change in GUVs was monitored under a microscope (Keyence, Mannheim, Germany) equipped with a 10x ocular and a 40x objective.

2.7.5 Surface pressure and potential of the monolayer

2.7.5.1 LPS-Re isotherm and peptide injection

A monolayer was obtained by gently spreading LPS onto the aqueous surface with a Hamilton syringe followed by incubation for 20 min to allow evaporation of organic solvents.

Surface tension-molecular area (π-A) and surface potential-molecular area (P-A) isotherms were recorded with a Langmuir film balance (Kibron, Helsinki,

Finland). The stock solution of LPS-Re (2 mg/ml in CHCl3/CH3OH (9/1 in v/v)) was spread onto the subphase. After the complete evaporation of the solvent (20 min), the film was compressed at a constant speed of 4.5 Å²/chain/min. Two types of buffer subphases (pH 7.4) were used to study the effect of Ca^{2+} ions, as follows: (i) a "Ca^{2+}-free" buffer containing 5 mM HEPES and 100 mM NaCl and (ii) a "calcium-loaded" buffer containing 50 mM $CaCl_2$.

The target molecular area was set to ~140 Å², corresponding to a surface pressure of ~17 or ~25 mN/m for calcium-free or calcium-loaded subphases, respectively, to compare the interaction between the peptide and LPS molecules at the same molecular area. When the target molecular area was reached, the monolayer was allowed to equilibrate for 20 min before peptide injection. The final concentration of the injected peptide was 2 μM.

2.7.5.2 Lipid isotherm

Compression (π-A) isotherms for lipids at 20 ± 1 °C on calcium-free and/or calcium-loaded buffers were conducted with a KSV NIMA Langmuir system (Biolin Scientific, Stockholm, Sweden) equipped with two Delrin barriers, a Teflon trough with a surface area of 86 cm^2, and a Wilhelmy paper sensor. The procedure was nearly the same as that for the LPS isotherm with minor modifications. The amount of lipid was adjusted to achieve an initial surface pressure below 1 mN/m. π-A isotherms were obtained by compressing the monolayer with two movable barriers at a constant rate of 5 mm/min.

2.7.6 Quartz Crystal Microbalance with Dissipation (QCM-D) for LPS and DOPC

Experiments using the quartz crystal microbalance with dissipation monitoring were performed at 25 ℃ using a QCM-D E4 system (Q-sense, Gothenburg, Sweden). The oscillation frequency shift (Δf) and the simultaneous energy dissipation change (ΔD) of the quartz crystal were recorded simultaneously. Changes in resonance frequency reflected the bound mass deposited on the surface of the quartz sensor, whereas changes in energy dissipation provided information on the roughness property of the adsorbed material (Dixon 2008).

An Au-coated crystal was purchased from Q-Sense (Gothenburg, Sweden). The quartz was first cleaned with a mixture of H_2O/NH_3 (25%)/H_2O_2 (30%) in a 5/1/1 ratio at 70 ℃ for 10 min; subsequently, the quartz was rinsed with MilliQ water and dried under a stream of nitrogen (Makky et al. 2010). The quartz was assembled into the quartz chamber and initially equilibrated with a loading buffer for 20 min, followed by DOPC liposome injection. After the completion of DOPC liposome adsorption, the quartz was then rinsed and loaded with the Ib-AMP4 peptide solution.

The procedure for the LPS-Re vesicle was almost the same, but was completed before LPS-Re adsorption. The quartz was first coated with octadecanethiol before the LPS-Re adsorption to provide a hydrophobic environment in which the LPS-Re would anchor.

2.7.7 Dynamic light scattering (DLS)

The radius of the prepared liposome was measured by DLS with a Zetasizer Nano-S (Malvern Instruments, Ltd., Worcestershire, UK). A homogenous DOPC liposome with diameter of ~200 nm was prepared as described and diluted 200 times in HEPES buffer with a final lipid concentration of ~26 μM. An Ib-AMP4 peptide concentration serial was prepared in HEPES buffer and mixed with an equal volume of liposome. For each measurement, the cuvette was equilibrated for 5 min at 20 ℃. The final result was recorded as an average of three measurements. All measurements were performed with a constant lipid concentration of ~13 μM in the presence of different concentrations of Ib-AMP4 peptide ranging from 2 μM to 30 μM.

2.7.8 Circular dichroism (CD) spectra

CD spectra were measured with a J-715 spectrometer (Jasco Corporation, Essex, UK) using a 0.1 cm path length quartz cuvette at 20 °C from 190 nm to 250 nm. All spectra were corrected by subtraction of the buffer spectra. The Ib-AMP4 concentration was fixed at 100 μM and supplemented with different amounts of liposome to obtain peptide/lipid ratios (P/L). The secondary structure was estimated with software provided by the manufacturer (Balhara et al. 2013).

2.7.9 Transmission electron microscope (TEM)

The cell sample was prepared as reported previously (Wu et al. 2010). Log-phase ATCC 25922 *Escherichia coli* cells were collected by centrifugation and resuspended in MilliQ water containing 500 μg/ml Ib-AMP4. The cells were incubated for 20 min and retrieved by centrifugation at 4,000 g for 5 min. The cell pellet was collected and then processed by prefixation with 2.5% glutaraldehyde in a 0.2 M phosphate buffer (pH 7.3), postfixation in 0.5% osmium tetroxide in a Millonigs constant-osmolarity phosphate buffer (pH 7.4), and dehydration in graded ethanol solutions. The dehydrated cell pellet was embedded in medium Taab Resin and polymerized for 24 h at 60 ℃. Slices (50 nm) were prepared and stained with aqueous uranyl acetate and lead citrate. Stained slices were examined using JEM-1010 TEM (JEOL, Tokyo, Japan).

2.8 Statistics

All experiments were repeated at least three times. Similar results were obtained. The MIC values were expressed as concentration range. The other values were analyzed by Excel and SigmaPlot software and expressed as the mean value from independent repeats.

Chapter 3. Expression and purification of Ib-AMP4 in *Escherichia coli*[*]

3.1 Abstract

AMPs represent a novel class of powerful natural antimicrobial agents. Ib-AMP4, which has two disulfide bonds, has been isolated from *I. balsamina*. Ib-AMP4 exhibits broad antimicrobial activity against plant pathogens. A large amount of Ib-AMP4 was required to study its potential as a clinical treatment. We presented the successful expression and purification of recombinant Ib-AMP4 from *E. coli*. An *E. coli*-specific gene for Ib-AMP4 was designed manually and inserted into a vector of pET32a for expression in *Escherichia coli* cells. After induction with 1 mM IPTG, a soluble fusion protein was expressed successfully. The Ib-AMP4 peptide was finally obtained with a purity of over 90% after nickel affinity chromatography, ultra filtration, enterokinase cleavage, and Sephadex size exclusion chromatography. Given the lack of posttranslational modification, the obtained peptide was activated by 5 μg/ml H_2O_2 to form two disulfide bridges.

[*] This chapter has been published as: "Fan, X., Schafer, H., Reichling, J., Wink, M., Bactericidal properties of the antimicrobial peptide Ib-AMP4 from *Impatiens balsamina* produced as a recombinant fusion-protein in Escherichia coli, Biotechnol J, 8 (2013) 1213-1220."

3.2 Introduction

AMPs can potentially be used to solve the drug resistance dilemma that has plagued global health in the last decade. AMP research has focused mainly on animal peptides rather than plant peptides because the latter have complex structures with multiple disulfide bonds. AMPs occur naturally in biological organisms, but at limited concentrations. AMPs have to be prepared in large amounts for use in laboratory research. To date, the most convenient and economic way of preparing AMPs is to express AMPs in prokaryotic cells. Given its well-characterized features, low cost, rapid replication, and simple manipulation, *Escherichia coli* has become the most popular organism for the prokaryotic expression of heterologous proteins (Samuelson 2010), even if some remaining issues, such as the post-transcriptional modification and disulfide bond formation, exist.

Escherichia coli can express proteins encoded by a transformed plasmid, and such capability offers many choices for different purposes. The target protein can be expressed by different strategies, such as single or fusion expression and cytoplasm expression or secretion expression coupled with different purification strategies downstream. Given that AMPs are bactericidal, their production in recombinant bacteria is far from trivial. Inclusion body expression has been reported in several cases. Another strategy involves the production of inactive fusion proteins, which has been successfully applied to *Escherichia*

coli to obtain various peptides, from large antibody proteins of over 30,000 kD to triple peptides comprising three amino acids. This approach can also be adopted for the production of AMPs (Katoh et al. 2010; Li et al. 2012; Wu et al. 2010).

Ib-AMP4 with 20 amino acids was firstly extracted from the seeds of *Impatiens balsamina* (Balsaminaceae) together with three other analogues (Tailor et al. 1997). In Ib-AMP4 (QWGRR**CC**GWGPGRRY**C**RRW**C**) the two intramolecular disulfide bonds are conserved. However, according to a later report, this is no prerequisite for its antimicrobial activity (Thevissen et al. 2005) though the conformation of short peptides restrained by disulfide bonds could modulate their stability in liquid media (Haag et al. 2012; Morehead et al. 1984; van Kraaij et al. 2000). Ib-AMP4 can be chemically synthesized, but we have chosen biotechnological production as an alternative. If this AMP should be used in clinical studies we would need large amounts of the peptides. In this case the biotechnological production would be cheaper than chemical synthesis.

We reported the successful production of Ib-AMP4 as a fusion protein in *Escherichia coli* and the Ib-AMP4's cleavage from the fusion protein, purification, and activation.

3.3 Results

3.3.1 Construction of plasmid pET32A-Trx-Ib-AMP4

The constructed plasmid is shown in Figure 9. The Ib-AMP4 gene was fused with a Trx gene to inhibit the antimicrobial activity of Ib-AMP4 during its expression. Thus, Ib-AMP4 was expressed as a fusion protein with its N-terminal coupled with the C-terminal of Trx. Between them was an rEk cleavage site, which allows the tidy excision of Ib-AMP4 from its fusion partner. The 6x His-tag between Ib-AMP4 and Trx was used as a purification tag.

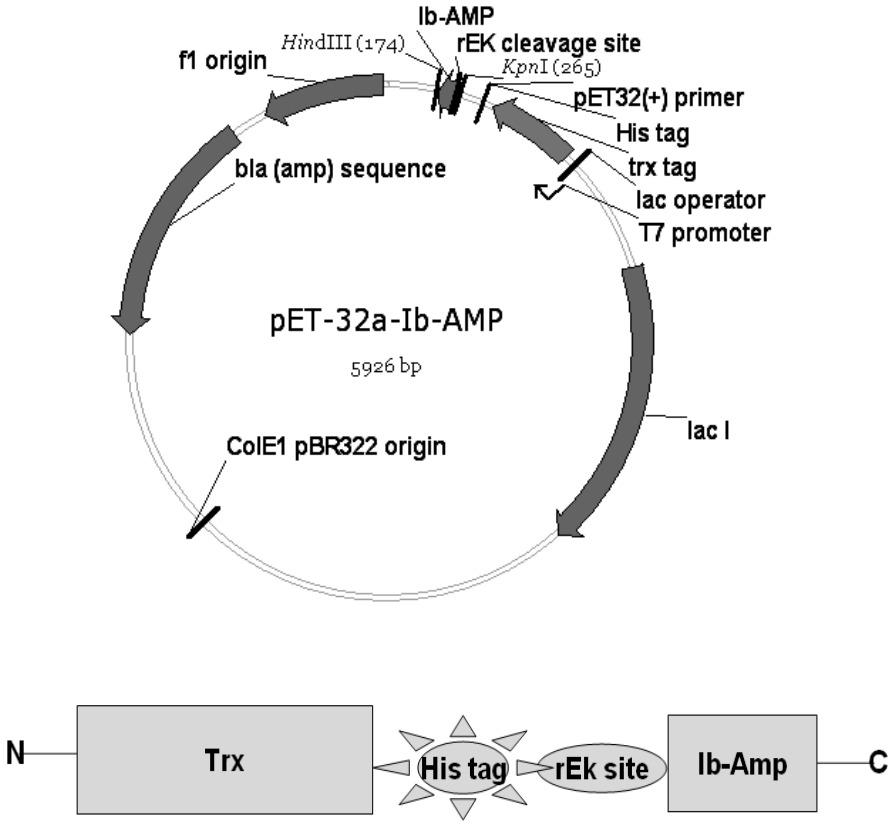

Figure 9. Design of the expression vector pET32a-Trx-Ib-AMP4. A) The DNA of Ib-AMP4 was inserted into vector pET32a between Hind III and Kpn I restriction sites. Vector pET32a possessed a T7 promoter which could be activated by lactose or IPTG. This vector also encoded a lactamase which rendered ampicillin resistance to the transformed bacteria as a screening marker. After expression, B) The peptide Ib-AMP4 was fused at

the C-terminal of a thioredoxin and between there were a 6X His tag and a rEk cleavage site, designed for the purification of Ib-AMP4.

3.3.2 Fusion expression and purification

The constructed plasmid *pET32A-Trx-Ib-AMP4* was transformed into an *Escherichia coli* BL21 strain for expression. The fusion protein was expressed within the cytoplasm mainly in a soluble form after IPTG induction and accounted for approximately 20% of the total protein in *Escherichia coli* cells, as shown by the SDS–PAGE results (Figure 10, lane 3). The fusion protein yield was approximately 50 mg/l culture. Most of the impurities were removed during affinity chromatography. The fusion protein carrying a His-tag with a purity of more than 80% was easily retrieved by nickel affinity chromatography (Figure 10, lane 6).

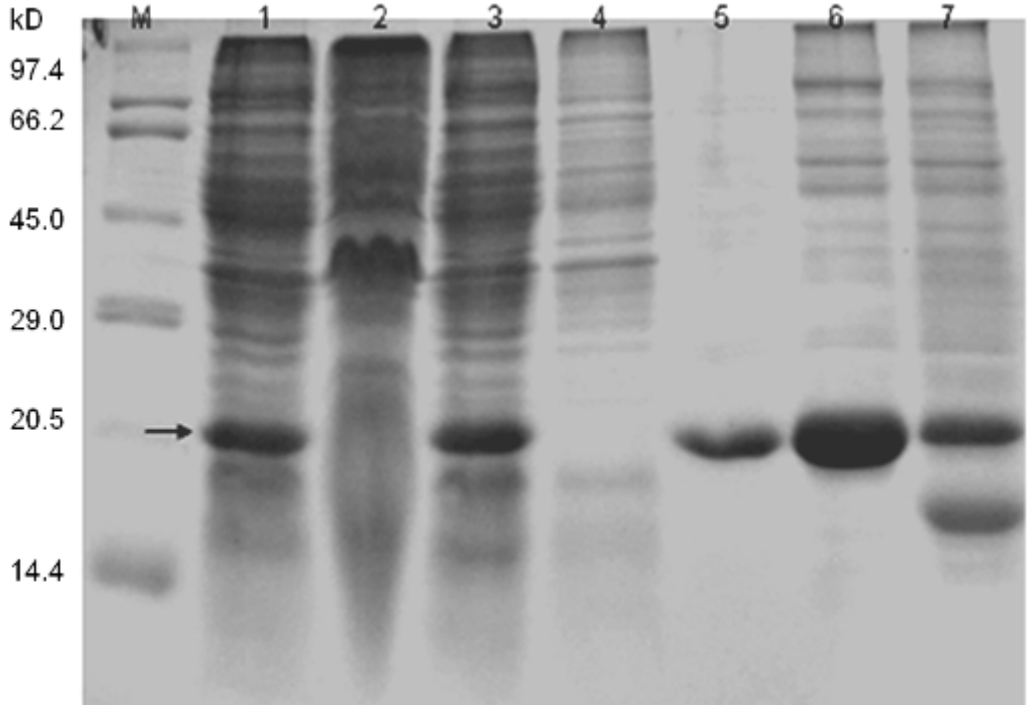

Figure 10. Expression and purification of Ib-AMP4. Lane M: size marker; lane 1: total protein after cell lysis; lane 2: insoluble protein after lysis; lane 3: soluble protein after lysis;

lane 4: impurity washed out from the nickel affinity column; lane 5: fusion protein retrieved by nickel affinity chromatography; lane 6: protein after ultrafiltration; lane 7: protein after rEk cleavage. The arrow points at the fusion protein.

3.3.3 rEK cleavage and Ib-AMP4 isolation

The elution from affinity chromatography was applied to the dialysis against the rEK cleavage buffer to adjust the pH and ion concentration. The protein solution was used for ultrafiltration (10 kD) (Figure 10, lane 6) after dialysis to concentrate the protein sample to 4 mg/ml. We removed an impurity (lower than 10 kD molecular weight, which would interfere with the subsequent step of Ib-AMP4 isolation. The fusion protein was cleaved into two fragments of 20 kD and 2.5 kD after the rEk cleavage (Figure 10, lane 7). Ib-AMP4 was isolated by applying the cleavage sample to Sephadex G25 to remove the fusion partner. A purity of higher than 90% for the peptide fraction was eventually reached (Figure 11A), and the final yield was approximately 8 mg Ib-AMP4 /l medium. Ib-AMP4 with an ultra purity of higher than 95% was obtained by using an extra purification step by HPLC. The MALDI-MS revealed the presence of a molecular ion of m/z 2542, which was consistent with the Ib-AMP4 theoretical mass (Figure 11B).

A

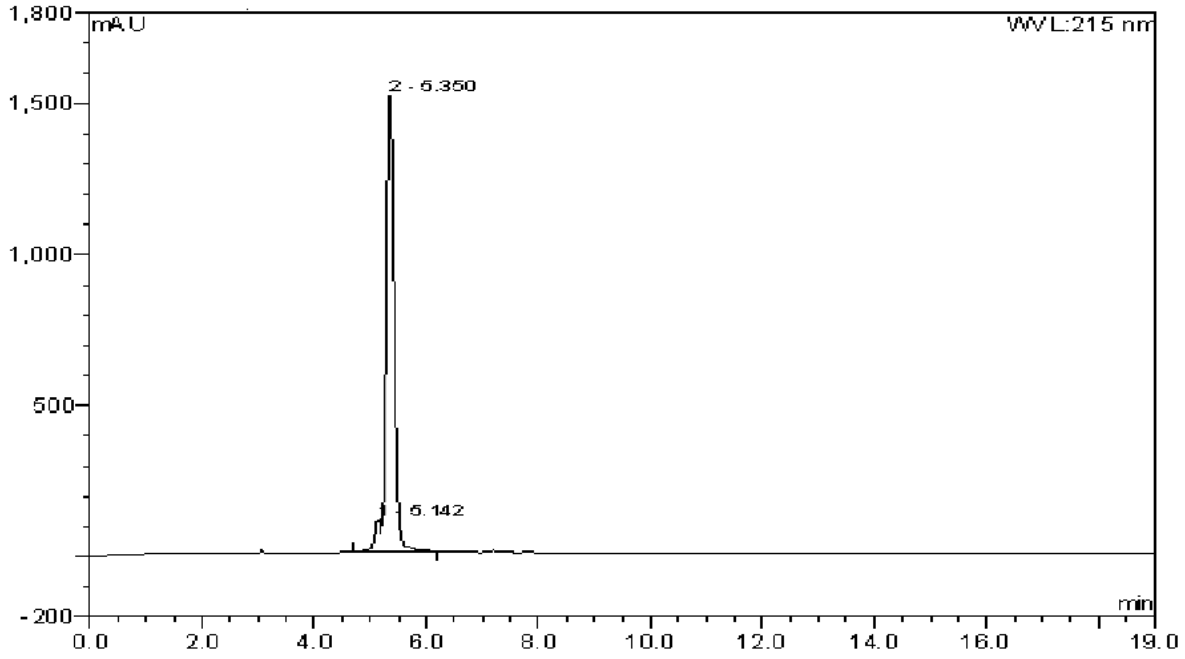
mAU
WVL:215 nm
2 - 5.350
5.142
min
1,800
1,500
1,000
500
-200
0.0
2.0
4.0
6.0
8.0
10.0
12.0
14.0
16.0
19.0

B

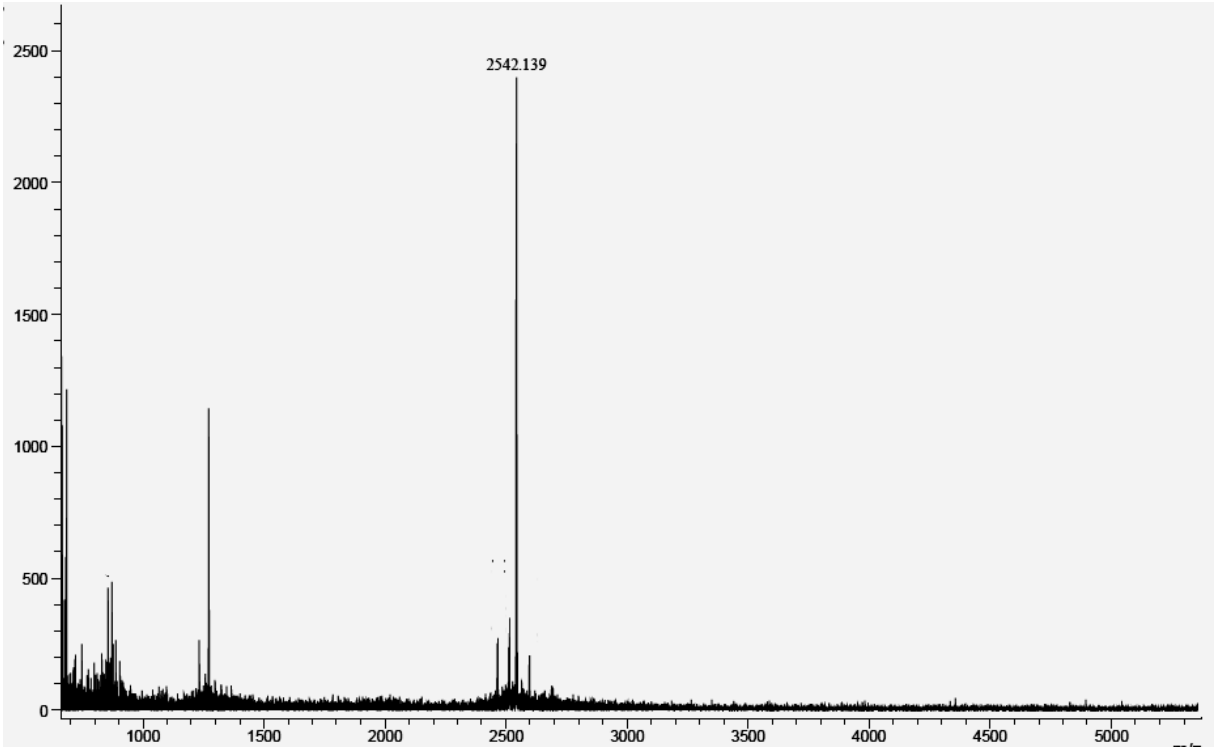
2542.139
2500
2000
1500
1000
500
0
1000
1500
2000
2500
3000
3500
4000
4500
5000

C

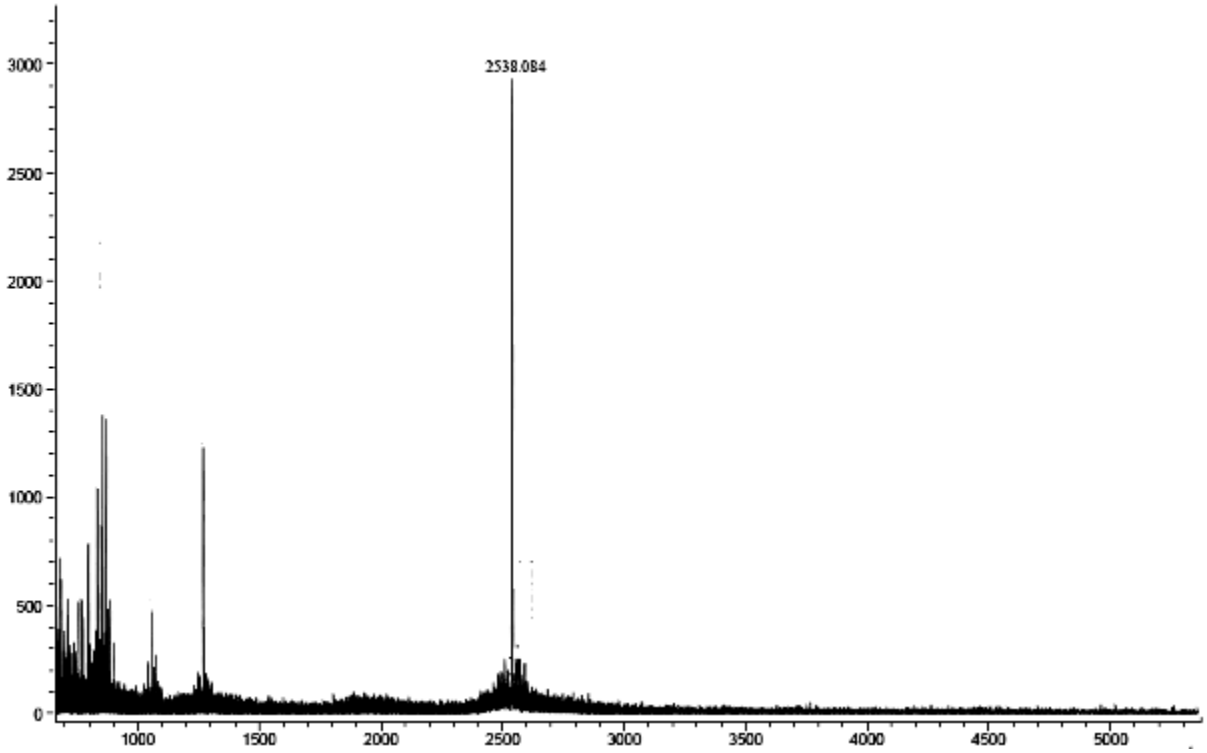

Figure 11. Spectral analysis of Ib-AMP4. A) Purity analysis by HPLC of Ib-AMP4 after Sephadex G-25 filtration; B) Mass spectrum of the purified Ib-AMP4; C) Mass spectrum of Ib-AMP4 after activation.

3.3.4 Activation and stability

Activation of the Ib-AMP4 can be shown by its improved MIC against *Staphylococcus aureus*, the smaller the MIC, the better the activation. As shown in Figure 12A, the peptide was hardly active before activation with a MIC of about 200 µg/ml, whereas samples stored at 4 °C were relatively stable and their activity was persistent until day 20, storage at 37 °C led to a loss of activity after 8 d. In addition, Ib-AMP4 also showed a good thermal stability (Figure 12B).

The disulfide bond failed to form within *Escherichia coli* cells because of the lack of posttranslational modification. Thus, an extra step of activation for Ib-AMP4 was required to form two disulfide bridges. The two disulfide bridges were formed by either self-oxidization by oxygen or by adding H_2O_2 at 5 μg/ml to the Ib-AMP4 solution. The result shows that self oxidization occurred slowly for several days and required a suitable temperature, such as RT. RT was not beneficial to the stability of Ib-AMP4. H_2O_2 application and significantly decreased the activation time to less than 24 h. Ib-AMP4 was adjusted to 400 μg/ml for activation to avoid a disulfide mismatch. A weight loss of 4 Da occurred after activation by 5 μg/ml H_2O_2, as determined by MS (Figure 12C). This change in M^+ indicated the formation of two intramolecular disulfide bonds.

A

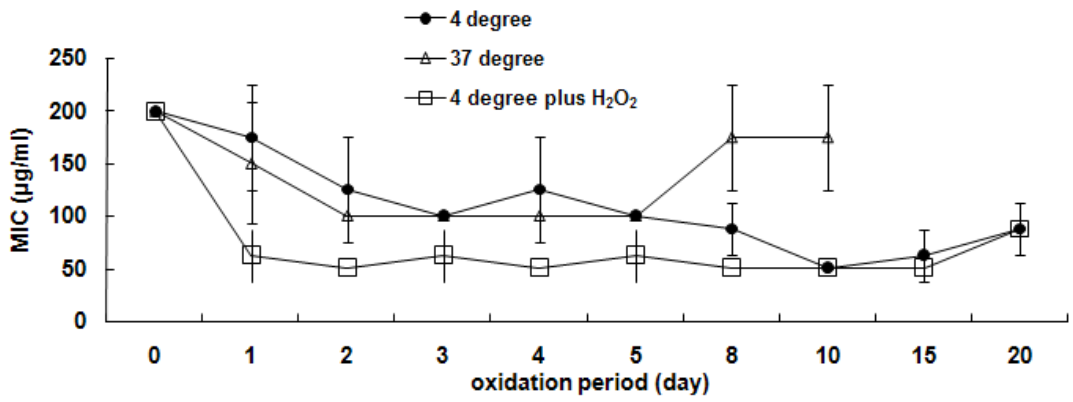

B

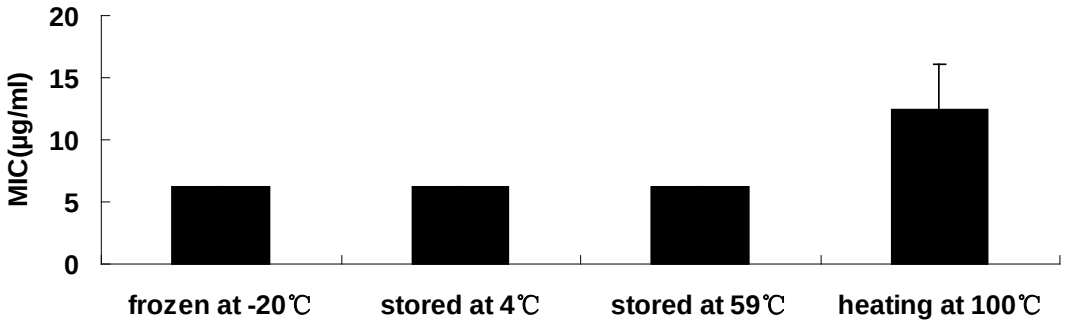

Figure 12. Activation and stability of Ib-AMP4. A) Activation of Ib-AMP4 and its bactericidal effect. Three lyophilized samples were dissolved in ddH_2O to a final concentration of 400 μg/ml, but were processed differently to optimize the condition for oxidation: Experiment 1: plus 5 μg/ml H_2O_2 and 4 °C; Experiment 2: without H_2O_2 at 37 °C; Experiment 3: without H_2O_2 at 4 °C. MIC values of three Ib-AMP4 preparations were determined against *Staphylococcus aureus* ATCC 25923. B) Thermal stability of Ib-AMP4. The active Ib-AMP4 samples were pretreated at different temperature and then tested their antimicrobial activity against *B. megaterium*. Antimicrobial activity of Ib-AMP4 was stable after several cycles of thawing-frozen or heat at 59 degree for 1 h, but 100 degree water bath reduced the antimicrobial efficiency.

3.4 Discussion

The expression of antimicrobial peptides remains an issue. Their production in plant seems very limited because of the poor expression, but they also could not be easily expressed in microorganism since they are antimicrobial agents. To solve this problem, fusion strategy was commonly adopted for expression of exogenous proteins in microorganisms including *Escherichia coli* and yeast (Katoh et al. 2010; Wu et al. 2010), but it always left extra amino acids in short peptides after protease cleavage. There were also some other papers

introduced the application of intein for expression of peptides without usage of protease. However, the cleavage was unpredictable and of poor yield (Diao et al. 2007; Hong et al. 2010). In this report, a pET32 plasmid expressing a fusion partner of thioredoxin was chosen to express a fusion protein, i.e. Ib-AMP4 with TRX, and an enterokinase cleavage domain was inserted directly before the target peptide. This construct allowed the controlled and sufficient cleavage of Ib-AMP4 from its fusion partner thioredoxin without leaving any extra amino acid.

As the figure of expression showed, there is only one band of fusion protein after purification which indicates almost no degradation happened. Instability of the recombinant protein might be expected, although BL21 is apparently deficient in the Ion and ompT proteases and many proteins produced in this strain are quite stable. The fusion chaperons function not only as an expression helper but also help the stability. The thioredexin partner from pET32 plamid is a homologous protein of *Escherichia coli* and confers resistance of the recombinant to inner protease degradation in *Escherichia coli* cells.

The results suggested that the soluble expression of the exogenous proteins should be performed under low temperature (Kiefhaber et al. 1991; Schein 1989; Xu et al. 2005). Referring to the previous researches, the temperature seemed to be the most important parameter influencing the soluble expression.

Under different temperatures, the heterogenetic protein could be expressed as different conformations, and it has been reported that growth at 37 °C causes some proteins to accumulate as inclusion bodies, while incubation at 28 °C leads to soluble, active protein . It is possible that the temperature could influence the activity of the protein synthases which decide the synthesis rate, and, moreover, the synthases with low activity under low temperature allow enough time for protein to refold into a correct conformation (Kiefhaber et al. 1991; Xu et al. 2005).

The purification steps appeared simple and efficient. The fusion protein easily achieved more than 80% purity after nickel affinity chromatography. Only three further steps were needed to obtain a purity of more than 90% for Ib-AMP4. We used ultrafiltration after nickel affinity chromatography because the elution solution consisted of several bands. This procedure was critical in removing protein fragments with an MW below 10,000 kD. The activity of Ib-AMP4 was firstly very low. We assumed that the weak activity was related to the failure to form disulfide bonds (Patel et al. 1998). Hence, Ib-AMP4 could be successfully activated by H_2O_2 after purification. Mass spectral analysis confirmed the activation by H_2O_2 and the formation of two disulfide bonds.

H_2O_2 is bactericidal and could thus interfere with the antimicrobial test. To exclude its effect, H_2O_2 was used at a maximum of 5 μg/ml for oxidation because all tested bacteria were unaffected by this concentration. Moreover,

most of the tested MICs of Ib-AMP4 were between 4 and 32 µg/ml. It means that the peptide preparation containing 5 µg/ml H_2O_2 has to be diluted for more than 10 times and the effect of H_2O_2 would become negligible.

In conclusion, Ib-AMP4 was successfully expressed in *Escherichia coli* cells as a fusion protein, and a simple approach to activate the peptide after enzymatic cleavage and purification could be established. This method might be useful for other AMPs with multiple disulfide bridges.

Chapter 4. Ib-AMP4 could selectively target bacteria but is sensitive to cations†

4.1 Abstract

As important constituents of the innate immune system, AMPs are active against infectious microorganisms, such as bacteria, and can distinguish host cells from invading pathogens. To evaluate the potential of Ib-AMP4 as a clinical medicine, its antimicrobial activity was studied. Ib-AMP4 was applied alone and in combination with current antimicrobial agents to human pathogens, including MDR strains. Ib-AMP4 cytotoxicity and hemolysis activity were investigated. The inhibitory effect of cations on the Ib-AMP4 antimicrobial activity was also explored.

Antimicrobial assays showed that most of the tested MICs were within the range of 2 mM to 20 mM, and Ib-AMP4's antimicrobial activity was independent of resistance to current antibiotics. Ib-AMP4 can efficiently target both susceptible and resistant bacteria, including MRSA and ESBL-producing *E. coli*. Given the unique antimicrobial mechanism of AMPs, the combination of Ib-AMP4 and other antimicrobial agents is a promising solution to the drug resistance problem. A genuine synergistic effect was achieved when Ib-AMP4

† This chapter has been published as: "Fan, X., Reichling, J., Wink, M., Antibacterial activity of the recombinant antimicrobial peptide Ib-AMP4 from *Impatiens balsamina* and its synergy with other antimicrobial agents against drug resistant bacteria, Pharmazie, 68 (2013) 628-630."

was used in combination with the plant monoterpene thymol or kanamycin against drug-resistant *Klebsiella pneumoniae* (KPC) ATCC700603, or with the antibiotics vancomycin or oxacillin against *Enterococcus faecalis* (VRE) ATCC51299.

Time kill experiments showed that Ib-AMP4 showed bactericidal activity within 10 min after application. Hemolysis and cytotoxicity assays indicated the selectivity of Ib-AMP4 toward the bacteria, which is an important prerequisite for clinical applications. However, Ib-AMP4 efficiency was generally inhibited by cations, especially divalent cations.

Recombinant Ib-AMP4 is an interesting and powerful AMP with bactericidal properties against Gram-positive and Gram-negative bacteria, including MDR pathogens. Ib-AMP4 is an interesting candidate for clinical studies involving patients with septicemia or for coating clinical devices, such as catheters.

4.2 Introduction

Until modern times most human deaths were caused by microbial infections. The discovery of antibiotics, beginning with that of penicillin in 1928, has revolutionized medicine, but many pathogens have since become resistant to antibiotics due to drug abuse and improper drug usage. 25,000 people in the European Union are presently dying each year from being seriously infected by resistant bacteria pathogens, mostly acquired in health-care settings (Carlet et al. 2012; Spellberg et al. 2004). Techniques of drug development today are much more powerful than in earlier decades, but most antimicrobial candidates being developed are variations on previous antibiotics or similar to them so they are likely to provoke new resistance, since similar targets are involved (Carlet et al. 2012; Spellberg et al. 2004). Drug R&D has plummeted, due to a shortage of research investment and innovation, while resistance to drugs keeps on developing faster and faster, threatening to lead us back into the pre-antibiotic era, when a mere scratch could be fatal (Carlet et al. 2012; Spellberg et al. 2004). The discovery of antibiotic with novel antimicrobial mechanism really becomes a matter of emergency.

Antimicrobial peptides (AMPs), produced by fungi, plants and animals, have received a lot of attention in having the potential to contribute solving the drug resistance problem. Unlike traditional antibiotics, AMPs seem to function like surfactants due to their amphiphilic character (Nan et al. 2011) but can

selectively target bacterial membranes and make them leaky (Li et al. 2012; Shenkarev et al. 2011; Tang and Hong 2009). AMPs can intercalate biomembranes and can disrupt them as a consequence, whereas traditional antibiotics target mainly bacterial metabolism or cell walls. This difference ensures a low cross-resistance (Reddy et al. 2009) and a good potential for synergy between AMPs and classical antibiotics (Aleinein et al. 2014; Nguyen et al. 2011).

The targeting of biomembranes by AMPs is thought to be achieved in three steps. At first, the peptides are electrostatically attracted by the negatively charged compounds from both the cell wall and cell membrane, i.e. LPS, PS and PG, which concentrate them on the bacterial surface (Lee et al. 2011; Nan et al. 2011). Next, the peptides approach the membrane and, due to their amphiphilic character, insert themselves into the lipid bilayers. Finally, leak channels are formed in bacterial membranes, which may disable cellular respiration and allows essential metabolites to leak out of the cells (Nguyen et al. 2011). Why some peptides selectively target Gram positive or Gram negative bacteria is still uncertain (Rahnamaeian 2011).

4.3 Results

4.3.1 Antimicrobial assay using susceptible strains

All susceptible species were obtained from ATCC. These bacteria are commonly referred to as standard bacteria because they have not developed any resistance to current antibiotics.

The results show that Ib-AMP4 is a broad-spectrum antimicrobial agent. It exhibits broad activity against both Gram-positive and Gram-negative bacteria (Table 4) with MICs between 1 and 20 μg/ml in sensitive bacteria. Some bacteria, such as *E. faecalis, Streptococcus agalactiae, S. oralis, S. epidermidis, K. oxytoca*, and *Pseudomonas aeruginosa*, showed low sensitivity (i.e., MIC values between 40 and 160 μg/ml). These differences may be due to cell wall and biomembrane composition (de la Fuente-Nunez et al. 2012).

Table 4. MICs for recombinant Ib-AMP4 against Gram-positive and Gram-negative bacteria.

Bacterial Species	ATCC No.	MIC (μg/ml)
Gram positive bacteria		
Bacillus megaterium	14581	0.63~1.25
Bacillus subtilis	6051	1.25~2.5
Micrococcus luteus	7468	2.5~5
Streptococcus agalactiae	27956	80~160
Enterococcus faecalis	29212	20~40
Staphylococcus oralis	35037	40~80
Staphylococcus epidermidis	14990	40~80
Staphylococcus aureus	29213	5~10
	25923	5~10
Staphyloccus saprophyticus	15305	1.25~2.5
Streptococcus pneumoniae	49619	10~20
Streptococcus pyogenes	12344	5~10
Enterococcus casseliflavus	700327	2.5~5
Enterococcus faecalis	51299	40~80
Gram negative bacteria		
Klebsiella oxytoca	700324	20~40
Klebsiella pneumoniae	700603	60~120
Escherichia coli	25922	5~10
	35150	4~8
Pseudomonas aeruginosa	27853	80~160

4.3.2 Antimicrobial assay over clinical isolates

Most of these clinical isolates were drug resistant, but no clear differences were observed between susceptible and resistant strains from the same species. The results of antimicrobial assays are summarized in Table 5.

Ib-AMP4 exhibited a broad activity spectrum over both Gram-positive and Gram-negative bacteria. Some bacteria, such as *E. faecium*, *E. cloacae*, *E. aerogenes*, *E. coli, S. haemolyticus*, and *Staphylococcus aureus*, were susceptible to Ib-AMP4 with MICs between 2 and 16 μg/ml. The other bacteria were less susceptible and showed susceptibility only with MICs between 32 and 128 μg/ml. *Acinetobacter calcoaceticus, P. aeruginosa*, and *Citrobacter freundii* were resistant to Ib-AMP4.

Table 5. Survey of Ib-AMP4 antibacterial activity (MIC values).

Bacteria	No.*	MIC (μg/ml)
Gram-negative bacteria		
Acinetobacter calcoaceticus	CI 110125202*	>128
Proteus vulgaris	CI 110125206	32~64
Proteus mirabilis	CI 110224201	32~64
	CI 110315208	64~128
Enterobacter cloacae	CI 110212223	4~8
	CI 100930201	4~8
Enterobacter aerogenes	CI 110307204	2~4
Serratia marcescens	CI 110126205	8~16
	CI 110127207	8~16
Pseudomonas stutzeri	CI 110207202	64~128
Pseudomonas aeruginosa	CI 110303204	>128
Klebsiella oxytoca	CI 110314209	32~64
Klebsiella aerogenes	CI 110307204	16~32
Citrobacter freundii	CI 110208201	>128
Escherichia coli	ATCC 25922	4~8
	CI 110316207**	4~8
	CI 110215211**	4~8
	CI 110215212**	4~8
Gram-positive bacteria		
Enterococcus faecium	CI 110125213	2~4

	CI 110201208	4~8
	CI 110211212	2~4
Streptococcus pneumoniae	CI 11021131	16~32
Staphylococcus haemolyticus	CI110127208	8~16
Staphylococcus epidermidis	CI 110126211	16~32
Staphylococcus aureus	ATCC 29213	4~8
	CI 110126209***	4~8
	CI 110126210***	4~8
	CI 110302214***	8~16

* CI clinical isolates; ATCC American type culture collection; ** ESBL-producing *Escherichia coli* was resistant to ampicillin, cefazolin, ceftazidime, cefepime, gentamicin, and cotrimoxazole; *** MRSA was resistant to penicillin, oxacillin, and cefotetan.

4.3.3 Ib-AMP4 combined with antimicrobial agents

The combination test indicated a slight additive effect between Ib-AMP4 and the antimicrobial agents (Table 6,7). Ib-AMP4 application reduced the use of these antimicrobial agents, and notable synergistic effects were achieved for Ib-AMP4 combined with oxacillin against MRSA and for Ib-AMP4 combined with vancomycin against VRE.

Table 6. Combination of Ib-AMP4 with other antimicrobial agents by the checkerboard method.

K. pneumoniae			*S. aureus*			*E. faecalis*		
Combination*	MIC (μg/ml)[1]	FIC[2]	Combination*	MIC (μg/ml)[1]	FIC[2]	Combination*	MIC (μg/ml)[1]	FIC[2]
$AgNO_3$ (8.75)			$AgNO_3$ (8.0)			$AgNO_3$ (45)		
1.75 μg/ml + P	106.67	1.09	2 μg/ml + P	11.85	0.72	9 μg/ml + P	71.11	1.06
2.63 μg/ml + P	71.11	0.89	3 μg/ml + P	7.9	0.69	18 μg/ml + P	71.11	1.22
3.5 μg/ml + P	47.41	0.79	4 μg/ml + P	7.9	0.82	27 μg/ml + P	4.16	0.55
4.38 μg/ml + P	31.6	0.76	5 μg/ml + P	7.9	0.94	36 μg/ml + P	1.23	0.68
Thymol (750)			Thymol (250)			Thymol (625)		
187.5 μg/ml + P	31.6	0.51	25 μg/ml + P	25	1.1	62.5 μg/ml + P	47.41	0.69
281.25 μg/ml + P	14.05	*0.49*	50 μg/ml + P	20	1	187.5 μg/ml + P	31.6	0.7
375μg/ml + P	14.05	0.62	125 μg/ml + P	8.446	0.84	250 μg/ml + P	14.05	0.58
468.75 μg/ml + P	9.36	0.7	150 μg/ml + P	6.33	0.85	312.5 μg/ml + P	6.24	0.58
EDTA (745)			EDTA (60)			Vancomycin (7.5)		
93.11 μg/ml + P	47.41	0.52	7.45 μg/ml + P	25	1.13	0.75 μg/ml + P	80	1.1
186.22 μg/ml + P	47.41	0.65	14.9 μg/ml + P	25	1.25	1.5 μg/ml + P	47.41	0.79
279.33 μg/ml + P	47.41	0.77	22.35 μg/ml + P	25	1.38	2.25 μg/ml + P	14.05	*0.48*
372.44 μg/ml + P	31.6	0.76	52.14 μg/ml + P	7.9	1.19	3 μg/ml + P	9.36	0.52
Vancomycin (120)			Oxicillin (50)			Oxicillin (32)	32	
12 μg/ml + P	120	1.1	5 μg/ml + P	11.25	0.55	3.2 μg/ml + P	44.8	0.66
24 μg/ml + P	120	1.2	10 μg/ml + P	8.44	0.54	6.4 μg/ml + P	25.6	0.52
36 μg/ml + P	120	1.3	15 μg/ml + P	6.33	0.55	9.6 μg/ml + P	19.2	0.54
48 μg/ml + P	120	1.4	20 μg/ml + P	4.75	0.59	12.8 μg/ml + P	2.4	*0.43*

* Checkerboard method was used for the combination test. Different combinations were obtained by testing the MICs of Ib-AMP4 in media with serial constant concentrations of indicated agents ranging from 0.1x MIC to 1x MIC. Values in brackets represent the MICs of indicated agents against respective bacteria. P represents the Ib-AMP4 peptide.

1 The values are the detected MICs of Ib-AMP4 in indicated combinations

2 FIC=FICA + FICB (FICA=MIC (A in combination with B)/MIC (A alone); FICB=MIC (B in combination with A)/MIC (B alone)). FIC >2.0 indicate antagonistic effects, 0.5<FIC< 2.0 indicate additive effects, and FIC<0.5 indicate synergistic effects (shown in Italic).

Table 7. Ib-AMP4 recovered the susceptibility of MDR strains to antimicrobial agents.

K. pneumoniae			*S. aureus*			*E. faecalis*		
Combination*	MIC (μg/ml)[1]	FIC[2]	Combination*	MIC (μg/ml)[1]	FIC[2]	Combination*	MIC (μg/ml)[1]	FIC[2]
Sanguinarine (46.875)			Sanguinarine (91.465)			Sanguinarine (7.812)		
0.2X Ib-AMP4	46.875	1.200	0.2X Ib-AMP4	1.099	0.950	0.2X	5.859	0.950
0.4X Ib-AMP4	35.156	1.150	0.4X Ib-AMP4	1.099	1.150	0.4X	3.296	0.822
0.6X Ib-AMP4	10.417	0.822	0.6X Ib-AMP4	0.824	1.163	0.6X	1.854	0.837
Quonolone (264)			Quonolone (16)			Quonolone (132)		
0.2X Ib-AMP4	264	1.200	0.2X Ib-AMP4	16	1.200	0.2X	74	0.763
0.4X Ib-AMP4	198	1.150	0.4X Ib-AMP4	12	1.150	0.4X	42	0.716
0.6X Ib-AMP4	148	1.163	0.6X Ib-AMP4	12	1.350	0.6X	10	0.675
Kanamycin			Kanamycin (4)			Kanamycin (750)		
0.2X Ib-AMP4	8	*0.378*	0.2X Ib-AMP4	4	1.200	0.2X	750	1.200
0.4X Ib-AMP4	5	*0.500*	0.4X Ib-AMP4	4	1.400	0.4X	422	0.963
0.6X Ib-AMP4	3	0.656	0.6X Ib-AMP4	3	1.350	0.6X	178	0.837
Berberine (250)			Berberine (16)			Berberine ()(250)		
0.2X Ib-AMP4	250	1.200	0.2X Ib-AMP4	16	1.200	0.2X	250	1.200
0.4X Ib-AMP4	250	1.400	0.4X Ib-AMP4	16	1.400	0.4X	250	1.400
0.6X Ib-AMP4	125	1.100	0.6X Ib-AMP4	4	0.850	0.6X	125	1.100

* 0.2X, 0.4X, 0.6X Ib-AMP4 indicate 0.2X, 0.4X or 0.6X MIC of Ib-AMP4 to respective bacterium was used in the combination. The MIC values were the tested MIC of indicated compounds in combination with Ib-AMP4.

1 The values are the detected MICs of indicated agents combined with a given concentration of Ib-AMP4

2 FIC=FICA + FICB (FICA=MIC (A in combination with B)/MIC (A alone); FICB=MIC (B in combination with A)/MIC (B alone)). FIC >2.0 indicate antagonistic effects, 0.5<FIC< 2.0 indicate additive effects, and FIC<0.5 indicate synergistic effects (shown in Italic).

4.3.4 Time-killing effect of Ib-AMP4

The bactericidal results revealed that 99% of *Staphylococcus aureus* cells were killed within 10 min after treatment with 20 μg/ml Ib-AMP4 (Figure 13). Compared with traditional antibiotics, Ib-AMP4 failed to kill bacterial cells by interfering with metabolism. Compared with vancomycin, Ib-AMP4 ruptured

the lipid membrane and caused an acute bactericidal effect, which prevented cells from developing resistance over time.

A

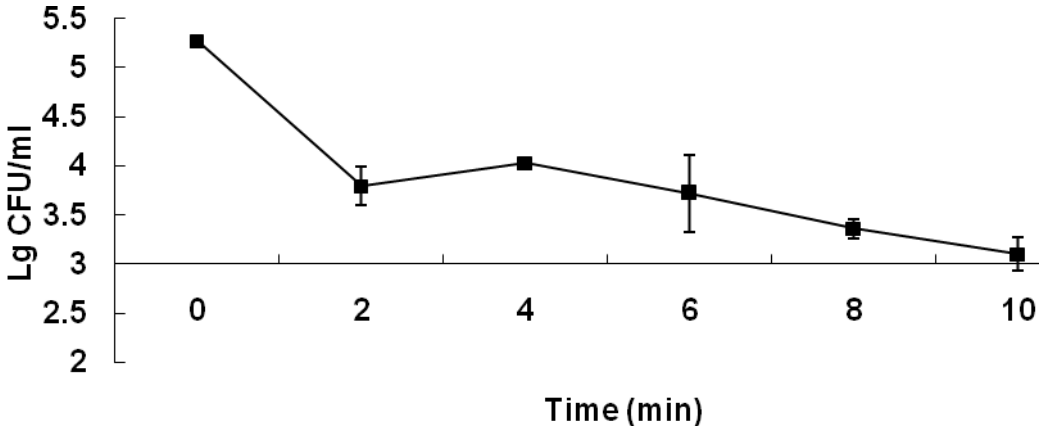

B

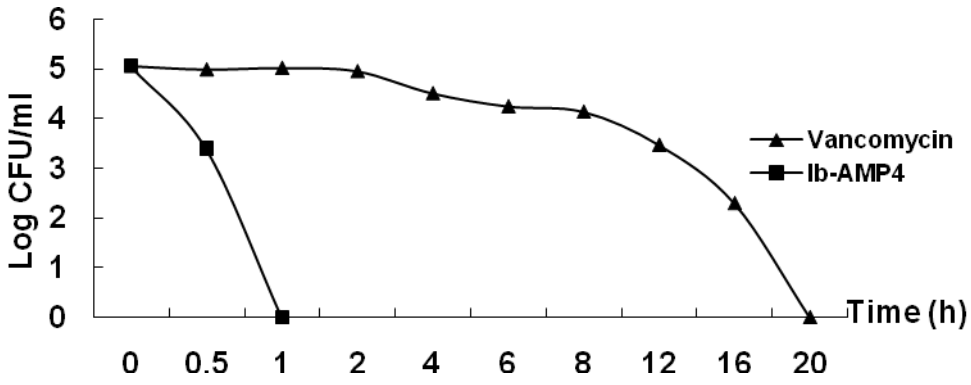

Figure 13. Rapid bactericidal effect of Ib-AMP4. A) Time killing curve of Ib-AMP4 against *Staphylococcus aureus* ATCC29213. Error bars indicate SD values. B) Comparison of bactericidal effects between Ib-AMP4 and vancomycin. Compared with Ib-AMP4, vancomycin targeted the cell wall, which caused a much slower bactericidal effect and allowed bacterial cells to develop resistance by metabolic alteration.

4.3.5 Anticancer effect and hemolysis activity

A potential membrane-disrupting effect of Ib-AMP4 on sheep erythrocytes and A459 cancer cells was investigated. H_2O_2 was introduced during the activation step. Thus, the maximal concentration of Ib-AMP4 applied to cancer cells was 200 mg/ml or lower. The antimicrobial assay results show that the MICs for most of these test bacteria were below 100 mg/ml. These concentrations used on cancer cells provided a good reference for the acute cytotoxicity of Ib-AMP4 in vivo.

The Ib-AMP4 cytotoxicity was limited. The peptide neither caused hemolysis nor inhibited cell proliferation (<2%) at concentrations lower than 100 μg/ml. Ib-AMP4 at 200 μg/ml caused 15% hemolysis of red blood cells and 8% inhibition of cell proliferation.

4.3.6 Cations affect AMPs

The cation effect on Ib-AMP4 antimicrobial activity was measured by supplementing the medium with extra monovalent cations (i.e., sodium or potassium) or divalent cations (i.e., calcium or magnesium). The MICs of Ib-AMP4 against *B. megaterium* in MH medium supplemented with different concentrations of salt were tested. The MIC of Ib-AMP4 against *B. megaterium* was 6.5 μg/ml in salt-free medium. Both monovalent and divalent cations prohibited Ib-AMP4 antimicrobial activity, but divalent cations were more effective than monovalent cations. The MIC obtained by adding 25 mM

calcium/magnesium was double that obtained by adding 400 mM sodium/potassium.

To understand the universal effect of cations on antimicrobial activity of Ib-AMP4, we also tested the MICs of Ib-AMP4 against 17 bacterial species in medium supplemented with 25 mM $CaCl_2$. Ib-AMP4 activity was inhibited by $CaCl_2$ in all tested species. The MICs increased to at least twice as high as those from the $CaCl_2$-free medium. The MIC increased by more than 10 times for some species, such as *E. coli*.

Table 8. MICs for recombinant Ib-AMP4 against gram positive and gram negative bacteria

Bacteria Species	ATCC No.	MIC	
		Calcium-free medium	Calcium-loaded medium
Gram-positive bacteria			
Bacillus megaterium	14581	1.25	10
Bacillus subtilis	6051	2.5	10
Micrococcus luteus	7468	5	20
Streptococcus agalactiae	27956	160	160
Enterococcus faecalis	29212	40	80
Staphylococcus oralis	35037	80	>200
Staphylococcus epidermidis	14990	80	>160
Staphylococcus aureus	29213	10	50
	25923	10	40
Streptococcus pneumoniae	49619	20	40
Streptococcus pyogenes	12344	10	40

Enterococcus casseliflavus	700327	5	20
Gram-negative bacteria			
Klebsiella oxytoca	700324	40	>160
Klebsiella pneumoniae	700603	120	160
Escherichia coli	25922	10	160
	35150	8	160)
Pseudomonas aeruginosa	27853	160	>160

A

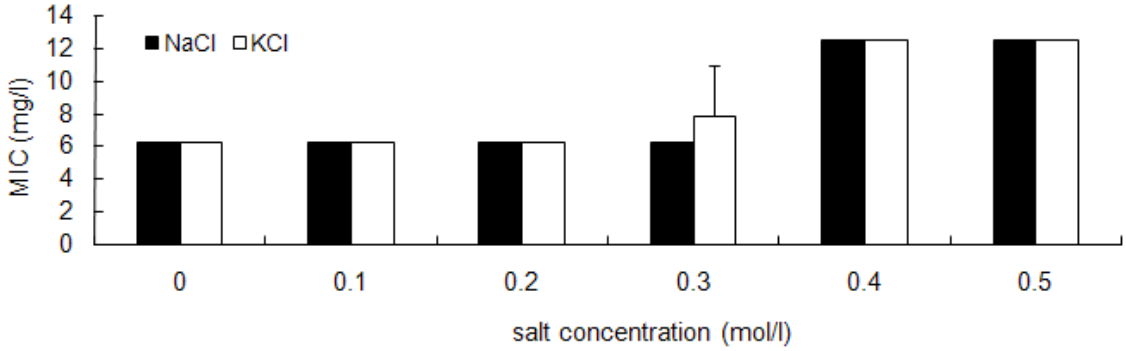

B

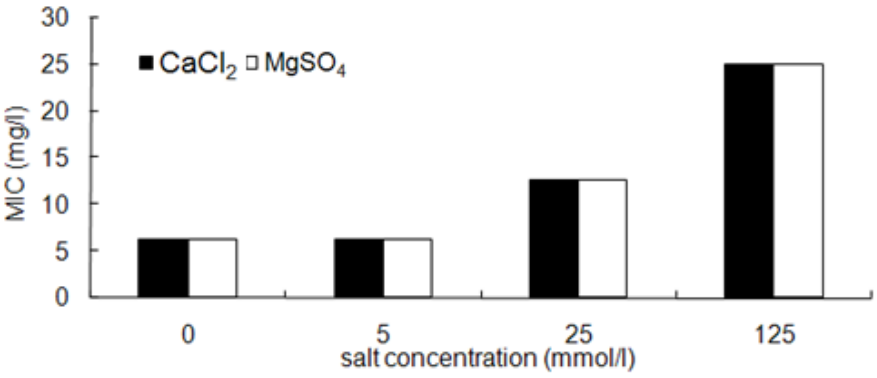

Figure 14. Cations affecting Ib-AMP4 antimicrobial activity. A) Inhibitory effect of monovalent sodium and potassium. B) Inhibitory effect of divalent calcium and magnesium.

4.4 Discussion

Ib-AMP4 was discovered as a highly effective agent against Gram positive bacteria but with much lower potential against Gram negative species such as *Escherichia coli* (Tailor et al. 1997). This result differs from our findings, as in our experiments Ib-AMP4 affected both gram-positive and gram-negative bacteria (Table 6,7). Although we tried the same medium and the same bacteria we could not confirm the original results [15].

AMPs sufficiently target either Gram-positive or Gram-negative bacteria in most cases (Hammami et al. 2009). Ib-AMP4 was effective against both Gram-positive and Gram-negative bacteria. At the moment, MRSA and ESBL-producing *Escherichia coli* are the two most widely prevalent drug resistant species in clinical settings (Table 1). Ib-AMP4 showed a promising effect on these two species. Similar MIC values were observed between drug resistant and susceptible strains, thereby indicating that Ib-AMP4 antibacterial activity was independent of the resistance of the species to other drugs. The Ib-AMP4 showed a mode of action that was different from that of traditional antibiotics, which showed no effect on drug-resistant pathogens. AMPs target and destroy the cell membrane. However, human cells also have membranes. Thus, many compounds that target cell membranes are not sufficiently selective for use in a clinical setting. Compared with eukaryotic cells, bacteria have more acidic phospholipids in their outer membranes and lack cholesterol.

Positively charged AMPs are prone to interacting with negatively charged substances and are selective toward bacteria (Epand and Epand 2011). Furthermore, the respiratory chain in bacteria is located in the plasma membrane, which has to be intact for the organism's function; AMPs that induce leakiness in cell membranes are ideal antibiotics because they disturb cellular respiration (Haddock and Jones 1977).

We tested the potential synergy of Ib-AMP4 combinations with established antimicrobial agents to further understand Ib-AMP4's antimicrobial potential. Silver has been used as an antibacterial agent for centuries before the discovery of the first modern antibiotics, such as penicillin. Silver could kill bacteria either indirectly by producing highly reactive oxygen species or directly by inactivating proteins (Davies and Etris 1997). Plant monoterpene thymol is another compound with a long history; thymol usage dates back to ancient Egypt when this compound was used to preserve mummies. Thymol interacts with bacterial membranes. Being a phenolic compound, thymol dissociates into a phenolate ion under physiological conditions; thus, thymol can interact with proteins (Rosenkranz and Wink 2008; Trombetta et al. 2005). Sanguinarine and berberine are quaternary ammonium salts isolated from plants and used as traditional medicines against infections. Membrane ion channels are predicted as their potential targets. EDTA causes instability in the cell membrane by chelating divalent cations. EDTA has already been used

with traditional antibiotics to overcome drug resistance (Aoki et al. 2010; Berges et al. 2007; Martin-Visscher et al. 2011; Raad et al. 2007). Vancomycin and oxacillin are cell wall inhibitors that block the crosslinking of the peptidoglycan net. Quinolone exerts antibacterial activity by preventing bacterial DNA from unwinding and duplicating. Kanamycin inhibits bacterial infection by interrupting bacterial protein translation. A promising combination of Ib-AMP4 with these antimicrobial agents is expected because their modes of action are different.

Some reports showed that AMPs could neutralize endotoxins such as LPS. Such findings are important as regards the outbreak of EHEC in Germany in 2011, which illustrated the fatal role of endotoxins produced by pathogens sensitive to antibiotics (Li et al. 2004). AMPs may be usefully applied under such conditions. If applied against acute septicemia antibiotics have the drawback of being slow to kill pathogens, letting them produce more life-threatening endo- and exotoxins (Mikkelsen and Gaieski 2011; Souza and Yuen 2012). In view of the rapid bactericidal activity and endotoxin binding ability of AMPs, AMP treatment could stop the production of endo- and exotoxins and neutralize them. Studies with animals suffering from septicemia are now needed, to find out whether or not Ib-AMP4 also works *in vivo*. If it does, it may be used in humans. Another application could be to coat medical devices such as catheter left in the human body for extended periods of time.

Such medical devices sometimes become infected and cause severe bacterial infections in patients. Furthermore, research is needed for adequate formulations which allow a stable and safe application.

Ions are physically essential for all living organisms and are involved in many vital cellular events, such as enzymatic catalysis and maintenance of transmembrane potential. Unlike mammalian cells where calcium is used to maintain the transmembrane potential, bacterial cells require a sufficient supply of cations, especially Ca^{2+} and Mg^{2+} for growth and metabolism. In the presence of a chelator for divalent cations, a bacterium would lose the original shape of its outer membrane. Mammalian cells use cations to regulate transmembrane channels for transport. Similarly, calcium can help in the construction of bacterial outer membrane, thereby affecting the permeability at the outer membrane and cell wall.

Ib-AMP4 was successfully purified from *Escherichia coli* cells. This peptide showed promising antimicrobial activity. Ib-AMP4 was sensitive to cations, but Ib-AMP4 killed most of the clinical isolates with MICs between 2 and 32 μg/ml. The peptide showed neither hemolysis nor cytotoxicity within this MIC range, which is the condition required for the clinical application of Ib-AMP4. Combined with traditional antimicrobial agents, Ib-AMP4 recovered the susceptibility of drug-resistant strains. Ib-AMP4's promising antimicrobial

effects, particularly on MRSA and ESBL-producing *E. coli*, indicated the significant potential of using Ib-AMP4 to solve drug resistance problems.

Chapter 5. Interaction between Ib-AMP4 with LPS and calcium effects

5.1 Abstract

Negatively charged LPS is an important component of the cell wall of Gram-negative bacteria and is closely related to AMP targeting. LPS can easily be purified and is an important model for studying the roles of cell walls and cell membranes in AMP targeting. Interaction between Ib-AMP4 with LPS and the Ca^{2+} effect were elucidated by monolayer experiments and QCM-D. Ib-AMP4 can intercalate into LPS-Re, and Ca^{2+} can potentially modulate such intercalation. LPS absorbed calcium ions at the headgroups and aligned into an orderly and compact matrix in the presence Ca^{2+}. Calcium ions were used by the cell wall to electrically repel Ib-AMP4 and thus to reduce the cell wall's permeability to Ib-AMP4.

5.2 Introduction

The initial interaction between AMPs and their target microbes occurs through electrostatic attraction. The AMP charge is highly associated with antimicrobial activity (Bessalle et al. 1992; Lee et al. 2013; Matsuzaki et al. 1997; Sato and Feix 2006; Yeaman and Yount 2003). AMPs from different species are also conserved by a highly positive charge (Gueguen et al. 2006; Seshadri Sundararajan et al. 2012; Wang et al. 2009).

The bacterial cell wall is located beyond the plasma membrane and protects bacterial cells as a first line of defense. All substances that enter or approach the bacterial cell membrane have to pass through the cell wall. Unlike the membrane channel that is only open for selected substances, the cell wall does not show any selectivity, but is related to drug resistance. A predicted mechanism underlying this phenomenon is that the bacterial cell's drug resistance can be promoted by modulating the cell wall's permeability.

In Gram-positve bacteria, the cell wall consists of multiple layers of peptidoglycan interspersed with teichoic acids which are unique to Gram-positive cell walls. Different from Gram-positive bacteria, the cell wall of Gram-negative bacteria is much complicated. Beyond the peptidoglycan layer, there is an extra layer of lipid membrane termed outer membrane for Gram-negative bacteria. This outer membrane is linked to the inner

peptidoglycan by lipoprotein and is anchored with lipopolysaccharide (LPS) at the outer leaflet.

The bacterial cell wall contains many negatively charged components that are highly related to the effective targeting of AMPs toward the cell membrane. These components can attract highly positively charged AMPs. These AMPs aggregate on the cell surface before inserting into the membrane. Several findings suggest that LPS induces AMP targeting. However, AMPs show irregularity in terms of their preferred target. Some AMPs can only efficiently target Gram-positive strains, whereas others can only target Gram-negative strains. The source of this bias remains unknown. The possible enhancers during AMP targeting are assumed to be charged components from the cell wall, charged phospholipids from the amphiphilic membrane, and negative transmembrane potential.

A Langmuir film is a single layer of insoluble molecules fabricated at the gas–liquid or liquid–liquid interface. This technology has been widely applied in the study of amphiphilic molecules and their interaction with other substances. The surface pressure area isotherm is the most important indicator of monolayer properties. The surface pressure area isotherm is obtained by measuring the surface pressure as a function of the water surface area available for each monolayer molecule upon compression. This isotherm is used to predict how molecules pack together and also provides information

about the internal force between molecules and compressibility of the monolayer.

As we showed in the antimicrobial test, Gram-negative bacteria showed relative strong resistance to Ib-AMP4 in calcium-loaded medium. To investigate the role of cell wall especially the Gram-negative bacteria cell wall and its interaction with calcium ions during Ib-AMP4 targeting, LPS, the Gram-negative cell wall special component, was employed to construct model system for study.

5.3 Result

5.3.1 LPS isotherm

In the π-A isotherms for LPS-Re, we observed the effect of calcium ions on condensation in the following data: (i) the onset of pressure increase appeared at the lower molecular area and (ii) the surface pressure was always lower than that in the calcium-free subphase in the same molecular area. These findings indicated that calcium affects the intermolecular interactions between LPS molecules when the headgroups were compact (Jeworrek et al. 2011).

In the surface potential-molecular area (P-A) isotherm, the surface potential on the calcium-loaded buffer was high. This finding indicates the incorporation of calcium ions into the headgroup region of LPS (Hagge et al. 2006). Given that

calcium has two positive charges, it can increase the effective molecular moment and affected the following: (i) the dipole moment of the polar headgroup and (ii) the tilt angle of the hydrocarbon chains. The effect of calcium on the effective molecular moment directed to the subphase surface was qualitatively observed using the Helmholtz equation at a constant molecular area as an assumption (Garcia-Verdugo et al. 2007).

The Helmhotz equation is as follows:

$$\Delta V = \frac{\mu \cos\theta}{A \varepsilon \varepsilon_0}$$

where the actual moment of the isolated molecule is ε and is aligned at some angle θ to the subphase normal. A is the area occupied by each molecule and ε_0 is the permittivity of free space.

A

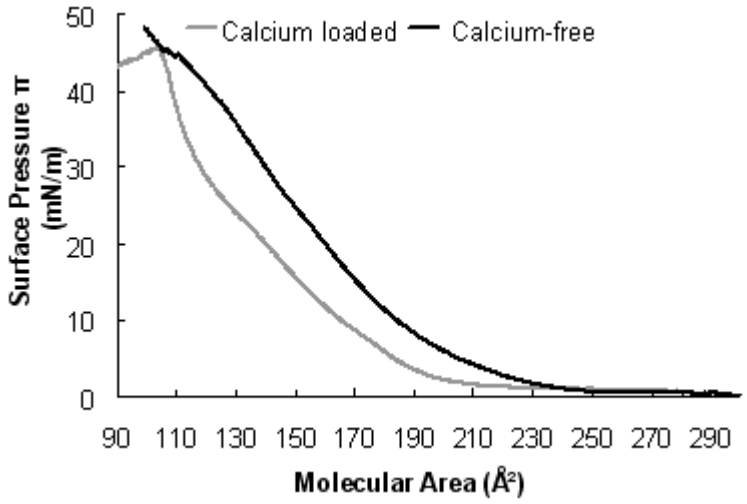

B

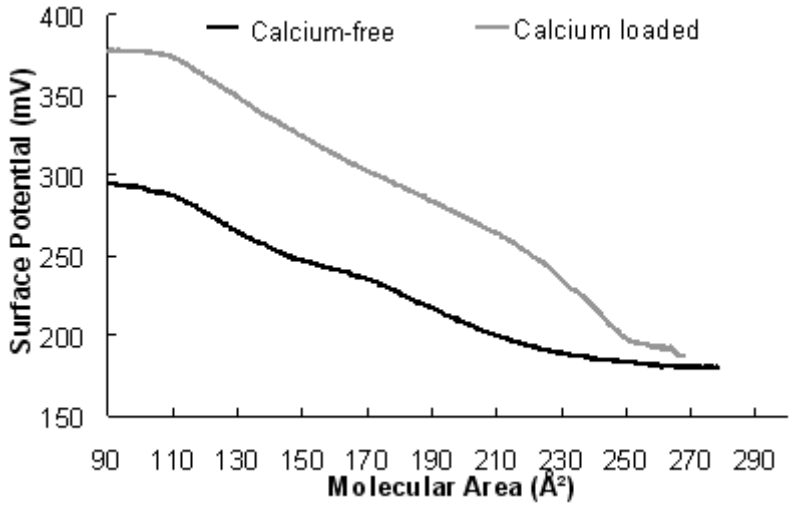

Figure 15. Isotherms for the LPS-Re monolayer in calcium-loaded and -free **buffers.** A) π-A isotherms for LPS-Re; B) P-A isotherms for LPS-Re.

5.3.2 Ib-AMP4 intercalation increases the LPS-Re monolayer surface pressure

To compare the insertion of Ib-AMP4 at different surface pressures and in different buffers, the monolayer was compressed to a target pressure of 10, 17, or 25 mN/m in calcium-free buffer, or 17 mN/m in calcium-loaded buffer separately. The Ib-AMP4 was injected after compression. The final Ib-AMP4 concentration was approximately 2 mM. The surface pressure of the LPS-Re monolayer increased after Ib-AMP4 injection. The pressure increase caused by Ib-AMP4 injection was negatively correlated with the surface pressure on the location where the drug was injected. Calcium prohibited the Ib-AMP4 intercalation in the calcium-loaded buffer at the same molecular area.

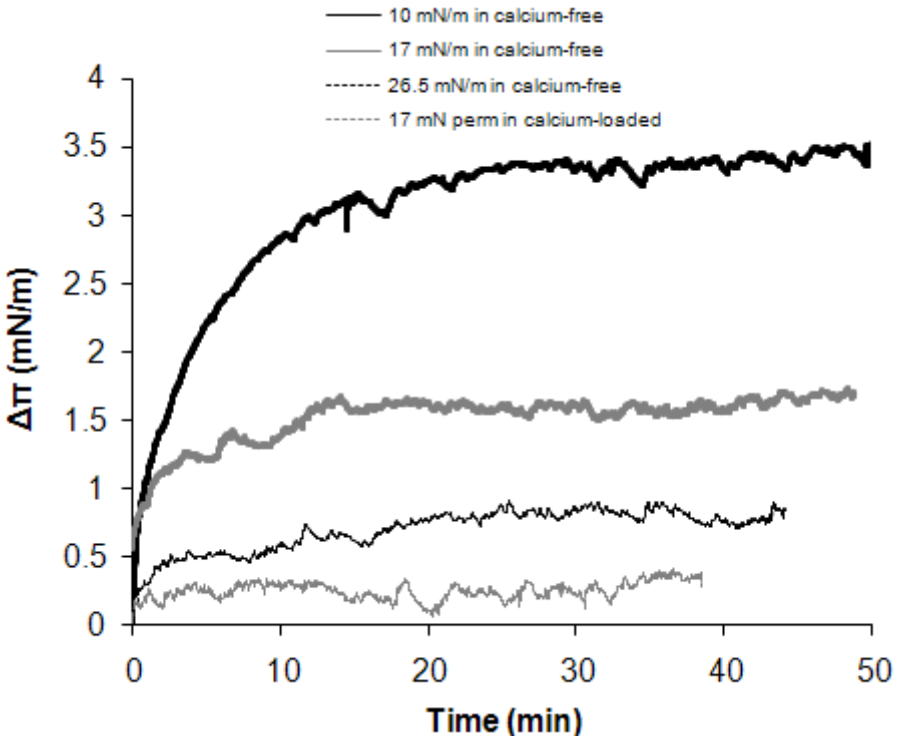

Figure 16. Ib-AMP4 intercalation increasing the surface pressure. The molecular area at 17 mN/m in the calcium-loaded buffer is equal to that at 25 mN/m in the calcium-free buffer. The pressure increase caused by Ib-AMP4 under different pressure and buffer treatments is plotted over time.

5.3.3 Study of Ib-AMP4 interaction with the LPS-Re vesicle by QCM-D

The unique fundamental frequency of ~5 MHz for a clean quartz crystal was recorded by the system before the LPS-Re was coated. After the injection of LPS-RE vesicles, the LPS-Re mass was continuously absorbed onto the surface, thereby resulting in a decrease in frequency, which finally became stable at -90 Hz below the fundamental frequency. The dissipation continued to increase, thereby indicating an increase in viscosity in the quartz surface. A

90 Hz frequency shift implied that the attached materials were probably intact vesicles.

An immediate mass loss amounting to -60 Hz was observed after applying Ib-AMP4 at 10 μg/ml. The LPS-Re vesicle/micelle was broken, and the major mass was removed from the quartz.

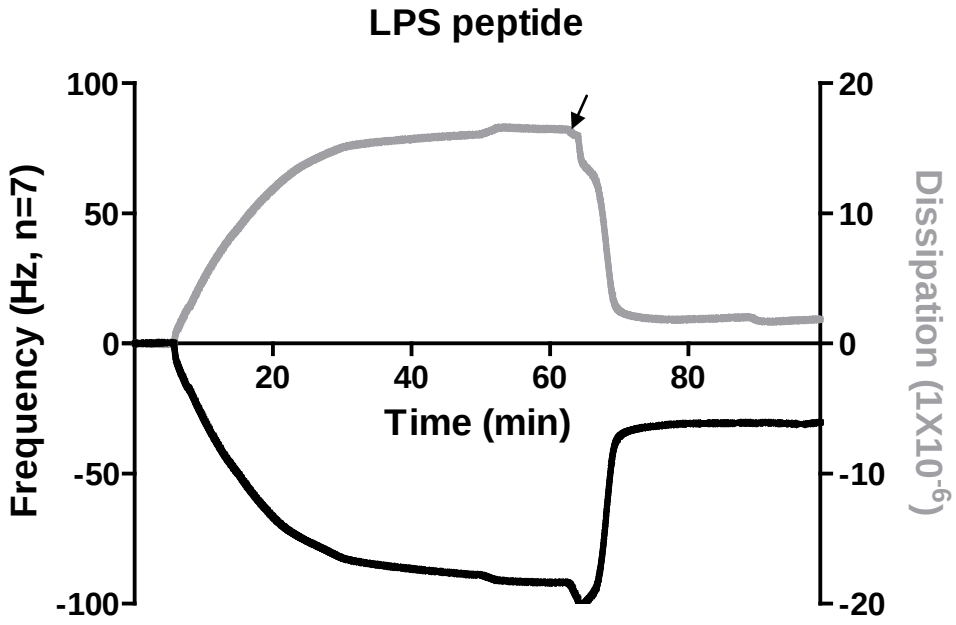

Figure 17. Study of Ib-AMP4 interaction with LPS-Re vesicles by QCM-D. The arrow indicates where the Ib-AMP4 was injected. The Ib-AMP4 injection disrupted the LPS-Re vesicles and removed most of the materials.

5.4 Discussion

Injecting Ib-AMP4 underneath an LPS-Re monolayer caused an instant adsorption at the monolayer interface, which showed a rapid interaction between these two opposite charged compounds. The peptide rupturing LPS vesicles at 10 μg/ml by QCM-D indicated affinity for Ib-AMP4 to the target on

LPS. The liposome disruption started with the peptide binding/insertion. These conditions suggest that the LPS layer located on the cell wall surface was electrically attractive and permeable to AMPs.

In the presence of Ca^{2+}, Ib-AMP4 absorption was dramatically reduced. The isotherm profile of LPS-Re was significantly modified by applying Ca^{2+} to the monolayer. The LPS-Re matrix became ordered and compact. This is in consistence with previous reports that cations were condensed at the LPS monolayer interface. The addition of Ca^{2+} dramatically resulted into a full replacement of K^+ from the interface (Abuillan et al. 2013; Oliveira et al. 2010). Therefore, Ca^{2+} built up an electrical defense before the entrance of the LPS monolayer. Peptide binding/penetration started with cation displacement. Replacing Ca^{2+} with a peptide rather than Na^+/K^+ was clearly difficult.

Ca^{2+} was unfavorable for Ib-AMP4 antimicrobial activities in all tested species during the antimicrobial assay; among these species, Gram-negative species showed strong resistance in the presence of Ca^{2+} (Fan et al. 2013). This might be considered in consistent with the result that calcium ions reduce the LPS permeability to Ib-AMP4 at the cell envelope and prevent Ib-AMP4 from approaching the target membrane by electrical repulsion.

Chapter 6. Interaction between Ib-AMP4 with lipid membrane

6.1 Abstract

Membrane breakage was the unique mechanism by which AMPs exert rapid bactericidal activity. A series of molecular events occurred in turn and finally resulted in the death of bacterial cells. QCM-D and CD measurements indicated that the initial binding of Ib-AMP4 with the membrane started at a critical concentration where Ib-AMP4 underwent a conformation change and adopted a special β-sheet form to insert into the liposome. Upon Ib-AMP4 insertion, the swollen liposome was not disassembled, as shown by the DLS measurement. Ib-AMP4 insertion induced leakiness and wrinkling of the liposome on the membrane surface, as shown by QCM-D. The leakage continued while a self-promoting insertion of Ib-AMP4 occurred. The intensive leakage finally eased after approximately 20 min.

The periodic leakage indicated the formation of transient pores across the liposome lipid bilayer, which probably occurred by a mechanism similar to that described for the sinking-raft model because Ib-AMP4 has a large hydrophilic headgroup coupled to a short and small hydrophobic tail. Surface pressure, line tension, and curvature strain were probably involved during the pore formation and resealing. Previous studies on DOPC single and DOPC/DOPG

binary monolayer in calcium-loaded and -free buffers implied that the charge property of lipid and cation species in the buffer affected Ib-AMP4 insertion, and such effect was independent from that of surface pressure. Cholesterol also prohibited Ib-AMP4-induced calcein leakage by changing the membrane compressibility and altering the membrane curvature. Furthermore, cations prevented Ib-AMP4 insertion by interrupting the conformational change of Ib-AMP4 during the insertion stage.

6.2 Introduction

Electrostatic forces exist in a long distance range, and interactions between lysine or arginine with phosphate groups in lipid bilayers are particularly strong; thus, negatively charged components from both the cell wall and membrane promote a mutual and vigorous attraction to highly charged cationic AMPs (Mavri and Vogel 1996). The initial interaction between AMPs with their target microbes is probably driven by electrostatic attraction. This view is also supported by the fact that AMPs from different species showed conserved highly positive charges (Gueguen et al. 2006; Seshadri Sundararajan et al. 2012; Wang et al. 2009).

The events that followed the initial binding comprised the transition stage, during which AMPs changed their binding affinity toward the membrane by altering their geometric conformation; a self-promoting association or multimerization of AMPs occurred, and AMPs were oriented perpendicular to the membrane (Huang 2000; Prado Montes de Oca 2013; Yeaman and Yount 2003). The membrane finally developed a transmembrane deficiency that could either be a hole or a channel. Different speculations have been presented for this stage, including the barrel-stave, toroid-pore, and carpet theories (Prado Montes de Oca 2013; Wimley 2010; Yeaman and Yount 2003). Besides the stable channel/pore complex formation suggested by carpet barrel or toroid theory, sinking-raft theory suggests that the transient

pore formation was due to mass imbalance caused by peptide preferential binding by self-association or self-assembly. This mass disproportion introduces a curvature strain along the outer membrane and forces the membrane to bend. Upon threshold concentration, the membrane breaks and the outer leaflet is linked to the inner leaflet for mass exchange. The membrane recovers again because the curvature stain dissipates as the result of the mass exchange.

A lipid bilayer is a good model for studying membranes. Expanding, contracting, and bending are the three main forms of deformation in the liposome bilayer (Disalvo and Simon 1995). Expanding and contracting are within-plane motions that are usually evaluated by the compressibility corresponding to the change in pressure vs. area per molecule in a membrane. Previous studies reported that membrane pressure prohibits pore formation (Farago and Santangelo 2005; Janmey and Kinnunen 2006; Karatekin et al. 2003; Matsuzaki et al. 1998). Membrane bending is an out-of-plane movement that is closely related to the curvature strain, which in turn is regulated by the nature of the constituent lipids (Heerklotz 2008). The compressibility and curvature strain are characteristic properties that can be used to estimate the deformation ability of a lipid bilayer.

QCM-D is a recently developed technique to study bilayers. A QCM-D sensor consists of a thin quartz disc that can be excited to oscillation by AC

application because of its piezoelectric properties. When a thin and rigid layer is attached to the sensor, the oscillation frequency (f) would decrease, according to the Sauerbrey relationship, as follows:

$$\Delta m = -\frac{C \cdot \Delta f}{n}$$

C=17.7ng Hz-1 cm-2 for a 5 MHz quartz crystal.
N=1, 3, 5, 7 is the overtone number.

The attached layer is “soft” and does not fully couple to the sensor in most cases. The mass was underestimated by the Sauerbrey relationship. This viscous film dampens the sensor’s oscillation. Energy dissipation (D) is introduced and defined as follows to estimate the viscosity:

$$D = \frac{E_{lost}}{2nE_{stored}}$$

Where E_{lost} is the energy lost (dissipated) during one oscillation cycle and E_{stored} is the total energy stored in the oscillator

Based on water coupling theory (Cho et al. 2007), the energy dissipation reflects the surface roughness.

Ib-AMP4 from *Impatients balsamina* represents an interesting and powerful AMP with bactericidal properties against Gram-positive and Gram-negative bacteria and MDR pathogens. However, Ib-AMP4 antibacterial activity is largely affected by ion concentrations. We aimed to determine the antimicrobial mechanism and to clarify how divalent cations inhibit Ib-AMP4 antimicrobial activity.

6.3 Result

6.3.1 Liposome leakage

Our liposome preparation reached a homogeneous size of ~200 nm in diameter after extrusion. The free calcein was effectively removed, and only stable and non-leaky liposome fractions from PD-10 chromatography were used for the leakage assay. The leakage percentages in 1% Triton X-100 and HEPES buffers were 100% and 0%, respectively.

Membrane disruption caused by Ib-AMP4 was studied using a calcein leakage kinetics assay. A series of peptide concentrations were added for the leakage assay. The P/L ratios used varied from 2.5/1 to 1/10. The release curve was characterized by a biphasic increase. A strong and instantaneous calcein release was observed within the first several minutes after peptide addition, followed by a slow and weak release that reached a plateau within 20 min.

The leakage ratio was positively correlated with the peptide at concentrations below 50 μg/ml. A maximal leakage of ~65% was obtained by applying the peptide at 50 or 100 μg/ml, whereas a minimal leakage of ~3% was obtained by applying the peptide at 0.2 μg/ml. The addition of 50 mM calcium into the reaction buffer decreased leakage at all tested peptide concentrations. Leakage decreased by at least 40% after calcium addition at concentrations

higher than 0.5 μg/ml. Such concentrations were within the MICs range for bacteria.

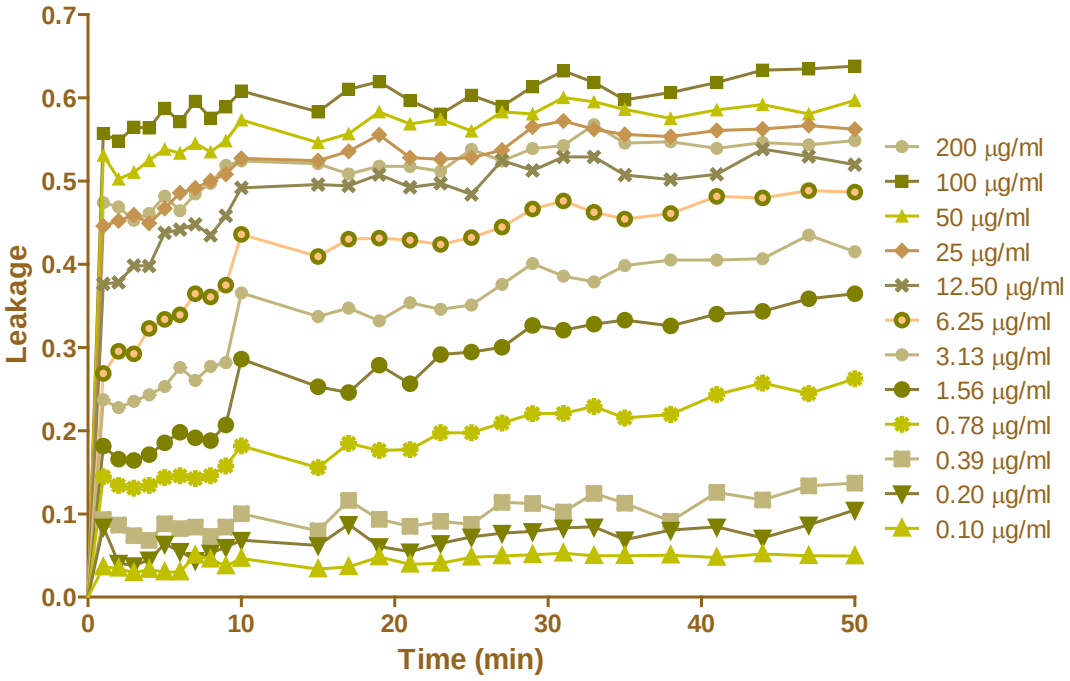

Figure 18. Kinetics of DOPC liposome leakage by Ib-AMP4 in the calcium-free buffer. A concentration series of Ib-AMP4 ranging from 0.1 μg/ml to 200 μg/ml was tested on the DOPC liposome. The calcein leakage intensity was positively correlated with Ib-AMP4 at concentrations lower than 200 μg/ml.

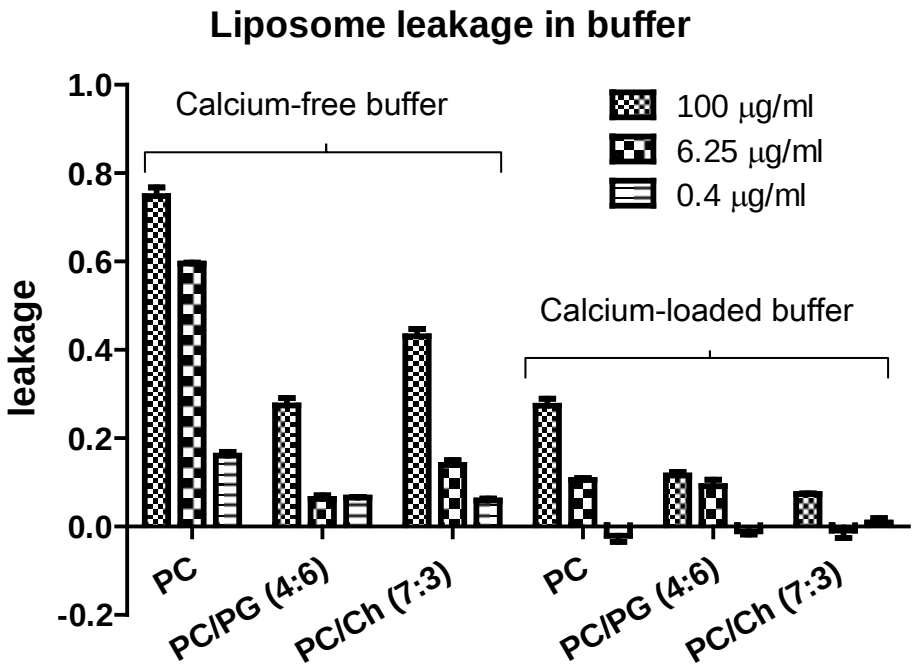

Figure 19. Liposome leakage after treated with different concentrations of Ib-AMP4. Liposome prepared by DOPC and its binary mixture with DOPG or cholesterol were used. High, medium, and low concentrations (i.e., 100, 6.25, and 0.4 μg/ml, respectively) of Ib-AMP4 were tested. PC, DOPC liposome; PC/PG (4:6), liposome of the binary mixture of DOPC/DOPG with a molar ratio of 4:6; PC/Ch (7:3), liposome of the binary mixture of DOPC/cholesterol with a molar ratio 7:3. The leakage percentages at 25 min after peptide application are plotted in bars.

The incorporation of DOPG or cholesterol into the DOPC membrane reduced the leakage percentage. Cholesterol and DOPG reduced the maximal leakage from ~80% to ~40% and ~30%, respectively. DOPC liposome and calcium addition inhibited the leakage of the mixed liposome, but the cholesterol-mixed liposome notably showed the lowest leakage after the addition of calcium.

6.3.2 Secondary structure of Ib-AMP4

The DOPC-bound peptide indicated that β -sheet was the effective conformation by which Ib-AMP4 exerted membrane activity. An inactive peptide without disulfide bonds only had 6.6% β-sheet, whereas an active peptide with disulfide bonds had 25.3%. Disulfide bonds seemed to promote the refolding of an unstructured Ib-AMP4 peptide. Both Mg^{2+} and SDS reduced the β-sheet percentage, and such decrease corresponded to a suppression of the Ib-AMP4 antimicrobial activity.

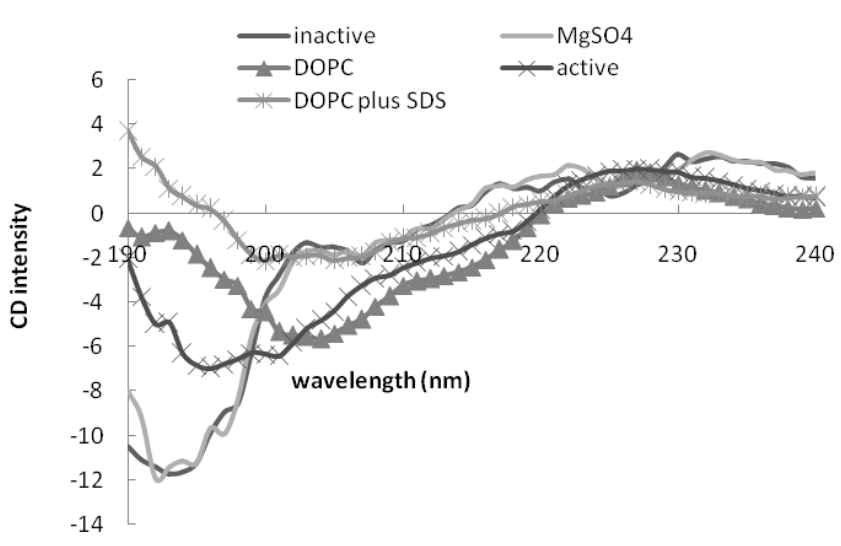

Figure 20. Secondary structures of Ib-AMP4 in different solutions.

Table 9. Second structure of the Ib-Amp4 peptide.

	Solvents*				
2D structure	MgSO4	Pure water	H_2O_2	DOPC	SDS
α-Helix	0	0	0	0	16.2
β-sheet	0	6.6	25.3	65.7	0
Turn	48.4	45.7	27.9	0	0
Random	51.6	47.7	46.9	34.3	83.8

*Ib-AMP4 peptide solved in “pure water” was inactive without disulfide bonds. The other samples were pre-treated with H_2O_2 to form disulfide bonds and were supplemented with different additives, such as DOPC, SDS, and $MgSO_4$, for CD measurements.

6.3.3 DLS

The prepared DOPC liposome showed an average size of ~165 nm in diameter. Size distribution results indicated that the whole liposome proportion was subject to a single peak, thereby suggesting that the liposome was prepared homogenously.

Addition of the peptide into the DOPC liposome with a P/L ratio varying from 1/6 to 2.5/1 failed to change the shape of the original size distribution curve. However, a minor mean size shift toward a larger diameter after peptide addition was observed. By contrast, the liposome melted down into tiny particles with a diameter of several nanometers in the presence of Triton X-100.

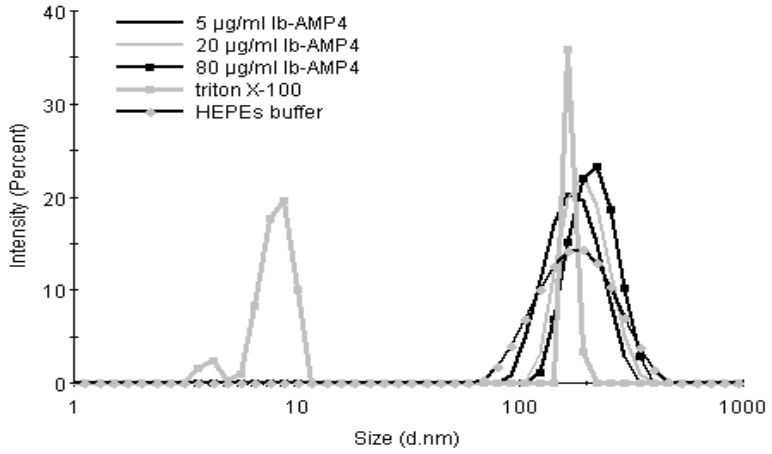

Figure 21. Size distribution of liposome by DSL after the addition of Ib-AMP4 or Triton X-100. The mean sizes of the liposome were 162.8, 186.3, 198.0, and 216.4 nm after the

addition of 0, 5, 20, and 80 μg/ml Ib-AMP4, respectively. Triton X-100 transformed liposomes into small particles with diameters of several nanometers.

6.3.4 TEM

Most of the *Escherichia coli* cells were disrupted, and a portion of their cytoplasm was released to the external environment after Ib-AMP4 treatment. Several cells slightly shrunk as they lost their original shape, but still maintained a round stick shape. The cell wall remained intact because the cells were still surrounded by a clear envelope. The cells became leaky, but most of their cytoplasm remained inside. The leakage zone showed a cloud-like shape, thereby implying that leakage was restricted to a local region and only a few leaky pores were formed.

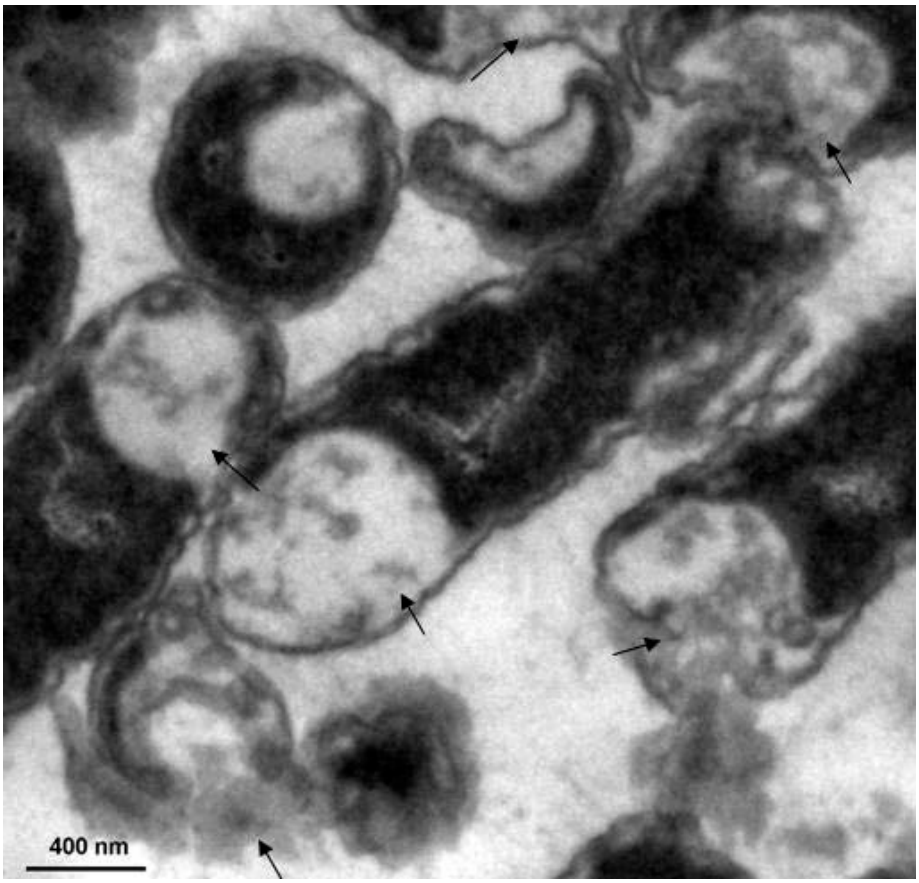

Figure 22. TEM image of Ib-AMP4 causing *Escherichia coli* cell leakage. Bacterial cells with condensed atom density appear black under TEM, whereas the bright areas represent either the extracellular buffer or leakage location where the cytoplasm was replaced by the water buffer. The arrows indicate leaky spots.

6.3.5 GUV image

The peptide started to diffuse from right to left in the sample chamber after peptide injection. The bilayer membrane rigidity increased with increasing peptide concentration. When the peptide reached the critical concentration, the GUVs suddenly exploded or started to shrink into a solid granule. This event occurred very rapidly, within 1 s on average. One of our photographs showed the step-by-step shrinkage of the GUVs. The image below indicates that a scar-like area was formed on the surface before the GUV started to shrink. The inner content continuously leaked out from the scar, and the GUV finally turned into a solid granule.

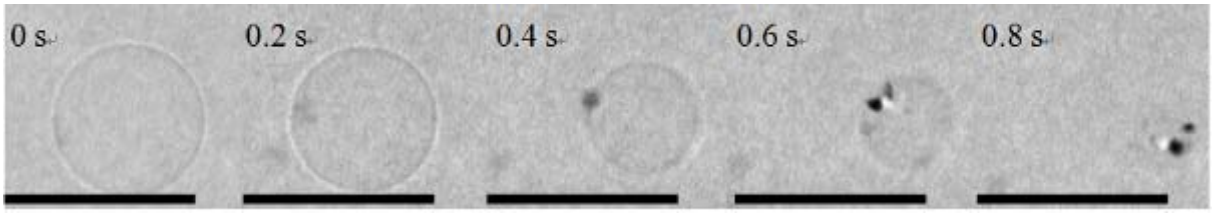

Figure 23. Documentation of GUV breakage by Ib-AMP4 using time elapse photography. The black bar indicates the amplification scale per 100 µm.

6.3.6 Isotherm for lipids

The π-A isotherm for DOPC is shown in Figure 24. The compression profiles of the calcium-loaded and -free buffers were similar, indicating an expanded isotherm without apparent phase transition. The expansion of the isotherm can

be explained by the loose structure formed by unsaturated double bonds in the alkyl chains of DOPC. In contrast to LPS-Re, calcium addition induced the onset of pressure increase at a low molecular area. Pressure was maintained at a high level throughout the compression, but the gap was only 1 mN/m to 3 mN/m, which was theoretically negligible. The condensation effect of divalent cations was also observed in other lipid monolayers (Ohki and Ohshima 1985; Ohshima and Ohki 1985; Yamaguchi et al. 1995).

The incorporation of DOPG into DOPC failed to change the shape of the π-A isotherm. The produced isotherm seemed to overlay with that obtained from the calcium-loaded buffer. Cholesterol incorporation apparently changed the π-A isotherm shape and resulted in low pressure throughout the compression.

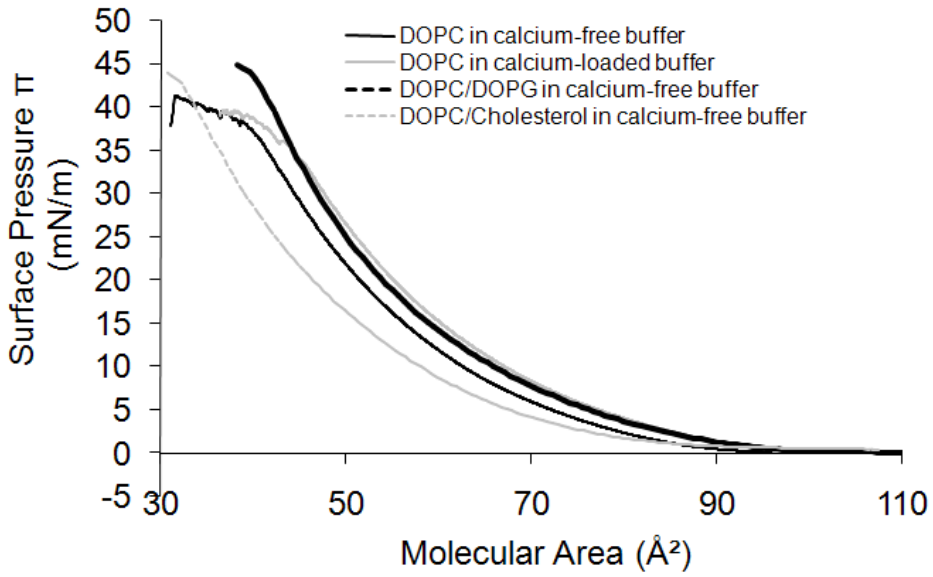

Figure 24. Surface pressure area isotherms for DOPC and their binary mixtures. Monolayer isotherms of DOPC both in calcium-free and -loaded buffers were measured to evaluate the effect of calcium ions. DOPG and cholesterol were mixed with DOPC at a 1:1 molar ratio and used for isotherm measurements.

6.3.7 DOPC QCM-D

DOPC was applied onto the quartz, and a bilayer was absorbed onto the surface, corresponding to a frequency shift of ~26 Hz. The dissipation values below 0.5 suggested that the bilayer was well deposited with good rigidity. A serial solution of different peptide concentrations ranging from 5 μg/ml to 400 μg/ml was applied to the DOPC bilayer. No apparent absorption was observed at concentrations lower than 400 μg/ml. At 400 μg/ml peptide concentration, a frequency shift of ~7 Hz was recorded. The washing step with the calcium buffer failed to change the binding/insertion. Consistent with the frequency, dissipation dramatically increased to 1.7 and higher after the application of the peptide at 400 μg/ml.

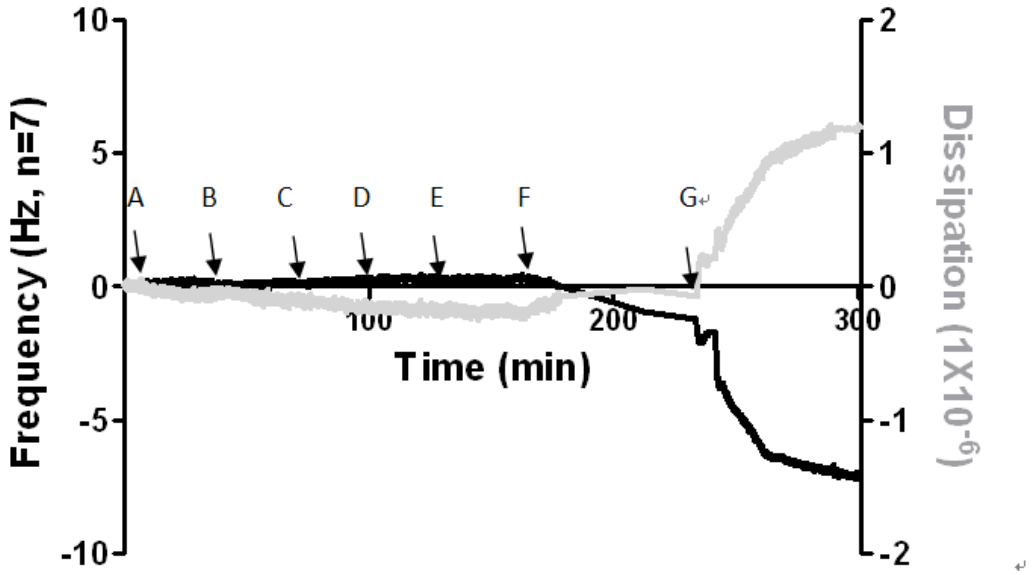

Figure 25. QCM-D for DOPC after the application of Ib-AMP4 at different concentrations. Before each injection, the quartz was equilibrated for at least 10 min until the curves were steady. The arrows indicate the injection spots. A, Ib-AMP4 at 5 μg/ml; B, Ib-AMP4 at 10 μg/ml; C, Ib-AMP4 at 20 μg/ml; D, Ib-AMP4 at 40 μg/ml; E, Ib-AMP4 at 80 μg/ml; F, Ib-AMP4 at 200 μg/ml; G, Ib-AMP4 at 400 μg/ml.

6.4 Discussion

The naturally occurring amino acid sequence for Ib-AMP4 comprises 20 amino acids. Hydrophobic amino acids are present symmetrically at position 2, 9 and 19. A multiple anti-parallel folding, which assembled the hydrophobic residues of Ib-AMP4, was the predicted reason for the membrane insertion. The disulfide restriction caused by connections at position 6, 20, 7 and 16, and the angle restriction by proline at position 9 indicated a quinary folding of each lamella comprising 4 to 5 amino acids. The basic charged groups of arginine only existed in pairs at the folding edge, whereas the hydrophobic residues were packed at the head.

Ib-AMP4 is not a true amphipathic molecule before the conformational change. Ib-AMP4 failed to show any surfactant activity in pure water or aquatic buffers (data not shown). An inducible conformation change is required for Ib-AMP4 to exert amphipathic insertion. The CD spectrum results failed to show an apparent secondary structure for Ib-AMP4 in an aquatic buffer after forming disulfide bonds, but the merit of the disulfide bond became evident when improved efficiency was obtained in antimicrobial tests after the formation of disulfide bonds (Fan et al. 2013). The presence of the membrane-bound peptide with a ~70% β-sheet implied that membrane insertion was a conformation-dependent process (Nguyen et al. 2011). The disulfide bond-restrained conformation probably represents an intermediate for the

unstructured peptide to fold into a β-sheet. Cations inhibited Ib-AMP4 antimicrobial efficiency by affecting the conformation transition stage because the β-sheet dissipated in the presence of magnesium cations or SDS was observed.

AMPs use a unique mechanism to selectively target bacteria and are a promising solution to overcome drug resistance. However, AMP's susceptibility to cations is the primary limitation for the wide application of AMPs. Cations, such as Ca^{2+} and Mg^{2+}, are physiologically essential in all cell types. Their effect on the antimicrobial efficiency of AMPs killing bacteria is an interesting topic.

As we discussed in the previous chapter, all substances entering or approaching the bacterial cell membrane pass through the cell wall. Unlike the cell membrane, which is only open for selected substances, the cell wall uses Ca^{2+} to reduce the permeability to Ib-AMP4. After crossing the cell wall, AMPs reach their real target, which is the cytoplasm membrane. Unlike the cell wall, the cell membrane is a sealed but selectively permeable bilayer. A lipid bilayer is a good model for studying the cell membrane. Spontaneous but slow leakage of calcein occurred in DOPC liposome, thereby indicating that the occasional opening of a membrane bilayer occurs naturally (Bordi et al. 2000). Membrane fluctuation transmits an occasional strain along the membrane where lipids move non-synchronously and dynamically changes the local

bilayer properties, such as thickness and tension; such properties are closely related to the insertion event (Santangelo and Farago 2007; Woodka et al. 2012). Membrane fluctuation initiates the occasional membrane hydrophobic exposure for AMP insertion.

Extended leakage can be caused by pore stabilization. Some studies suggest that surfactants stabilize pores by reducing the line tension, which helps reseal pores (Farago and Santangelo 2005; Janmey and Kinnunen 2006; Karatekin et al. 2003). Unlike the line tension, membrane surface tension drives the opening of the membrane (Farago and Santangelo 2005; Janmey and Kinnunen 2006; Karatekin et al. 2003; Matsuzaki et al. 1998). Logically, the opposing surface pressure prohibits the pore-formation on the membrane. Curvature is another important factor affecting membrane flexibility or fluctuation.

From an energy perspective, previous experiments have proven that the insertion of amphipathic molecules into a lipid membrane is driven by enthalpy (i.e., energy minimization) (Yeaman and Yount 2003). The hydrophobic insertion is energetically favored and would occur spontaneously as the membrane expands and as the inserted peptides lose potential energy. However, the membrane cannot expand freely in a liposome where interior pressure increases after insertion. The potential energy produced by increased interior pressure is energetically unfavored. An alternative is to create a wrinkle

on the surface. DOPC/PC is a kind of lipid with a spontaneous negative curvature strain, but the outer leaflet bends positively. Therefore, curvature frustration occurs at the bilayer's outer leaflet. Stress caused by the curvature failure, which stores elastic potential to an extent, favors insertion only if an opposite curvature strain is introduced (Marsh et al. 2006). Line tension, which is considered as the energy compensation for the hydrophobic exposure of a lipid membrane, drives the resealing of hydrophobic exposure. The value of line tension, such as in a pore of a given size, on a membrane depends on the length of the hydrophobic tail of the constituent lipids (Janmey and Kinnunen 2006). The energy compensation for hydrophobic exposure is smaller for a molecule from a membrane with a smaller or shorter hydrophobic tail. This condition explains why Ib-AMP4, which has a small hydrophobic region, can drive a self-promoting insertion and can stabilize pores.

Consistent with bactericidal kinetics (Fan et al. 2013), liposome leakage occurred for ~20 min and was dynamically constant for up to 24 h. Membrane corruption is the primary bactericidal effect of Ib-AMP4. This temporary leakage implied that the membrane was opened transiently, but no large mass from the membrane was removed. This condition was suggested by the DLS results, wherein neither apparent size change nor new particle generation was observed for the liposome after treatment with peptides at concentrations reaching 80 μg/ml. At these concentrations, ~70% leakage was observed in

the leakage assay. We can distinguish the peptide membrane disruption mechanism from a carpet mechanism, which is a characteristic of small particle generation. Apparently, the peptide employed a non-membrane-lytic mechanism. Given that the peptide structure restrained by two disulfide bonds failed to reach a sufficient length to expand across the bilayer of ~5 nm, the barrel-stave pore mechanism was not applicable for Ib-AMP4.

Rinsing with a subphase without a peptide failed to decrease the binding mass, which indicates a strong affinity between Ib-AMP4 and DOPC lipid in the settled buffer environment. Nevertheless, no apparent adsorption was observed at concentrations up to 200 μg/ml, but absorbed mass dramatically increased after Ib-AMP4 at 400 μg/ml was applied. This finding implies the existence of a threshold at which the peptide affinity towards the lipid bilayer dramatically increased. A reasonable explanation is that the binding/insertion target was not exposed until the threshold concentration was reached. A self-promoting event for peptide binding/insertion was assumed.

The observed threshold by QCM-D was between 200 and 400 μg/ml. The threshold was much bigger than the sufficient concentration observed in the leakage assay using the same liposome species. This finding can be attributed to the changes in flexibility/fluctuation for the DOPC bilayer after immobilization (Karatekin et al. 2003; Matsuzaki et al. 1998). The immobilized

membrane with one side anchored to the quartz results in high stiffness and low flexibility (Disalvo and Simon 1995; Heerklotz 2008).

The increase in the dissipation indicates the roughness of the DOPC bilayer surface after peptide insertion/binding. DOPC is prone to introducing a negative curvature strain onto the outer lipid leaflet (Heerklotz 2008), whereas Ib-AMP4 introduces a positive curvature strain because of its large hydrophilic headgroup and small hydrophobic tail. When Ib-AMP4 is aligned with the lipid, a fluctuant wrinkle instead of smooth adjacency occurs. The energy compensation for hydrophobic exposure of an Ib-AMP4 molecule with a small hydrophobic tail is smaller than that of a long lipid tail. Therefore, the induced weakness at the adjacent place increases the membrane's propensity to open at local places where a peptide is already inserted. This finding explains the self-promoting insertion of Ib-AMP4 into the membrane and also clarifies why leakage is constrained at a local place, as observed by TEM.

The GUV image provides information on the pore formation. Before reaching the threshold concentration, the GUV membrane became increasingly rigid and then started to shrink when a pore was produced on the surface. However, unlike much smaller bacterial cells or small, unilamellar vesicle liposomes, GUVs are sensitive to osmotic pressure changes or curvature strain caused by peptide addition.

How the membrane opens pores across the bilayer is still unknown, but pore opening is certainly dependent on peptide insertion. A high number of insertions cause increased leakage. These mechanisms outlined in the introduction suggest different pore forming patterns, but they all ignore the fact that the membrane would open spontaneously. Does the inner leaflet really need to adopt a similar mechanism to open in the same way as the outer leaflet? Determining what occurs in the inner layer is difficult because the area is hardly accessible for any monitor.

The incorporation of a negatively charged DOPG into the membrane failed to increase leakage, but rather decreased the leakage caused by Ib-AMP4. This finding is consistent with the antimicrobial assay results wherein *Escherichia coli* exhibited stronger resistance to Ib-AMP4 than *Staphylococcus aureus* in salt-containing medium. However, their susceptibility to Ib-AMP4 was comparable in salt-free medium. If the net charge of the bacterial cells defines their susceptibility to AMPs, then the usefulness of all AMPs should be the same or similar. The preferred bacterial targets were distinguished for different AMPs, and the susceptibility to AMPs was unpredictable in terms of bacterial charge property. Therefore, charged lipids affect AMP distribution on the membrane surface, but this electrostatic effect is not as simple as we expected (Yamaguchi et al. 1995).

DOPG and DOPC share a very similar structure with only small differences existing at the headgroup, which introduced a negative charge to the DOPG. Thus, a comparison between DOPC and DOPC/DOPG mixture liposome/monolayer would contribute to the study on the effect of charge during membrane disruption. As expected, the DOPG incorporation failed to alter the isotherm curve shape, but slightly increased the surface pressure at the same molecular area. However, this increase is theoretically negligible. Compressibility is independent of charge during membrane expansion. Calcium addition produced nearly the same effects as DOPG incorporation into DOPC in both isotherm and calcein-leakage assays. This result could indicate that incorporating a negative charge to the membrane produces an effect similar to that obtained when cations are added into the environmental buffer. As of this writing, we lack sufficient case studies to reach such a conclusion, but determining the relationship linking buffer ions, membrane charges, and compressibility is interesting.

The DOPG-mixed lipid bilayer can prevent deep insertion of the peptide by electrostatically absorbing the peptide at the lipid headgroup or using the same approach as that used for LPS to prohibit peptide binding by electrostatic repulsion. The compressibility has been modified by adding DOPG into DOPC, but only slightly. Unlike DOPG, cholesterol is a truly neutral compound, but with a strong negative curvature potential. Some reports state that negative

curvature-inducing lipids can prohibit pore formation (Matsuzaki et al. 1998). Other studies suggest that cholesterol can prevent membrane opening by increasing the line tension (Farago and Santangelo 2005). Thus, cholesterol plays a versatile role during membrane stabilization.

The insertion finally eased after attenuating the bound Ib-AMP4 into the bulk context of the DOPC lipid-forming wrinkle on the surface as indicated by QCM-D. Deductively, this insertion decreased the compressibility of the bilayer as insertion occupied space and increased the membrane lateral pressure. The curvature failure was also fixed by introducing Ib-AMP4 of a spontaneous positive strain, which changed the bending modulus, thereby affecting the membrane flexibility/fluctuation (Zilman and Granek 1996). This condition explains why the liposome finally became resistant to the peptide, and why the calcein leakage of DOPC stopped increasing at concentrations above 50 μg/ml.

Ib-AMP4 can use a quartered mechanism to rupture the DOPC membrane. (i) The binding/insertion event is initiated by an occasional strain burst that opens gaps temporarily between adjacent molecules and exposes the hydrophobic area. The solution peptides therefore obtain access to the hydrophobic area of the outer leaflet for insertion by chance. Along with this insertion, a conformation change in the bound peptide significantly increases the interaction between lipids and bound peptides. (ii) This insertion increases the

tendency of opening the outer leaflet prone because the peptides introduce opposite spontaneous curvature strains to the bulk lipids on the membrane. Thus, the insertion spot would widen and more peptide insertions occur through a self-promoting mechanism. (iii) Thus, a transmembrane pore develops by a particular mechanism. The lateral pressure and line tension quickly reseal the pore and attenuate the bound peptides into the bulk lipid context. This triple cycle i.e., insertion-pore-resealing, occurs several times. (iv) Finally, the bilayer becomes resistant to the peptide after intensive insertion and reaches a stable stage where leakage was significantly decreased. Calcium ions can decrease LPS permeability to Ib-AMP4 at the cell envelope and also prevent the interaction between Ib-AMP4 and lipids by either electrical repulsion or interruption of peptide transformation.

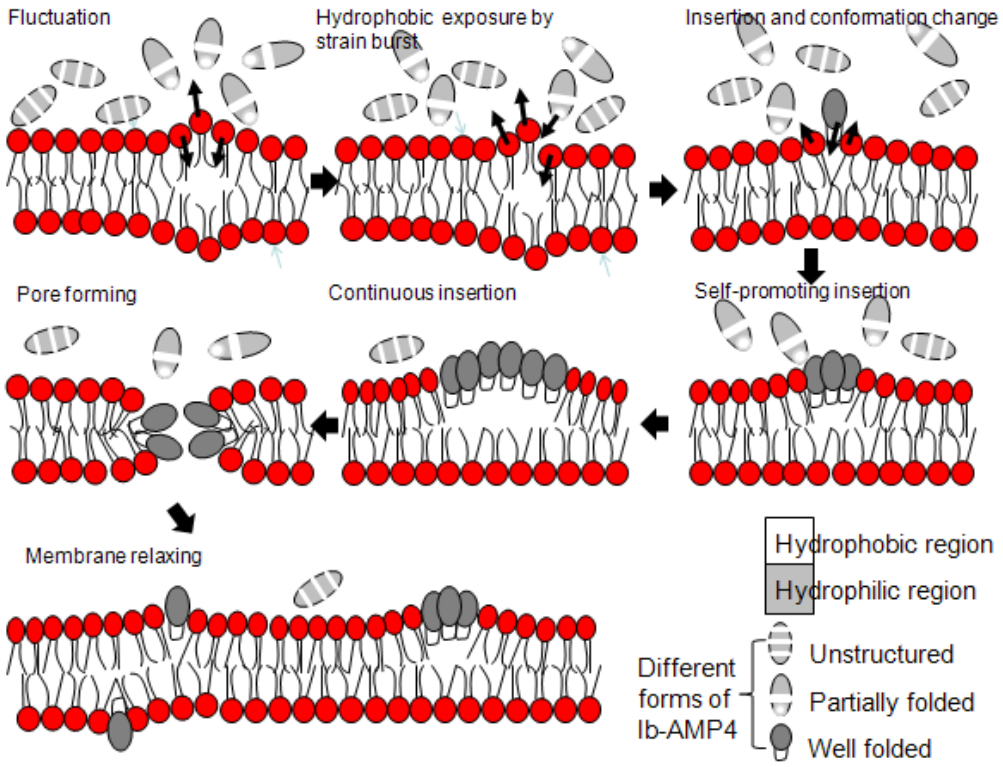

Figure 26. Scheme for membrane interaction with Ib-AMP4. Ib-AMP4 needs to adopt a proper structure to intercalate into membrane. This insertion probably follows a mechanism similar to sinking-raft. The curvature strain, line tension and surface tension are involved during pore formation and resealing.

Reference

Abuillan, W., Schneck, E., Korner, A., Brandenburg, K., Gutsmann, T., Gill, T., Vorobiev, A., Konovalov, O., Tanaka, M., Physical interactions of fish protamine and antisepsis peptide drugs with bacterial membranes revealed by combination of specular x-ray reflectivity and grazing-incidence x-ray fluorescence, Phys Rev E Stat Nonlin Soft Matter Phys, 88 (2013) 012705.

Aleinein, R. A., Schafer, H., Wink, M., Secretory ranalexin produced in recombinant *Pichia pastoris* exhibits additive or synergistic bactericidal activity when used in combination with polymyxin B or linezolid against multi-drug resistant bacteria, Biotechnol J, 9 (2014) 110-119.

Alekshun, M. N., Levy, S. B., Molecular mechanisms of antibacterial multidrug resistance, Cell, 128 (2007) 1037-1050.

Aoki, N., Ishii, Y., Tateda, K., Saga, T., Kimura, S., Kikuchi, Y., Kobayashi, T., Tanabe, Y., Tsukada, H., Gejyo, F., Yamaguchi, K., Efficacy of Calcium-EDTA as an inhibitor for metallo-beta-lactamase in a mouse model of *Pseudomonas aeruginosa* Pneumonia, Antimicrobial Agents and Chemotherapy, 54 (2010) 4582-4588.

Balhara, V., Schmidt, R., Gorr, S. U., DeWolf, C., Membrane selectivity and biophysical studies of the antimicrobial peptide GL13K, Biochimica Et Biophysica Acta-Biomembranes, 1828 (2013) 2193-2203.

Berges, L., Rodriguez-Villalobos, H., Deplano, A., Struelens, M. J., Prospective evaluation of imipenem/EDTA combined disc and Etest for detection of metallo-beta-lactamase-producing Pseudomonas aeruginosa, Journal of Antimicrobial Chemotherapy, 59 (2007) 812-813.

Bessalle, R., Haas, H., Goria, A., Shalit, I., Fridkin, M., Augmentation of the antibacterial activity of magainin by positive-charge chain extension, Antimicrob Agents Chemother, 36 (1992) 313-317.

Bi, H. M., Yang, B., Wang, L., Cao, W. W., Han, X. J., Electroformation of giant unilamellar vesicles using interdigitated ITO electrodes, Journal of Materials Chemistry A, 1 (2013) 7125-7130.

Bordi, F., Cametti, C., Motta, A., Ion permeation across model lipid membranes: A kinetic approach, Journal of Physical Chemistry B, 104 (2000) 5318-5323.

Carlet, Jean, Jarlier, Vincent, Harbarth, Stephan, Voss, Andreas, Goossens, Herman, Pittet, Didier, Ready for a world without antibiotics? The pensieres antibiotic resistance call to action, in: Antimicrobial Resistance and Infection Control, 2012, pp. 11.

Carlet, Jean, Jarlier, Vincent, Harbarth, Stephan, Voss, Andreas, Goossens, Herman, Pittet, Didier, Forum, the Participants of the 3rd World Healthcare-Associated Infections, Ready for a world without antibiotics? The Pensieres Antibiotic Resistance Call to Action, in: Antimicrobial Resistance and Infection Control, 2012, pp. 11.

Chatterjee, S., Chatterjee, D. K., Jani, R. H., Blumbach, J., Ganguli, B. N., Klesel, N., Limbert, M., Seibert, G., Mersacidin, a new antibiotic from *Bacillus* In vitro and In vivo antibacterial activity, Journal of Antibiotics, 45 (1992) 839-845.

Cho, N. J., D'Amour, J. N., Stalgren, J., Knoll, W., Kanazawa, K., Frank, C. W., Quartz resonator signatures under Newtonian liquid loading for initial instrument check, J Colloid Interface Sci, 315 (2007) 248-254.

Davies, R. L., Etris, S. F., The development and functions of silver in water purification and disease control, Catalysis Today, 36 (1997) 107-114.

de la Fuente-Nunez, C., Mertens, J., Smit, J., Hancock, R. E., The bacterial surface layer provides protection against antimicrobial peptides, Appl Environ Microbiol, 78 (2012) 5452-5456.

Diao, H., Guo, C., Lin, D., Zhang, Y., Intein-mediated expression is an effective approach in the study of beta-defensins, Biochem Biophys Res Commun, 357 (2007) 840-846.

Disalvo, E.A., Simon, S.A., Permeability and Stability of Lipid Bilayers, in, CCR Press, 1995, pp. 288.

Dixon, M. C., Quartz crystal microbalance with dissipation monitoring: enabling real-time characterization of biological materials and their interactions, J Biomol Tech, 19 (2008) 151-158.

Elion, G. B., Singer, S., Hitchings, G. H., Antagonists of nucleic acid derivatives. VIII. Synergism in combinations of biochemically related antimetabolites, J Biol Chem, 208 (1954) 477-488.

Engstrom, Y., Induction and regulation of antimicrobial peptides in *Drosophila*, Developmental and Comparative Immunology, 23 (1999) 345-358.

Epand, R. F., Savage, P. B., Epand, R. M., Bacterial lipid composition and the antimicrobial efficacy of cationic steroid compounds (Ceragenins), Biochim Biophys Acta, 1768 (2007) 2500-2509.

Epand, R. M., Epand, R. F., Bacterial membrane lipids in the action of antimicrobial agents, Journal of Peptide Science, 17 (2011) 298-305.

Estes, D. J., Mayer, M., Electroformation of giant liposomes from spin-coated films of lipids, Colloids Surf B Biointerfaces, 42 (2005) 115-123.

Fan, X., Reichling, J., Wink, M., Antibacterial activity of the recombinant antimicrobial peptide Ib-AMP4 from *Impatiens balsamina* and its synergy with other antimicrobial agents against drug resistant bacteria, Pharmazie, 68 (2013) 628-630.

Fan, X., Schafer, H., Reichling, J., Wink, M., Bactericidal properties of the antimicrobial peptide Ib-AMP4 from *Impatiens balsamina* produced as a recombinant fusion-protein in *Escherichia coli*, Biotechnol J, 8 (2013) 1213-1220.

Farago, O., Santangelo, C. D., Pore formation in fluctuating membranes, J Chem Phys, 122 (2005) 44901.

Ferraro, Mary Jane, Methods for dilution antimicrobial susceptibility tests for bacteria that grow aerobically: Approved standard, Clinical and laboratory standards institute, 2005.

Fischer, W., Lipoteichoic acid and lipids in the membrane of *Staphylococcus aureus*, Medical Microbiology and Immunology, 183 (1994) 61-76.

Galanos, C., Luderitz, O., Westphal, O., A new method for the extraction of lipopolysaccharides, Eur J Biochem, 9 (1969) 245-249.

Garau, G., Di Guilmi, A. M., Hall, B. G., Structure-based phylogeny of the metallo-beta-lactamases, Antimicrob Agents Chemother, 49 (2005) 2778-2784.

Garcia-Verdugo, I., Canadas, O., Taneva, S. G., Keough, K. M., Casals, C., Surfactant protein A forms extensive lattice-like structures on 1,2-dipalmitoylphosphatidylcholine/rough-lipopolysaccharide-mixed monolayers, Biophys J, 93 (2007) 3529-3540.

Gueguen, Y., Garnier, J., Robert, L., Lefranc, M. P., Mougenot, I., de Lorgeril, J., Janech, M., Gross, P. S., Warr, G. W., Cuthbertson, B., Barracco, M. A., Bulet, P., Aumelas, A., Yang, Y., Bo, D., Xiang, J., Tassanakajon, A., Piquemal, D., Bachere, E., PenBase, the shrimp antimicrobial peptide penaeidin database: sequence-based classification and recommended nomenclature, Dev Comp Immunol, 30 (2006) 283-288.

Haag, A. F., Kerscher, B., Dall'Angelo, S., Sani, M., Longhi, R., Baloban, M., Wilson, H. M., Mergaert, P., Zanda, M., Ferguson, G. P., Role of cysteine residues and disulfide bonds in the activity of a legume root nodule-specific, cysteine-rich peptide, Journal of Biological Chemistry, 287 (2012) 10791-10798.

Haddock, B. A., Jones, C. W., Bacterial respiration, Bacteriol Rev, 41 (1977) 47-99.

Hagge, S. O., Hammer, M. U., Wiese, A., Seydel, U., Gutsmann, T., Calcium adsorption and displacement: characterization of lipid monolayers and their interaction with membrane-active peptides/proteins, BMC Biochem, 7 (2006) 15.

Hall, M. J., Middleton, R. F., Westmacott, D., The fractional inhibitory concentration (FIC) index as a measure of synergy, J Antimicrob Chemother, 11 (1983) 427-433.

Hammami, R., Ben Hamida, J., Vergoten, G., Fliss, I., PhytAMP: a database dedicated to antimicrobial plant peptides, Nucleic Acids Research, 37 (2009) D963-D968.

Heerklotz, H., Interactions of surfactants with lipid membranes, Q Rev Biophys, 41 (2008) 205-264.

Herold, C., Chwastek, G., Schwille, P., Petrov, E. P., Efficient electroformation of supergiant unilamellar vesicles containing cationic lipids on ITO-coated electrodes, Langmuir, 28 (2012) 5518-5521.

Higgins, JPT, Cochrane handbook for systematic reviews of interventions, version 5.1.0 ed., Wiley-Blackwell, West Sussex, 2011.

Hong, I., Kim, Y. S., Choi, S. G., Simple purification of human antimicrobial peptide dermcidin (MDCD-1L) by intein-mediated expression in *E.coli*, J Microbiol Biotechnol, 20 (2010) 350-355.

Huang, H. W., Action of antimicrobial peptides: Two-state model, Biochemistry, 39 (2000) 8347-8352.

Janmey, P. A., Kinnunen, P. K., Biophysical properties of lipids and dynamic membranes, Trends Cell Biol, 16 (2006) 538-546.

Jenssen, H., Hamill, P., Hancock, R. E., Peptide antimicrobial agents, Clin Microbiol Rev, 19 (2006) 491-511.

Jeworrek, C., Evers, F., Howe, J., Brandenburg, K., Tolan, M., Winter, R., Effects of specific versus nonspecific ionic interactions on the structure and lateral organization of lipopolysaccharides, Biophysical Journal, 100 (2011) 2169-2177.

Karatekin, E., Sandre, O., Guitouni, H., Borghi, N., Puech, P. H., Brochard-Wyart, F., Cascades of transient pores in giant vesicles: line tension and transport, Biophys J, 84 (2003) 1734-1749.

Katoh, A., Fujihara, H., Ohbuchi, T., Onaka, T., Young, W. S., 3rd, Dayanithi, G., Yamasaki, Y., Kawata, M., Suzuki, H., Otsubo, H., Murphy, D., Ueta, Y., Specific expression of an oxytocin-enhanced cyan fluorescent protein fusion transgene in the rat hypothalamus and posterior pituitary, J Endocrinol, 204 (2010) 275-285.

Kiefhaber, T., Rudolph, R., Kohler, H. H., Buchner, J., Protein aggregation in vitro and in vivo: a quantitative model of the kinetic competition between folding and aggregation, Biotechnology (N Y), 9 (1991) 825-829.

Klaenhammer, T. R., Bacteriocins of lactic-acid bacteria, Biochimie, 70 (1988) 337-349.

Kohanski, M. A., Dwyer, D. J., Collins, J. J., How antibiotics kill bacteria: from targets to networks, Nature Reviews Microbiology, 8 (2010) 423-435.

Kumar, Sanath, Mukherjee, Mun Mun, Varela, Manuel F., Modulation of bacterial multidrug resistance efflux pumps of the major facilitator superfamily, International Journal of Bacteriology, 2013 (2013) 15.

Lee, E. K., Kim, Y. C., Nan, Y. H., Shin, S. Y., Cell selectivity, mechanism of action and LPS-neutralizing activity of bovine myeloid antimicrobial peptide-18 (BMAP-18) and its analogs, Peptides, 32 (2011) 1123-1130.

Lee, J. K., Park, S. C., Hahm, K. S., Park, Y., Antimicrobial HPA3NT3 peptide analogs: placement of aromatic rings and positive charges are key determinants for cell selectivity and mechanism of action, Biochim Biophys Acta, 1828 (2013) 443-454.

Lewis, K., Platforms for antibiotic discovery, Nat Rev Drug Discov, 12 (2013) 371-387.

Li, P., Li, X., Saravanan, R., Li, C. M., Leong, S. S. J., Antimicrobial macromolecules: synthesis methods and future applications, Rsc Advances, 2 (2012) 4031-4044.

Li, P., Wohland, T., Ho, B., Ding, J. L., Perturbation of lipopolysaccharide (LPS) micelles by Sushi 3 (S3) antimicrobial peptide. The importance of an intermolecular disulfide bond in S3 dimer for binding, disruption, and neutralization of LPS, J Biol Chem, 279 (2004) 50150-50156.

Makky, A., Michel, J. P., Kasselouri, A., Briand, E., Maillard, P., Rosilio, V., Evaluation of the specific interactions between glycodendrimeric porphyrins, free or incorporated into liposomes, and concanavaline A by fluorescence spectroscopy, surface pressure, and QCM-D measurements, Langmuir, 26 (2010) 12761-12768.

Marsh, D., Shanmugavadivu, B., Kleinschmidt, J. H., Membrane elastic fluctuations and the insertion and tilt of beta-barrel proteins, Biophys J, 91 (2006) 227-232.

Martin-Visscher, L. A., Yoganathan, S., Sit, C. S., Lohans, C. T., Vederas, J. C., The activity of bacteriocins from Carnobacterium maltaromaticum UAL307 against Gram-negative bacteria in combination with EDTA treatment, Fems Microbiology Letters, 317 (2011) 152-159.

Matsuzaki, K., Nakamura, A., Murase, O., Sugishita, K., Fujii, N., Miyajima, K., Modulation of magainin 2-lipid bilayer interactions by peptide charge, Biochemistry, 36 (1997) 2104-2111.

Matsuzaki, K., Sugishita, K., Ishibe, N., Ueha, M., Nakata, S., Miyajima, K., Epand, R. M., Relationship of membrane curvature to the formation of pores by magainin 2, Biochemistry, 37 (1998) 11856-11863.

Mavri, J., Vogel, H. J., Ion pair formation of phosphorylated amino acids and lysine and arginine side chains: a theoretical study, Proteins, 24 (1996) 495-501.

Mikkelsen, M. E., Gaieski, D. F., Antibiotics in sepsis: Timing, appropriateness, and (of course) timely recognition of appropriateness, Critical Care Medicine, 39 (2011) 2184-2186.

Morales-Penningston, N. F., Wu, J., Farkas, E. R., Goh, S. L., Konyakhina, T. M., Zheng, J. Y., Webb, W. W., Feigenson, G. W., GUV preparation and imaging: Minimizing artifacts, Biochimica Et Biophysica Acta-Biomembranes, 1798 (2010) 1324-1332.

Morehead, H., Johnston, P. D., Wetzel, R., Roles of the 29-138 disulfide bond of subtype A of human alpha interferon in its antiviral activity and conformational stability, Biochemistry, 23 (1984) 2500-2507.

Morein, S., Andersson, A. S., Rilfors, L., Lindblom, G., Wild-type *Escherichia coli* cells regulate the membrane lipid composition in a "window" between gel and non-lamellar structures, Journal of Biological Chemistry, 271 (1996) 6801-6809.

Nan, Y. H., Park, I. S., Hahm, K. S., Shin, S. Y., Antimicrobial activity, bactericidal mechanism and LPS-neutralizing activity of the cell-penetrating peptide pVEC and its analogs, J Pept Sci, 17 (2011) 812-817.

Nguyen, L. T., Haney, E. F., Vogel, H. J., The expanding scope of antimicrobial peptide structures and their modes of action, Trends Biotechnol, 29 (2011) 464-472.

Nizet, V., Antimicrobial peptide resistance mechanisms of human bacterial pathogens, Curr Issues Mol Biol, 8 (2006) 11-26.

Ohki, S., Ohshima, H., Divalent cation-induced phosphatidic acid membrane fusion. Effect of ion binding and membrane surface tension, Biochim Biophys Acta, 812 (1985) 147-154.

Ohshima, H. , Ohki, S., Effects of divalent cations on the surface tension of a lipid monolayer-coated air/water interface, Journal of Colloid and Interface Science, 103 (1985) 85-94.

Oliveira, R. G., Schneck, E., Quinn, B. E., Konovalov, O. V., Brandenburg, K., Gutsmann, T., Gill, T., Hanna, C. B., Pink, D. A., Tanaka, M., Crucial roles of charged saccharide moieties in survival of gram negative bacteria against protamine revealed by combination of grazing incidence x-ray structural characterizations and Monte Carlo simulations, Phys Rev E Stat Nonlin Soft Matter Phys, 81 (2010) 041901.

Patel, S. U., Osborn, R., Rees, S., Thornton, J. M., Structural studies of *Impatiens balsamina* antimicrobial protein (Ib-AMP1), Biochemistry, 37 (1998) 983-990.

Plumb, J. A., Cell sensitivity assays: the MTT assay, Methods Mol Med, 88 (2004) 165-169.

Prado Montes de Oca, E., Antimicrobial peptide elicitors: new hope for the post-antibiotic era, Innate Immun, 19 (2013) 227-241.

Raad, I., Hanna, H., Dvorak, T., Chaiban, G., Hachem, R., Optimal antimicrobial catheter lock solution, using different combinations of minocycline, EDTA, and 25-percent ethanol, rapidly eradicates organisms embedded in biofilm, Antimicrobial Agents and Chemotherapy, 51 (2007) 78-83.

Rahnamaeian, M., Antimicrobial peptides: modes of mechanism, modulation of defense responses, Plant Signal Behav, 6 (2011) 1325-1332.

Ratledge, C , Wilkinson, E SG, Microbial lipids, 3rd ed ed., London: Academic Press, 1988.

Reddy, P., Chadaga, S., Noskin, G. A., Antibiotic considerations in the treatment of multidrug-resistant (MDR) pathogens: a case-based review, J Hosp Med, 4 (2009) E8-15.

Rinaldi, A. C., Antimicrobial peptides from amphibian skin: an expanding scenario - Commentary, Current Opinion in Chemical Biology, 6 (2002) 799-804.

Rosenkranz, V., Wink, M., Alkaloids induce programmed cell death in bloodstream forms of trypanosomes (*Trypanosoma b. brucei*), Molecules, 13 (2008) 2462-2473.

Samuelson, J. C., Recent developments in difficult protein expression: a guide to *E. coli* strains, promoters, and relevant host mutations, Methods Mol Biol, 705 (2010) 195-209.

Santangelo, C. D., Farago, O., Membrane fluctuations around inclusions, Journal of Computer-Aided Materials Design, 14 (2007) 103-109.

Sato, H., Feix, J. B., Peptide-membrane interactions and mechanisms of membrane destruction by amphipathic alpha-helical antimicrobial peptides, Biochim Biophys Acta, 1758 (2006) 1245-1256.

Schein, Catherine H. , Production of soluble recombinant proteins in bacteria, Bio/Technology, 7 (1989) 1141-1149.

Seshadri Sundararajan, V., Gabere, M. N., Pretorius, A., Adam, S., Christoffels, A., Lehvaslaiho, M., Archer, J. A., Bajic, V. B., DAMPD: a manually curated antimicrobial peptide database, Nucleic Acids Res, 40 (2012) D1108-1112.

Shenkarev, Z. O., Balandin, S. V., Trunov, K. I., Paramonov, A. S., Sukhanov, S. V., Barsukov, L. I., Arseniev, A. S., Ovchinnikova, T. V., Molecular mechanism of action of beta-hairpin antimicrobial peptide arenicin: oligomeric structure in dodecylphosphocholine micelles and pore formation in planar lipid bilayers, Biochemistry, 50 (2011) 6255-6265.

Shimojo, R. Y., Iwaoka, W. T., A rapid hemolysis assay for the detection of sodium channel-specific marine toxins, Toxicology, 154 (2000) 1-7.

Souza, A. C. P., Yuen, P. S. T., How can antibiotics worsen acute kidney injury but improve survival in experimental sepsis?, Critical Care Medicine, 40 (2012) 685-686.

Spector, A. A., Yorek, M. A., Membrane lipid composition and cellular function, J Lipid Res, 26 (1985) 1015-1035.

Spellberg, B., Powers, J. H., Brass, E. P., Miller, L. G., Edwards, J. E., Trends in antimicrobial drug development: Implications for the future, Clinical Infectious Diseases, 38 (2004) 1279-1286.

Tailor, R. H., Acland, D. P., Attenborough, S., Cammue, B. P., Evans, I. J., Osborn, R. W., Ray, J. A., Rees, S. B., Broekaert, W. F., A novel family of small cysteine-rich antimicrobial peptides from seed of *Impatiens balsamina* is derived from a single precursor protein, J Biol Chem, 272 (1997) 24480-24487.

Tang, M., Hong, M., Structure and mechanism of beta-hairpin antimicrobial peptides in lipid bilayers from solid-state NMR spectroscopy, Mol Biosyst, 5 (2009) 317-322.

Teixeira, V., Feio, M. J., Bastos, M., Role of lipids in the interaction of antimicrobial peptides with membranes, Prog Lipid Res, 51 (2012) 149-177.

Thevissen, K., Francois, I. E., Sijtsma, L., van Amerongen, A., Schaaper, W. M., Meloen, R., Posthuma-Trumpie, T., Broekaert, W. F., Cammue, B. P., Antifungal activity of synthetic peptides derived from *Impatiens balsamina* antimicrobial peptides Ib-AMP1 and Ib-AMP4, Peptides, 26 (2005) 1113-1119.

Trombetta, D., Castelli, F., Sarpietro, M. G., Venuti, V., Cristani, M., Daniele, C., Saija, A., Mazzanti, G., Bisignano, G., Mechanisms of antibacterial action of three monoterpenes, Antimicrobial Agents and Chemotherapy, 49 (2005) 2474-2478.

van Kraaij, C., Breukink, E., Rollema, H. S., Bongers, R. S., Kosters, H. A., de Kruijff, B., Kuipers, O. P., Engineering a disulfide bond and free thiols in the lantibiotic nisin Z, Eur J Biochem, 267 (2000) 901-909.

Wang, G., Li, X., Wang, Z., APD2: the updated antimicrobial peptide database and its application in peptide design, Nucleic Acids Res, 37 (2009) D933-937.

WHO, Antimicrobial resistance: global report on surveillance For more information: http://www.who.int/drugresistance/documents/surveillancereport/en/, (2014).

WHO, Combat antimicrobial resistance, For more information: http://www.who.int/world-health-day/2011 (2011).

WHO, *Staphylococcus aureus* (hospital isolates): percentage of methicillin-resistant strains, Latin America and the Caribbean, For more information http://www.who.int/mediacentre/factsheets/fs194/en/ (2007).

Wimley, W. C., Describing the mechanism of antimicrobial peptide action with the interfacial activity model, ACS Chem Biol, 5 (2010) 905-917.

Woodka, A. C., Butler, P. D., Porcar, L., Farago, B., Nagao, M., Lipid bilayers and membrane dynamics: insight into thickness fluctuations, Phys Rev Lett, 109 (2012) 058102.

Wu, G. Q., Wu, H. B., Li, L. X., Fan, X. B., Ding, J. X., Li, X. F., Xi, T., Shen, Z. L., Membrane aggregation and perturbation induced by antimicrobial peptide of S-thanatin, Biochemical and Biophysical Research Communications, 395 (2010) 31-35.

Wu, Y., Ren, C., Gao, Y., Hou, B., Chen, T., Zhang, C., A novel method for promoting heterologous protein expression in *Escherichia coli* by fusion with the HIV-1 TAT core domain, Amino Acids, 39 (2010) 811-820.

Xu, H. M., Zhang, G. Y., Ji, X. D., Cao, L., Shu, L., Hua, Z. C., Expression of soluble, biologically active recombinant human endostatin in *Escherichia coli*, Protein Expr Purif, 41 (2005) 252-258.

Yamaguchi, T., Nishizaki, K., Itai, S., Nemoto, M., Ohshima, H., Adsorption of divalent-cations onto the membrane-surface of lipid emulsion, Colloids and Surfaces B-Biointerfaces, 5 (1995) 49-55.

Yeagle, P. L., Cholesterol and the cell membrane, Biochim Biophys Acta, 822 (1985) 267-287.

Yeaman, M. R., Yount, N. Y., Mechanisms of antimicrobial peptide action and resistance, Pharmacological Reviews, 55 (2003) 27-55.

Zilman, A. G., Granek, R., Undulations and dynamic structure factor of membranes, Phys Rev Lett, 77 (1996) 4788-4791.